STUDIES ON GRAPHENE

A Thesis

submitted in partial fulfillment of the

requirements of the degree of

Master of Science [Engg.]

by

K. S. Subrahmanyam

Chemistry and Physics of Materials Unit
Jawaharlal Nehru Centre for Advanced Scientific Research
(A Deemed University)
Bangalore – 560 064
July 2008

Dedicated

To

AMMA, NANNA

DECLARATION

I hereby declare that the matter embodied in this thesis entitled "**Studies on Graphene"** is the result of investigations carried out by me under the supervision of Prof. C. N. R. Rao, FRS at the Chemistry and Physics of Materials Unit, Jawaharlal Nehru Centre for Advanced Scientific Research, Bangalore, India and that it has not been submitted elsewhere for the award of any degree or diploma.

In keeping with the general practice in reporting scientific observations, due acknowledgement has been made whenever the work described is based on the findings of other investigators.

_____

K. S. Subrahmanyam

CERTIFICATE

I hereby certify that the matter embodied in this thesis entitled "**Studies on Graphene**" has been carried out by Mr. k. s. subrahmanyam, at the Chemistry and Physics of Materials Unit, Jawaharlal Nehru Centre for Advanced Scientific Research, Bangalore, India under my supervision and that it has not been submitted elsewhere for the award of any degree or diploma.

_____

Prof. C. N. R. Rao, FRS

(Research Supervisor)

ACKNOWLEDGEMENTS

I am extremely grateful to Prof. C. N. R. Rao, FRS for suggesting me research problems and guiding me throughout. He has been a constant source of inspiration for me. I greatly admire his enthusiasm towards science. I express my hearty gratitude to him for giving me an opportunity to work under his guidance.

I would like to express my sincere thanks to Dr. A. Govindaraj who has helped me a great deal in carrying out the various experiments. It has been a good learning experience working with him in the lab.

I am thankful to Usha Madam, Basavaraj, Anil, Vasu and Selvi, for their help with the various characterization techniques.

I am thankful to Dr. M. Eswaramoorthy and Saikrishna for their help in BET surface area measurements.

I am thankful to Dr. A. Sundaresan for magnetic measurements facility and Prof. G. U. Kulkarni for XPS facility.

I thank Bhat, Neenu, Vivek, Rakesh, and Gomathi for their help with the Raman measurements, Dr. Neena, Dr. Kunal, Vijay, Kalyani for their help with the AFM measurements, Bhuvana for her help with the XPS measurements, Pranab and Vengadesh for their help with the magnetic measurements.

I would like to thank my lab members Vivek, Chandu, Kalyani, Bhat, Gomathi, Kanishka, Rakesh, Leela, Sandeep, Neenu, Basanth, Anupama and Barun for their help and co-operation.

I am thankful to the faculty members of JNC and IISc for their courses. In particular, I would like to thank Prof. S. Balasubramanian, Prof. Swapan Pati, Prof. Umesh V Waghmare, Prof. Chandrabhas Narayana, Dr. M. Eswaramoorthy, and Dr. A. Sundaresan from JNC and Prof. S. Ranganathan from IISc.

I am thankful to Ravi, Nishaj, Dharma, Shithal, Satish, and Vikas of computer lab for their help.

I would like to thank Mrs. Indumati Rao and Mr. Sanjay S. R. Rao for their encouraging words and hospitality.

I am thankful to all academic staff members (Mrs. Sukanya, Dr. Princy).

I am thankful to office members (Mrs. Sashi, Gowda, Victor and Mrs. Sudha).

I am thankful to all work shop members (Arogyanathan, moorthy and sunil).

I would like to thank Mr. M. Srinivasa Rao, my teacher, who has been giving constant encouragement and suggestions in my life.

I would like to thank Rakesh, Kalyan, Chandu, Sahu, Neenu, Leela, Krishna, Gomathi, and Dr. A. Govindaraj for their help in writing thesis.

I would like to thank all HCU faculty, classmates and friends.

Special thanks to my friends Subbareddy, Chary, Sinu, Raja, Madhu soodhan, Balu, Ganesh, Koti, Guru, Nagarjuna, Bochkar, Vijji, Venki, Rag, Koteswar, Mohan, Naidu, Nag babu, Anand, Kasi, Kiran, Shesu, Prasad, Suresh, Srinu, Leela, Rakesh, Krishna, Vijay, Gopi, Siddhu, Mahesh, Phani, KKR, Kalyani, Dr. Thiru, Neenu, Radha, manu, Vivek, Chandu,

Bhat, Gomathi, Anupama, Kanishka, Sandy, Basanth, Barun, Reji, Ved, Saiki, kalyan, Srinivasraj, Dinesh, Claudy, Raju, Sahu, Madhu, Gurunath, Shipra, Venky, Pranab, Srinivasraj, Mukthi, kiran batta, Manojith, Sabyasachi, Prakash, Sameer, Sudip, Anil, Mighfar and Satthi.

I would like thank all my teachers, friends and relatives at my native place.

Heartfelt thanks to my parents, annyya and akka for being there for me always.

PREFACE

The thesis presents the results of studies on graphene. Part 1 consists of brief introduction to graphene. The scope of the present investigations is described in Part 2. Experimental and related aspects form Part 3 followed by a discussion of results in Part 4. Part 5 gives conclusions.

Different synthetic routes, including newly discovered arc discharge route have been employed and the samples so obtained characterized by utilizing different techniques such as electron microscopy, Raman spectroscopy, atomic force microscopy, and X-ray diffraction. Graphene samples prepared by different routes have been investigated for surface areas and gas storage applications. Interestingly, these samples have shown good uptakes of both H_2 and CO_2. Different ways to functionalize graphene have been explored. Amidation and reaction with organosilane or organotin reagents solubilize graphene in organic solvents where as wrapping with surfactants gives water soluble graphene. The π-π interaction with a pyrene derivative solubilizes graphene in dimethylformamide. Decoration of graphene with metal nano particles has been achieved in a single processing step through polyol reduction method. Electon transfer kinetics of different graphenes and their use as electrode material in supercapacitors have been investigated.

Summary

The results obtained from the investigations of graphene are summarized below.

Graphene has been synthesized by four different methods namely, pyrolysis of camphor under reducing conditions (CG), exfoliation of graphitic oxide (EG), conversion of nanodiamond (DG) and arc evaporation of graphite rod in hydrogen atmosphere (AG). The samples were examined by X-ray diffraction (XRD), transmission electron microscopy (TEM), atomic force microscopy, Raman spectroscopy and thermogravimetric analysis. Raman spectroscopy shows EG and DG to exhibit smaller in-plane crystallite size around 4-5 nm, while CG exhibits higher in-plane crystallite size of around 10 nm. From XRD and AFM studies, HG turns out be the best means of preparing graphene with a small number of layers.

Graphene samples prepared by the exfoliation of graphitic oxide, conversion of nanodiamond and arc-discharge of graphite rod in reductive atmosphere have been investigated for gas adsorption properties. These samples show high Brunauer-Emmett-Teller (BET) surface area values ranging from 238 to1550 m^2/g at 1 atm and 77 K. Graphene samples prepared by us exhibit good hydrogen uptake at 1 atm and 77 K, the uptake going up to 1.7 wt %. The hydrogen uptake varies linearly with the surface area, and the extrapolated value of hydrogen uptake by single-layer graphene works out to be just above 3 wt %. The H_2 uptake at 100 atm, 298 K is found to be 3 wt % or more, suggesting thereby the single-layer graphene would exhibit much higher uptakes. Equally interestingly, the graphene samples prepared by us show high uptake of CO_2, the value reaching up to 35 wt % at 1 atm and 195 K. The first principles calculations show that hydrogen molecule sits parallely on each six-membered ring of the graphene layer and can accommodates up to 7.7 wt % of hydrogen on single-layered graphene. CO_2 molecules sit alternatively in a parallel fashion on

the rings to give a maximum uptake of 37.93 wt % in single-layer graphene. Presence of more than one layer of graphene causes a decrease in the H_2 uptake. The present study shows that the H_2 uptake by graphene is comparable to that of single-walled carbon nanotubes and other carbon-based materials.

Solubilization of graphene in organic solvents has been accomplished through covalent functionalization, involving the preparation of a long-chain alkylamide derivative, and by interaction with an organosilane or an organotin reagents such as hexadecyltrimethoxysilane and dibutyldimethoxytin. Water-soluble graphene has been produced by extensive acid treatment of EG or treatment with polyethylene glycol. Non-covalent modification of graphene has been done through π-π interaction by using 1-pyrenebutanoic acid succinimidyl ester, which gives stable dispersions in dimethylformamide. Interaction of graphene with surfactants (IGP, SDS and CTAB) produced stable aqueous dispersions, Igepal being effective even at low concentrations.

Graphene has been decorated with Pt and Ag nanoparticles, through microwave-assisted polyol reduction of metal salts. TEM analysis shows the size of decorated Pt particles was around 10 nm, while silver was around 5 nm.

Electrochemical redox properties of the graphene samples prepared by three different methods have been studied. Among those three sampes EG behaves similar to that of basal plane in graphite, where as DG and CG exhibit slightly better kinetics. Graphene samples were investigated as electrode materials in electrochemical supercapacitors. The samples prepared by exfoliation of graphitic oxide and by the transformation of nanodiamond exhibit high specific capacitance in aq. H_2SO_4, the value reaching up to 117 F/g. By using an ionic liquid, the operating voltage has been extended to 3.5 V (instead of 1 V in the case of

aq. H_2SO_4), the specific capacitance and energy density being 75 F/g and 31.9 Whkg–1 respectively.

Papers based on these studies have appeared in J. Mater. Chem. (2008) and J. Chem. Sci (2008). Two papers have been accepted for publication in J. Phys. Chem. C and Nanosci. Nanotech. Letts.

1. INTRODUCTION

1.1 Allotropes of carbon

Carbon is one of the most interesting elements in the Periodic Table and plays a unique role in nature. The formation of carbon [Fig 1] in stars as a result of the merging of three particles, known as triple alpha process is a crucial process that leads to the existence of all the relatively heavy elements in the universe [1].

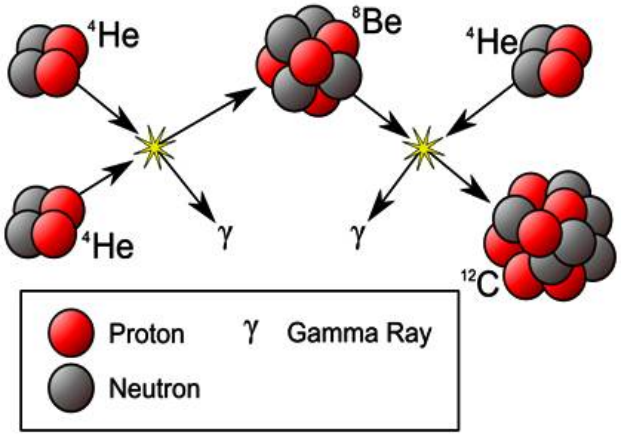

Fig 1: Overview of the Triple-alpha process

$$2He^{4} + 2He^{4} \rightarrow 4Be^{8}$$

$$4Be^{8} + 2He^{4} \rightarrow 6C^{12} + \gamma + 7.367 \text{ MeV}$$

Carbon has the ability to form very long chains interconnecting C-C bonds known as catenation. This ability allows carbon to form an almost infinite number of compounds; in fact, there are more known carbon-containing compounds than all the compounds of the other chemical elements. The capability of carbon atoms to form complicated networks [2] is

fundamental to organic chemistry and the basis for the existence of life, at least in its known forms. Even elemental carbon demonstrates unusually complicated behavior, forming a number of very different structures. It forms many allotropes such as diamond and graphite including recently discovered fullerenes [3-5] and nanotubes [6].

Among those, diamond and graphite are much popular and have known since ancient times, while recently discovered fullerenes and nanotubes are currently a focus of attention for many physicists and chemists. Thus, only three-dimensional (diamond, graphite),

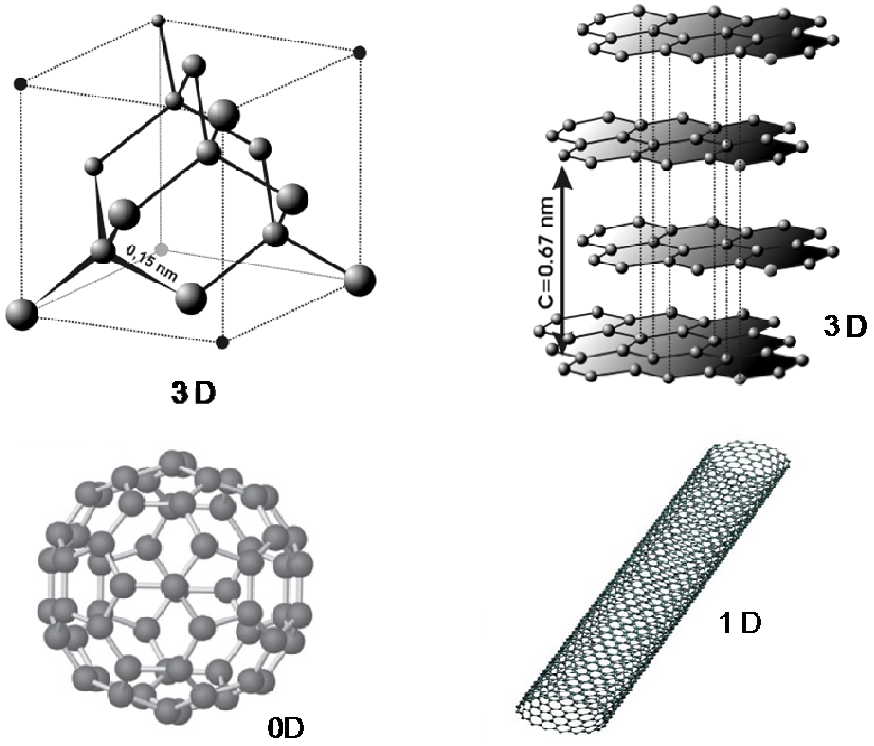

Fig 2: 3D, 1D and 0D allotropes of carbon

one-dimensional (nanotubes), and zero-dimensional (fullerenes) allotropes of carbon were known [Fig 2]. The two-dimensional form was conspicuously missing, resisting any attempt at experimental observation – until recently.

1.2 Brief history of graphene

The two-dimensional form of carbon known as graphene (or '2D graphite') is a flat monolayer of carbon atoms tightly packed into a honeycomb lattice, and is a basic building block for graphitic materials of all other dimensionalities. It can be wrapped up into 0D

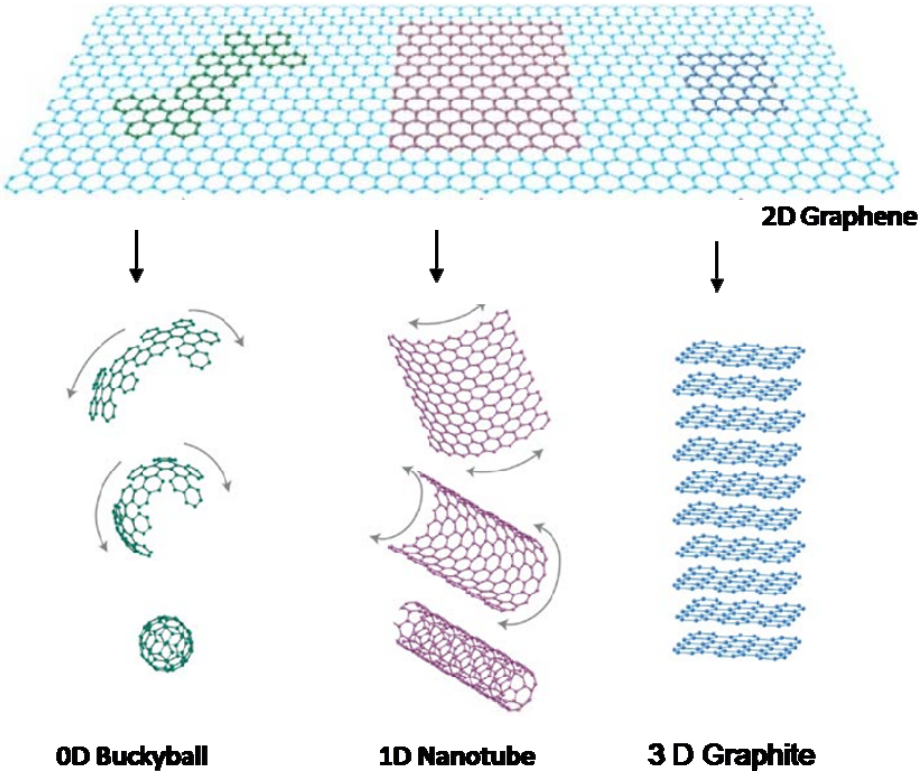

Fig 3: Mother of all graphitic forms

fullerenes, rolled into 1D nanotubes or stacked into 3D graphite [Fig 3]. It has been theoretically studied for sixty years [7-9] and it is used as the starting point for all calculations of various carbon based materials like graphite, carbon nanotubes and fullerenes. Even though it is known as an integral part of 3D materials, graphene was presumed not to exist in the free state and was believed to be unstable with respect to the formation of curved structures such as soot, fullerenes and nanotubes. At the same time, attempts to synthesize these two-dimensional atomic crystals have usually failed, ending up with nanometer-size crystallites [10] supporting the above assumption.

Suddenly in 2004, this two-dimensional form, which was considered earlier as an 'academic' material turned into reality, when free-standing graphene was obtained by a group of physicists from Manchester University.

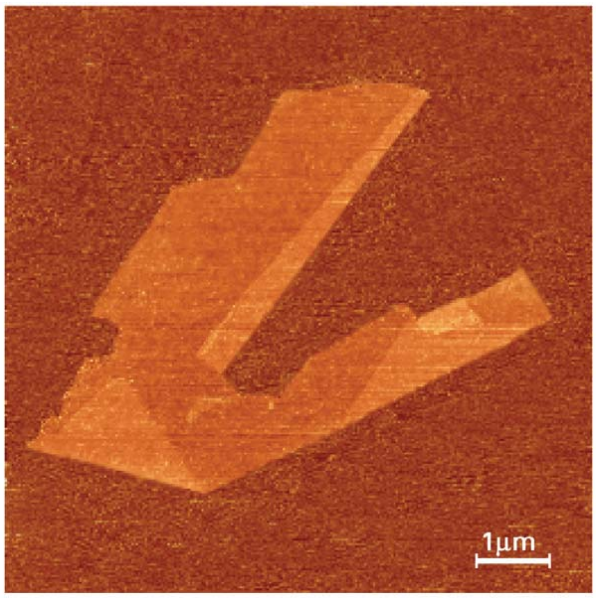

Fig 4: Atomic force microscopy image of a graphene crystal on top of an oxidized Si substrate

The group led by Andre Geim and Kostya Novoselov used a very different and, at first glance, even naive approach to obtain graphene and lead a revolution in the field. They started with three-dimensional graphite and extracted a single sheet (a monolayer of atoms) using a technique called micromechanical cleavage [11,12] [Fig 4]. Graphite is a layered material and can be viewed as a number of two-dimensional graphene crystals weakly coupled together – exactly the property used by the Manchester team. By using this top-down approach and starting with large, three-dimensional crystals, the researchers avoided all the issues with the stability of small crystallites. Furthermore, the same technique has been used by the group to obtain two-dimensional crystals of other materials [11], including boron nitride, some dichalcogenides, and the high-temperature superconductor Bi-Sr-Ca-Cu-O.

1.3 Types of graphene

Obviously, a single atomic plane is a 2D crystal, whereas 100 layers should be considered as a thin film of a 3D material. But it is also interesting to know how many number of layers are needed before the structure is regarded as 3D. In case of graphene, it was shown that the electronic structure rapidly evolves with the number of layers, approaching the 3D limit of graphite at 10 layers [13]. Moreover, only graphene and to a good approximation its bilayer has simple electronic spectra: they are both zero-gap semiconductors (they can also be referred to as zero-overlap semimetals) with one type of electron and one type of hole. For three or more layers, the spectra become increasingly complicated: Several charge carriers appear and the conduction and valence bands start notably overlapping [13]. This allows single-, double- and few- (3 to <10) layer graphene to

be distinguished as three different types of 2D crystals (‘graphenes’). Thicker structures should be considered, to all intents and purposes, as thin films of graphite.

1.4 Stability of graphene

The physical structure of graphene is interesting and also quite puzzling. On the one hand, graphene appears to be a strictly two-dimensional material, exhibiting such a high crystal quality that electrons can travel submicrometre distances without scattering. On the other hand, perfect two-dimensional crystals cannot exist in the free state, according to both theory and experiments reported earlier [11,14–18]. This incompatibility can be avoided by arguing that all the graphene structures studied so far were an integral part of larger three-dimensional structures, either supported by a bulk substrate or embedded in a three-dimensional matrix [11,19-21]. But amazingly, recently individual graphene sheets [Fig 5] freely suspended on a micro fabricated scaffold in vacuum or in air have been reported [22].

Fig 5: TEM image of a suspended graphene membrane

(Scale bar, 500 nm)

Whether a strictly two-dimensional (2D) crystal can exist was first raised theoretically more than 70 years ago by Peierls [14,15] and Landau [16,17]. They showed that, in the standard harmonic approximation [23], thermal fluctuations should destroy long-range order, resulting in melting of a 2D lattice at any finite temperature. Furthermore, Mermin and Wagner proved that a magnetic long-range order could not exist in one and two dimensions [17] and later extended the proof to crystalline order in 2D [18]. Importantly, numerous experiments on thin films have been in accord with the theory, showing that below a certain thickness, typically of dozens of atomic layers, the films become thermodynamically unstable (segregate into islands or decompose) unless they constitute an inherent part of a three-dimensional (3D) system (such as being grown on top of a bulk crystal with a matching lattice) [24-26]. However, although the theory does not allow perfect crystals in 2D space, it does not forbid nearly perfect 2D crystals in 3D space. Indeed, a detailed analysis of the 2D crystal problem beyond the harmonic approximation has led to the conclusion [27-29] that the interaction between bending and stretching long-wavelength phonons could in principle stabilize atomically thin membranes through their deformation in the third dimension [29].

1.5 Electronic structure of graphene

Graphene has two atoms per unit cell, which results in two ‘conical’ points per Brillouin zone where band crossing occurs, K and K’. Near these crossing points, the electron energy is linearly dependent on the wave vector. Actually, this behavior follows from symmetry considerations [30] and thus, is robust with respect to long-range hopping processes [Fig 6]. The interesting point is that, the charge carriers in graphene behave as

massless relativistic particles [31,32].The Dirac equation describes relativistic quantum particles with spin ½, such as electrons. The essential feature of the Dirac spectrum, following from the basic principles of quantum mechanics and relativity theory, is the existence of antiparticles.

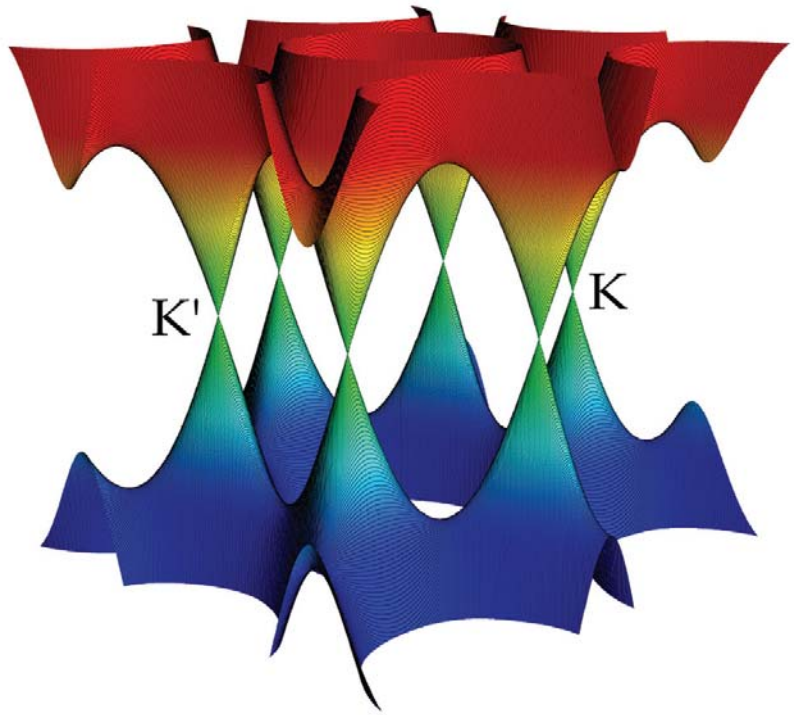

Fig 6: Band structure of graphene

This fundamental property of the Dirac equation is often referred to as the charge-conjugation symmetry. For Dirac particles with mass m, there is a gap between the minimal electron energy, $E_0 = mc^2$, and the maximal positron energy, $-E_0$ (c is the speed of light). When the electron energy $E >> E_0$, the energy is linearly dependent on the wave

vector k, E = cħk. For massless Dirac fermions, the gap is zero and this linear dispersion law holds at any energy. In this case, there is an intimate relationship between the spin and motion of the particle: spin can only be directed along the propagation direction (say, for particles) or only opposite to it (for antiparticles). In contrast, massive spin-½ particles can have two values of spin projected onto any axis. In a sense, we have a unique situation here: charged massless particles. Although this is a popular textbook example, no such particles have been observed before. The fact that charge carriers in graphene are described by a Dirac-like spectrum, rather than the usual Schrödinger equation for nonrelativistic quantum particles, can be seen as a consequence of graphene's crystal structure. This consists of two equivalent carbon sublattices A and B [Fig 7]. Quantum-mechanical hopping between the sublattices leads to the formation of two energy bands, and their intersection near the edges of the Brillouin zone yields the conical energy spectrum.

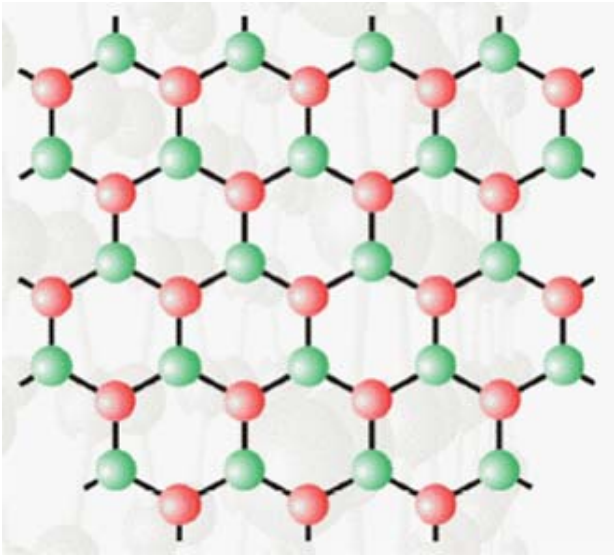

Fig 7: Crystallographic structure of graphene. Atoms from different sublattices(A and B) are marked different colors.

As a result, quasiparticles in graphene exhibit a linear dispersion relation $E = \hbar k \upsilon_F$, as if they were massless relativistic particles (for example, photons) but the role of the speed of light is played here by the Fermi velocity $\upsilon_F \approx c/300$. Because of the linear spectrum, one can expect that quasiparticles in graphene behave differently from those in conventional metals and semiconductors, where the energy spectrum can be approximated by a parabolic (free electron- like) dispersion relation.

1.6 Ballistic conductivity

Graphene's quality clearly reveals itself in a pronounced ambipolar electric field effect [Fig 8] such that charge carriers can be tuned continuously between electrons and holes in concentrations as high as 10^{13} cm^{-2} and their mobilities μ can exceed 15,000 cm^2 V^{-1} s^{-1} even under ambient conditions [11,12,33,34]. Moreover, the observed mobilities weakly depend on temperature T, which means that μ at 300 K is still limited by impurity scattering, and therefore can be improved significantly, perhaps, even up to $\approx$ 100,000 cm^2 V^{-1} s^{-1}. Although some semiconductors exhibit room-temperature μ as high as $\approx$ 77,000 cm^2 V^{-1} s^{-1} (namely, InSb), those values are quoted for undoped bulk semiconductors. In graphene, μ remains high even at high concentration (>1012 cm^{-2}) in both electrically and chemically doped devices [35], which translates into ballistic transport on the submicrometre scale (currently up to ≈0.3 μm at 300 K). A further indication of the system's extreme electronic quality is the quantum Hall effect (QHE) that can be observed in graphene even at room temperature, extending the previous temperature range for the QHE by a factor of 10 [36].

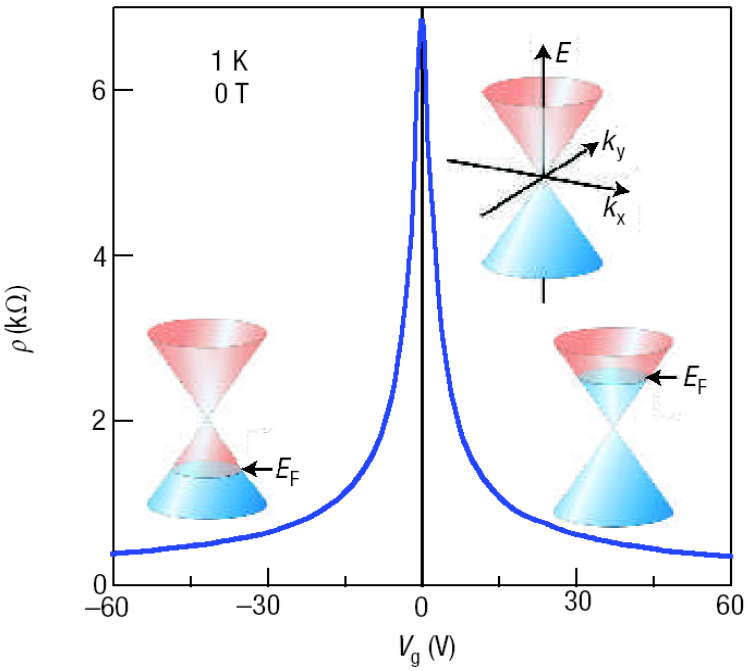

Fig 8: Ambipolar electric field effect in Single-layer graphene

Although there is nothing particularly relativistic about electrons moving around carbon atoms, their interaction with the periodic potential of graphene's honeycomb lattice gives rise to new quasiparticles that at low energies E are accurately described by the (2+1)-dimensional Dirac equation with an effective speed of light $v_F \approx 10^6$ $m^{-1}s^{-1}$. These quasiparticles, called massless Dirac fermions, can be seen as electrons that have lost their rest mass (m_0) or as neutrinos that acquired the electron charge. The relativistic like description of electron waves on honeycomb lattices has been known theoretically for many

years, never failing to attract attention, and the experimental discovery of graphene now provides a way to probe quantum electrodynamics (QED) phenomena by measuring graphene's electronic properties.

1.7 Anomalous quantum Hall effect

Quantum Hall effect is a phenomenon that Hall resistance (Hall voltage/channel current) in two dimensional electron systems is quantized to the ratio of fundamental physical constant under the condition of low temperature and high magnetic field.

$$R_H = V_H/I_x = h/ie^2$$

Where R_H is Hall resistance, V_H is Hall voltage, I_x is channel current, *h* is Planck constant, *e* is elementary charge and i is integer number. Quantized Hall resistance has a dimension of resistance and is independent on sample size or materials.

Graphene, consisting of an isolated single atomic layer of graphite, is an ideal realization of a two-dimensional system in which Quantum Hall effect can be observed. However, its behaviour is expected to differ markedly from the well-studied case of quantum wells in conventional semiconductor interfaces. This difference arises from the unique electronic properties of graphene, which exhibits electron–hole degeneracy and vanishing carrier mass near the point of charge neutrality [37,38]. Indeed, a distinctive half-integer quantum Hall effect has been predicted theoretically [39–41], as has the existence of a non-zero Berry's phase (a geometric quantum phase) of the electron wave function—a consequence of the exceptional topology of the graphene band structure [42,43].

Recent advances in micromechanical extraction and fabrication techniques for graphite structures [12,44–47] now permit such exotic two-dimensional electron systems to be probed experimentally. They observed an unusual half integer quantum Hall effect for both electron

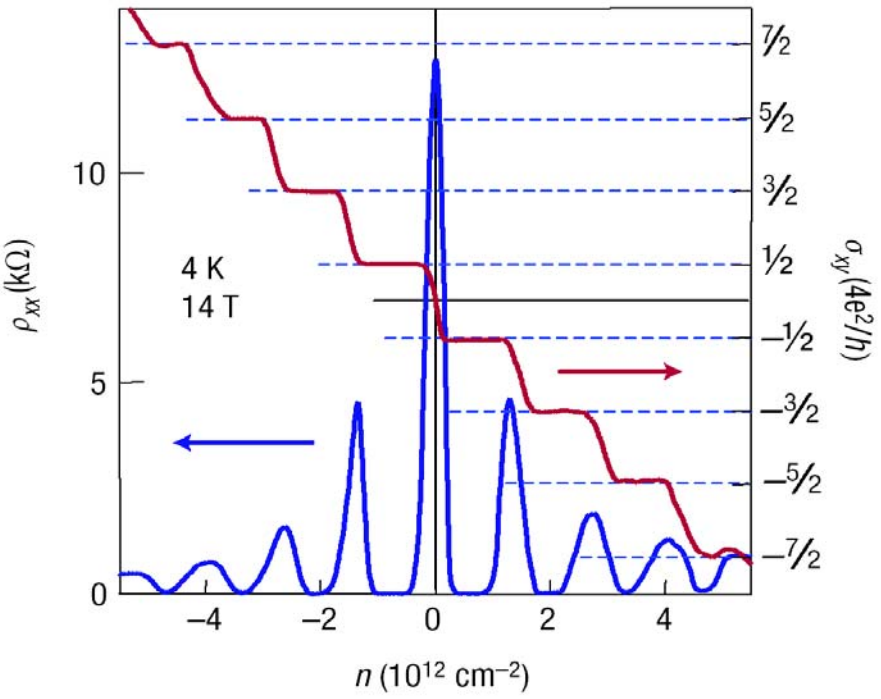

Fig 9: Anomalous QHE in single layer Graphene

and hole carriers in graphene [Fig 9], by adjusting the chemical potential with the use of the electric field effect. The relevance of Berry's phase to these experiments is confirmed by magneto-oscillations. These unusual quantum transport phenomena may lead to new applications in carbon-based electronic and magneto-electronic devices.

1.8 Quantum Hall effect at room-temperature

As with many other quantum phenomena, the observation of the QHE usually requires low temperatures, typically below the boiling point of liquid helium (48). Efforts to extend the QHE temperature range by, for example, using semiconductors with small effective masses of charge carriers have so far failed to reach temperatures above 30 K [49, 50]. These

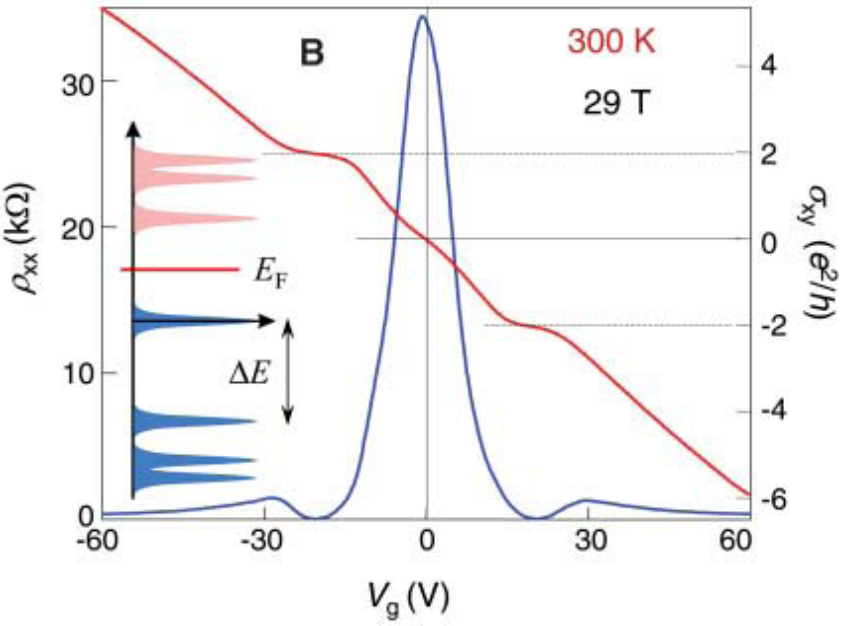

Fig 10: Room-temperature QHE in graphene

efforts have been done to observe apparently fragile quantum phenomena under ambient conditions and the pragmatic need to perform metrology at room, or at least liquid-nitrogen, temperatures. The QHE can be observed in graphene even at room temperature [Fig 10] due to the highly unusual nature of charge carriers in graphene, which behave as massless relativistic particles (Dirac fermions) and move with little scattering under ambient conditions [33].

1.9 Anomalous QHE in bilayer graphene

For two carbon layers, the nearest-neighbor tight-binding approximation predicts a gapless state with parabolic bands touching at the K and K' points, instead of conical bands [51, 52]. More accurate consideration [53] gives a very small band overlap (about 1.6 meV).

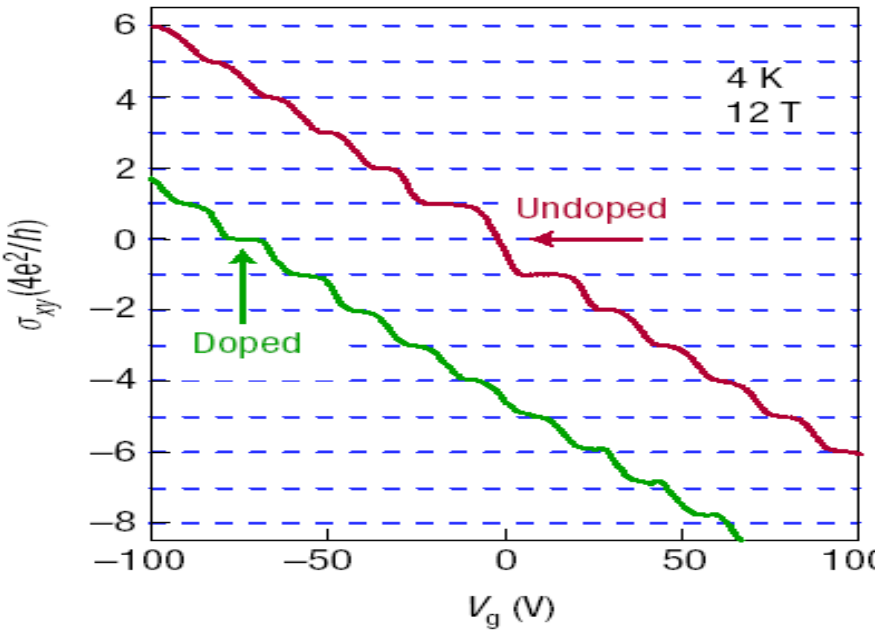

Fig 11: Anomalous QHE in bilayer grapheme

But at, larger energies, bilayer graphene can be treated as a gapless semiconductor. At the same time, the electron states are still characterized by chirality and by the Berry phase. Exact solution of the quantum mechanical equation for this kind of spectrum in the presence of a homogeneous magnetic field gives the result [51, 52] Eυ α √υ (υ- 1) and, thus, the number of states with zero energy (υ= 0 and υ= 1) is twice that of monolayer graphene As a

result, the QHE for bilayer graphene differs from both single-layer graphene and conventional semiconductors, as found experimentally [51] [Fig 11].

1.10 Conductivity with out charge carriers

An important observation in graphene is that its zero-field conductivity σ does not disappear in the limit of vanishing n but instead exhibits values close to the conductivity quantum e^2/h per carrier type [33]. Figure 12, shows the lowest conductivity σ (min) measured near the neutrality point for nearly 50 single-layer devices. For all other known material such a low conductivity unavoidably leads to a metal–insulator transition at low temperature but no sign of the transition has been observed in graphene down to liquid-helium temperature. Bilayer graphene also exhibits a minimum conductivity of the order of e^2/h per carrier type [51], which indicates that it is chirality, rather than the linear spectrum, that is more important.

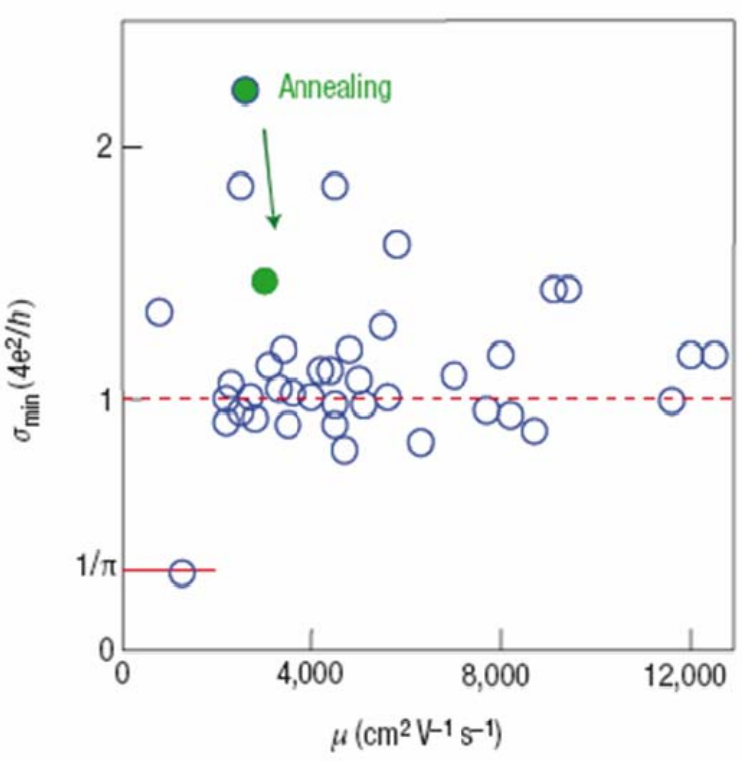

Fig 12: Minimum conductivity of graphene.

1.11 Composites

Graphite is soft and flaky, and cannot be used in load-bearing structures. This problem could be solved by making a composite material of graphene sheets and polymers. The manufacturing of such composites requires not only that graphene sheets be produced on a sufficient scale but that they also be incorporated, and homogeneously distributed, into various matrices. Unfortunately, owing to their hydrophilic nature, graphene oxide sheets can only be dispersed in aqueous media that are incompatible with the most organic polymers. In addition, graphite oxide is electrically insulating, unlike graphite, which limits its usefulness for the synthesis of conductive nanocomposites. It has been demonstrated [54-57] however, that the electrical conductivity of graphite oxide can be significantly increased by chemical reduction, presumably owing to the restoration of a graphitic network of sp^2 bonds. But reduction of exfoliated graphene oxide nanoplatelets in water results in their irreversible coagulation [54], which then makes dispersion within a polymer matrix at the individual sheet level impossible.

However Stankovich *et al*. reported a novel approach for the preparation of graphene-polymer composites via complete exfoliation of graphite and molecular-level dispersion of individual, chemically modified graphene sheets within polymer hosts, overcoming above difficulties [58]. A polystyrene–graphene composite [Fig 13] reported by Stankovich et al. exhibits a percolation threshold of ~ 0.1 volume percent for room-temperature electrical conductivity, the lowest reported value for any carbon-based composite except for those involving carbon nanotubes [59], at only 1 volume percent, this composite has a conductivity of ~ 0.1 Sm^{-1}, sufficient for many electrical applications [60].

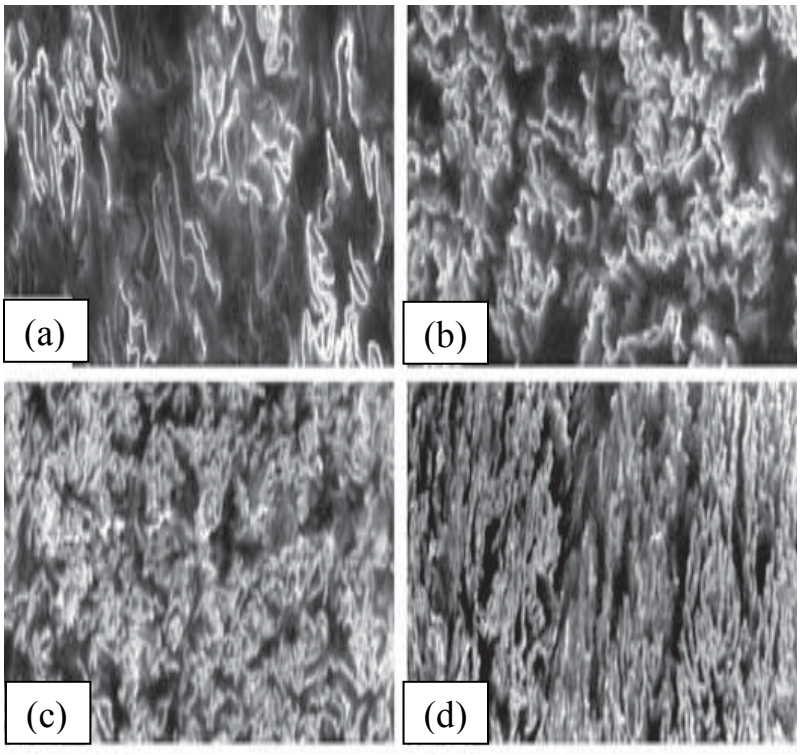

Figure 13: SEM images of graphene–polystyrene composite. a–d, SEM images of the composites reveal different morphologies of the graphene sheets, including their packing, at different concentrations (vol.%): a, 0.24; b, 0.96; c, 1.44; and d, 2.4.

By employing directed-flow assembly method D. A. Dikin et al. reported a method to yield a novel graphene oxide paper-like material possessing a unique layered structure in which individual compliant graphene oxide sheets are interlocked together in a near-parallel fashion [61]. The large interaction surfaces between these sheets, their corrugation at the atomic scale, and their wrinkled morphology at the submicrometre scale allow for a highly effective load distribution across the entire macroscopic sample, and thus make this material more resilient than traditional carbon- and clay-based papers.

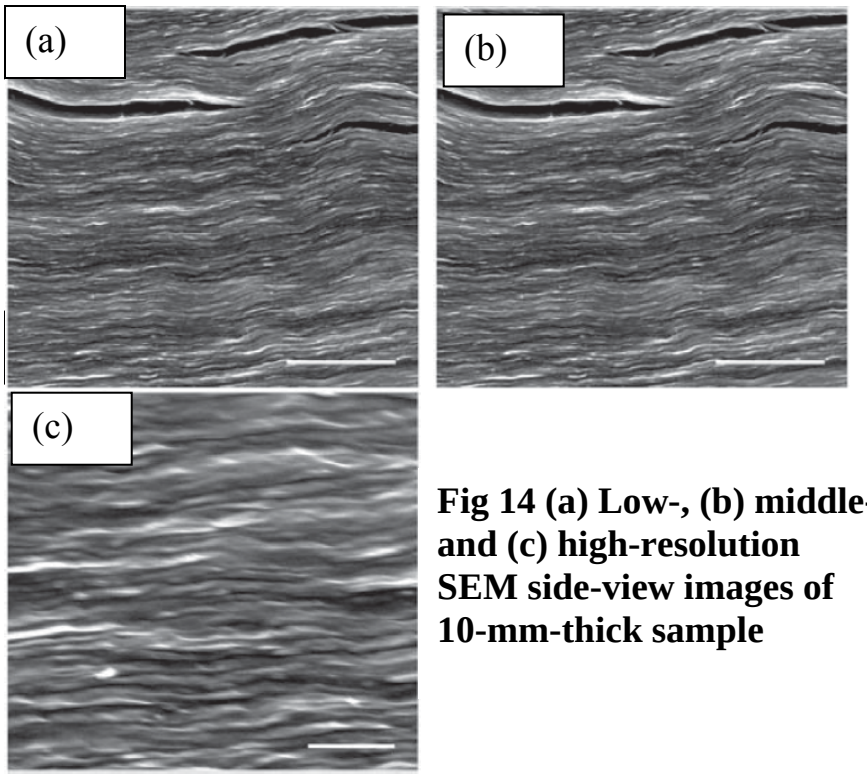

Fig 14 (a) Low-, (b) middle- and (c) high-resolution SEM side-view images of 10-mm-thick sample

The graphene composites could be very useful: for example, in the manufacture of fuselages for aircraft, which must combine low weight, high strength and electrical conductivity. This last property is necessary for protection against lightning strikes while in flight. The potential properties of these graphene sheet-based composites thus appear promising due to the extremely high aspect ratios of the graphene sheets having the average lateral dimension about 1 mm. The intrinsic mechanics of the sheets, their crumpling, wrinkling and folding, and whether they can be processed to be non-crumpled sheets (for example, so that layering could be more effectively achieved) are important issues for further study.

1.12 Sensors

Solid-state gas sensors are renowned for their high sensitivity, which in combination with low production costs and miniature sizes—have made them ubiquitous and widely used in many applications [62,63]. Recently, a new generation of gas sensors has been demonstrated using carbon nanotubes and semiconductor nanowires [64,65]. The ultimate aim of any detection method is to achieve such a level of sensitivity that individual quanta of a measured entity can be resolved. In the case of chemical sensors, the quantum is one atom or molecule. Such resolution has so far been beyond the reach of any detection technique, including solid-state gas sensors hailed for their exceptional sensitivity [62-65]. The fundamental reason limiting the resolution of such sensors is fluctuations due to thermal motion of charges and defects [66], which leads to intrinsic noise exceeding the sought-after signal from individual molecules, usually by many orders of magnitude. But the micrometer-size sensors made from graphene are capable of detecting individual events when a gas molecule attaches to or detaches from graphene's surface [67].

The operational principle of graphene devices is based on changes in their electrical conductivity, due to gas molecules adsorbed on graphene's surface [Fig 15] and acting as donors or acceptors, similar to other solid-state sensors [62-65]. However, the following characteristics of graphene make it possible to increase the sensitivity to its ultimate limit and detect individual dopants.

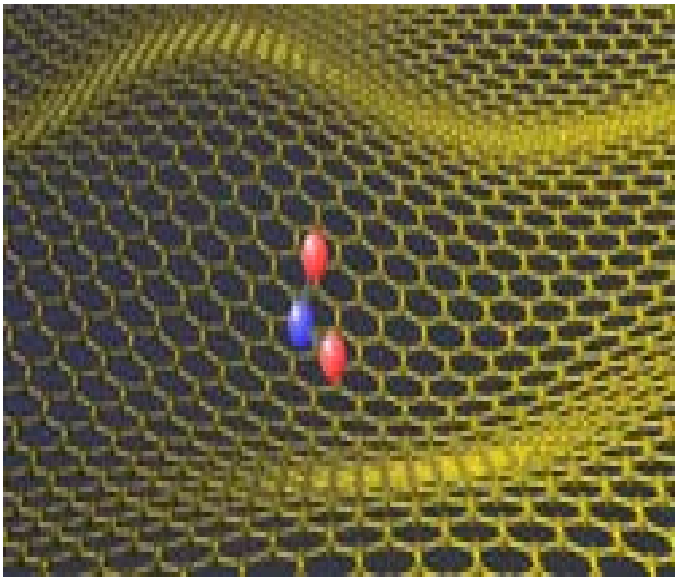

Fig 15: Graphene sheets could detect just a single molecule of nitrogen dioxide

First, graphene is a strictly two-dimensional material and, as such, has its whole volume exposed to surface adsorbates, which maximizes their effect. Second, graphene is highly conductive, exhibiting metallic conductivity and, hence, low Johnson noise even in the limit of no charge carriers [11, 33, 34], where a few extra electrons can cause notable relative changes in carrier concentration (n). Third, graphene has few crystal defects [11, 33, 34, 68], which ensures a low level of excess (1/f) noise caused by their thermal switching [66]. Fourth, graphene allows four-probe measurements on a single crystal device with electrical contacts that are ohmic and have low resistance. All these features contribute to make a unique combination that maximizes the signal-to-noise ratio to a level sufficient for

detecting changes in a local concentration by less than one electron charge, e, at room temperature.

1.13 Electrodes in solar cells

Transparent conducting films are an essential part of many gadgets including common liquid crystal displays for computers, TVs and mobile phones. Traditionally, thin metallic or metal oxide films are used for these purposes [69]. At the same time, there is a constant search for new types of conductive thin films, as existing technologies are often complicated (e.g. thin metallic films require anti-reflection coating) and expensive (often using noble or rare metals). Furthermore, many of the widely used metal oxides exhibit nonuniform absorption across the visible spectrum [70] and are chemically unstable (for instance, (commonly used indium tin oxide (ITO, In_2O_3: Sn) is known to inject oxygen [71] and indium [72] ions into the active media of a device). Recently carbon nanotube films have been produced [73] and used as an alternative transparent conductor in various photonic devices including electric-field-activated optical modulators [73], organic solar cells [74], and liquid crystal displays [75]. The experimental discovery of graphene brought a new alternative to the ubiquitous ITO. Recently graphene was employed as a transparent conductive coating for photonic devices and showed that its high transparency and low resistivity make this two dimensional crystal ideally suitable for electrodes in solar cells and liquid crystal devices [Fig 16].

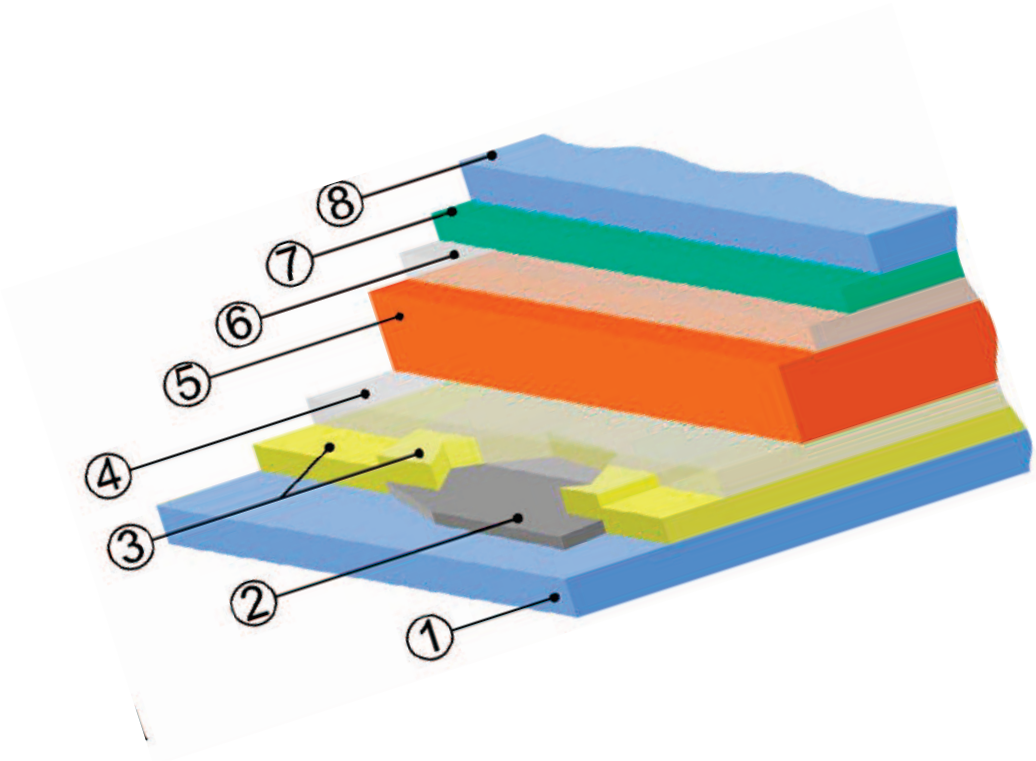

Fig 16 (a) Schematic diagram of liquid crystal device typical layer thicknesses in brackets: 1, glass (1 mm); 2, graphene; 3, Cr/Au contact surrounding graphene flake (5 nm Cr + 50 nm Au); 4, alignment layer (polyvinyl alcohol) (40 nm); 5, liquid crystal (20 μm); 6, alignment layer (40 nm); 7, ITO (150 nm); 8, glass (1 mm). The graphene flake is surrounded by a nontransparent Cr/Au contact.

1.14 Support membrane for transmission electron microscopy

Graphene is effectively the thinnest material that we can make out of atoms. Surprisingly, it is also very strong, thanks to a lack of crystal boundaries to break along and very strong bonds between carbon atoms (carbon nanotubes are made from rolled up graphene, and it has been suggested that cabling made from nanotubes would be strong enough to create an elevator into space). As a result, we can use it to hold micro- and

nanoscopic objects to look at in an electron microscope (e.g. DNA, nanoparticles) in a similar way we use glass slides in an optical microscope. Graphene is the perfect material for this job as it is made only of carbon, it is very thin, so it will not interfere with TEM images taken as much as other materials, and has a very simple crystal structure so can easily be eliminated from diffraction patterns.

1.15 Molecular sieves

The open honeycomb structure of graphene means it might be possible to use it as a net or sieve for atoms and small molecules, since only objects of this size will be able to fit through the lattice. So it could, be used in a way analogous to a filter paper, trapping large molecules and allowing smaller ones to pass.

1.16 Graphene may be the new silicon

The new two dimensional form of carbon called graphene is fast replacing silicon (the material at the heart of all computer chips) in electronics. It could allow electronics to process information and produce radio transmissions 10 times better than silicon-based devices. Usage of graphene produces faster and more powerful cell phones, computers as well as other electronics. However, until now, the switch from silicon to carbon had not been possible because of unavailability of graphene in the same form as the silicon used to make chips: a single crystal of material 8 or 12 inches wide. The hurdle in achieving these is that the largest single-crystal graphene sheets made to date have been no wider than a couple millimeters, not big enough for a single chip.

1.17 Graphane

Graphane is a “hypothetical” saturated hydrocarbon derived from a single graphene sheet with formula CH. All of the carbon atoms are in sp^3 hybridization forming a hexagonal network and the hydrogen atoms are bonded to carbon on both sides of the plane in an alternating manner. Graphane is predicted to be stable on the basis of first-principles total energy calculations with a binding energy comparable to other hydrocarbons such as benzene, cyclohexane, and polyethylene.

Hydrocarbons are the simplest organic compounds made only of carbon and hydrogen Atoms [76]. Some of them occur naturally in the form of crude oil and natural gas. Others are synthesized such as polyethylene and other plastics. They are readily oxidized to produce carbon dioxide and water with a considerable release of energy; therefore, they are usually good fuels. All known hydrocarbons, until now, are molecules that consist of a carbon backbone with hydrogen atoms attached. The backbone can be a linear chain, a ring, or combinations of both. On the contrary, graphane is the first extended two-dimensional covalently bonded hydrocarbon. Graphane is predicted to be a semiconductor, because of its novel structure and low dimensionality. There is a fully fluorinated analog, poly-(carbon monofluoride) with formula CF, which has been synthesized before [77]. Because fluorine is known to replace hydrogen in many hydrocarbons, the existence of this fully fluorinated form gives further support to prediction of this new academic material.

Graphane has two favorable conformations: a chair-like conformer with the hydrogen atoms alternating on both sides of the plane and a boat-like conformer with the hydrogen atoms alternating in pairs. In the chair conformer, every C-C bond connects carbon atoms with hydrogen attached at opposite sides of the plane.

The calculated C-C bond length of 1.52 Å is similar to the sp^3 bond length of 1.53 Å in diamond and is much greater than 1.42 Å characteristic of sp^2 carbon in graphene. The boat conformer has two different types of C-C bonds: those connecting carbons bonded to hydrogen atoms on opposite sides of the plane with a bond length of 1.52 Å and those connecting carbon atoms bonded to hydrogen atoms on the same side of the plane with a bond length of 1.56 Å, slightly longer due to H-H repulsion.

The C-H bond length of 1.1 Å is similar in both conformers and typical of hydrocarbon compounds. The graphane bonds are fully saturated and there is no opportunity for hydrogen bonding between the sheets.

2. SCOPE OF THE PRESENT INVESTIGATIONS

2.1 Synthesis and characterization of graphenes

The approach to prepare graphene reported by Novoselov et al. based on the scotch tape technique allows production of graphene crystallites up to 100 μm in size. [12].The quality of the samples produced is so good that both ballistic transport and a quantum Hall effect (QHE) [34, 36] can be observed easily. This makes graphene a promising candidate for future electronic applications, such as ballistic field-effect transistors (FETs). While this approach may suffice for certain physical measurements, so it is necessary to prepare graphene in large quantities for other studies and applications. We have therefore attempted to investigate different synthetic routes, which can provide graphene with yield.

In order to prepare graphene in large quantities, we have employed four known methods, based on exfoliation of graphitic oxide (EG) [78], conversion of nanodiamond (DG) [79], reductive pyrolysis of camphor (CG) [80], and arc evaporation of silicon carbide rod in reductive atmosphere (SG) [81].

We have prepared several samples following above procedures and characterized by employing different techniques known as AFM, TEM, X-ray diffraction and Raman spectroscopy. This is because, there is no information in literature about characterization of graphene obtained by different methods, particularly incase of samples those have more than one layer.

We have developed a new method to prepare graphene by doing arc evaporation of graphite rod in H_2 atmosphere with out using any catalyst. This new method makes use of the knowledge that, it is difficult to obtain carbon nanotubes by employing arc evaporation of

graphite rod in H_2 atmosphere. It appears that H_2 plays a key role in the formation of graphene sheets by resisting them to role into tubular form.

2.2 Surface area of graphenes and uptake of H_2 and CO_2 by graphene

High surface area materials

High surface area materials are materials which have large surface to volume ratio. Consider for example a chunk of material in the shape of a sphere of radius R. Its surface to volume ratio is 3/R. Thus, for smaller pieces of materials, the surface to volume ratio is larger. For pieces of matter on a nanometer scale (nanoparticles), the contribution of the surface to the overall properties of such matter becomes very important. For example, in a nanoscopic particle with a diameter of 5 nm, about half of its atoms are on its surface (low-coordination-number atoms). This is why the techniques and methods of surface science are needed to describe properties of nanoscopic matter. Even the macroscopic pieces of nanostructured materials can have high surface area, since their nanoscopic constituents can arrange in such a way to still have a large exposed surface. For example, single-walled carbon nanotube materials consist of carbon nanotube bundles. The bundles are made of several tens of carbon nanotubes and thus have a large exposed surface. Bundles are in a macroscopic material organized in such a way that their large surface still remains exposed (a particular bundle is not shielded by other bundles in the material).

Commercial applications of high surface area materials already are in the multibillion dollar range, primary contributions to this economic basis are air separation, petroleum and petrochemical processing, environmental cleanup, chemical sensing, fine chemical catalysis [84, 85], packaging [86-87], and chemical separation [88] applications.

Economic incentives for the development and application of high surface area materials are expected to substantially increase in view of increasing environmental stress, their role as important components of chemical sensors [89, 90], potential applications in biotechnology, and increasing energy and agricultural consumption demands.

Control of the nanostructure and the nanostructure interface in composite phases can be expected to provide breakthroughs in a number of applications: parallel processing where high density image processing coupled with high space velocity or turnover is required; applications involving pattern recognition, biomaterials synthesis, and design; biotechnology applications; development of small lapel-worn toxic agent detectors for military and in general, chemical sensing technology where highly selective, rapid detection is required. Breakthroughs are less likely in current bulk processing applications, particularly in the historically more mature air separation, petroleum, and petrochemical industries. The cost of reconfiguring present technologies and plants operating at a relatively high efficiency is a formidable barrier. Nevertheless, the magnitude of the economic impact generated by even small improvements in many of these areas is so substantial that nanostructure-directed modification of the present approaches is still being and will continue to be sought.

We have prepared several graphene samples by exfoliation of graphitic oxide (EG), conversion of nanodiamond (DG) and arc evaporation of graphite (HG). Some of these samples have been subjected H_2 treatment at high temperature and further acid treatment. We have studied surface areas of the different samples by employing Brunauer-Emmett-Teller (BET) method at 1 atm and 77 K employing QuantaChrome Autosorb-1 instrument. These samples showed BET surface areas values in the range of 238 - 1550 m^2/g.

Hydrogen Storage

The use of hydrogen for transportation, personal electronics and other portable power applications requires an effective hydrogen storage medium. Existing technology for hydrogen storage is limited to compressed gas and liquefaction, both of which are used now in demonstration vehicles. Compressed gas, even at the highest practical pressure of 10,000 psi, is still a bulky way to store hydrogen that requires a significant fraction of the trunk space in a small car to enable a 500 km driving range. Liquid hydrogen takes up slightly more than half the volume of 10,000 psi compressed gas, but it loses 30–40% of its energy in liquefaction. Although gas and liquid storage are useful as temporary options in a provisional hydrogen economy, more compact and efficient storage media are needed for a mature hydrogen economy.

The most promising hydrogen storage routes are in solid materials that chemically bind or physically adsorb hydrogen at volume densities greater than that of liquid hydrogen. The challenge is to find a storage material that satisfies three competing requirements: high hydrogen density, reversibility of the release/charge cycle at moderate temperatures in the range of 70–100°C to be compatible with the present generation of fuel cells, and fast release/charge kinetics with minimum energy barriers to hydrogen release and charge. The first requires strong chemical bonds and close atomic packing; the second requires weak bonds that are breakable at moderate temperature; and the third requires loose atomic packing to facilitate fast diffusion of hydrogen between the bulk and the surface, as well as adequate thermal conductivity to prevent decomposition by the heat released upon hydriding. Although several materials have been found that satisfy one or more of the requirements, none has proven to satisfy all three. In addition to these basic technical criteria, viable storage media must satisfy cost, weight, lifetime, and safety requirements as well [91].

The US Department of Energy considers 6 wt % H_2 uptake in a solid for it to be suitable for automobile applications.

The recent developments in nanoscience hold promise for meeting the difficult hydrogen storage challenge. The small dimensions of nanoscale materials minimize the diffusion length and time for hydrogen atoms to travel from the interior to the surface. The large relative surface area provides a platform for dissociation of molecular hydrogen to atomic hydrogen, a prerequisite for diffusion and for chemical bonding with the host. The surface area can be tailored with a monolayer of catalyst to promote dissociation, and surface curvature can be adjusted through the size of the nanoparticles to create unbonded orbitals that promote reactivity with hydrogen.

We have measured the H_2 uptake of various EG, DG and HG samples by employing a QuantaChrome Autosorb-1 instrument at 1 atm and 77 K. We have also measured H_2 adsorption at high pressures employing a home-built apparatus.

Uptake of CO_2

The increasing atmospheric CO_2 concentration, mainly caused by fossil fuel combustion, has led to concerns about global warming. Most of the emissions of CO_2 to the atmosphere from the electricity generation and industrial sectors are currently in the form of flue gas from combustion, in which the CO_2 concentration is typically 4-14 % by volume, although CO_2 is produced at high concentrations by a few industrial processes. The high flow rates of these flue gases lead to a fast filling of the storage reservoirs. For these reasons it is preferred to produce a relatively pure stream of CO_2 for transport and storage; this process is called CO_2 capture. Adsorbents, such as zeolites, pillared clays, and hydrotalcite [92-95],

loading amines on porous materials, such as silica gel and carbon, has been found to be a promising way for achieving the effective adsorption of CO_2 [96–99] .

We have studied CO_2 uptake of graphene samples prepared by different methods. These experiments carried out by employing QuantaChrome Autosorb-1 instrument at 1 atm and 195 K.

2.3 Functionalization and solubilization of graphene

Chemistry occurs in solution. Modern synthetic chemistry and biological processes primarily take place in the solution phase. But unfortunately pristine graphene is insoluble in many liquids such as water, polymer resins, and most solvents. Thus it is difficult to evenly disperse in a liquid matrix such as epoxies and other polymers. To make graphene more easily dispersible in liquids, it is necessary to physically or chemically attach certain molecules or functional groups to graphene without significantly changing its desirable properties. This process is called functionalization. The production of robust composite materials requires strong covalent chemical bonding between the filler particles and the polymer matrix, rather than the much weaker vander Waals physical bonds which occur if graphene is not properly functionalized.

Even though much progress has not been occurred on graphene functionalization, plenty of investigations have been carried out on functionalization of single-walled carbon nanotubes (SWNTs), which are considered as rolled form of graphene. SWNTs are extremely resistant to wetting [122]. They typically exist as ropes or bundles 10-25 nm in diameter that are a few micrometers long; the SWNT ropes are entangled together in the solid state to form

a highly dense, complex network structure. These factors, coupled with the fact that these pseudo-1D graphitic cylinders do not have any surface functional groups, make them very difficult to disperse in organic media [123]

It is possible to wet the SWNT raw soot in refluxing nitric acid [124, 125] whereby the end caps of the tubes are oxidized to carboxylic acid and other weakly acidic functionalities [125, 126, 127]. These "acid-purified" SWNTs can be dispersed in various amide-type organic solvents under the influence of an ultrasonic force field [128]. However, the nitric acid treatment introduces defects on the nanotube surface [129], oxidizes the carbon nanotubes, and produces impurity states at the Fermi level of the nanotubes [130]. The defect sites that are introduced into the carbon nanotubes can be used to shorten and eventually destroy the carbon nanotubes under similar oxidizing conditions [125, 131-134]. The shortened tubes (s-SWNTs) are better solvated by amide solvents than the full-length SWNTs. The addition of a long-chain hydrocarbon at the ends of the shortened (100-300 nm) carbon nanotubes could render the functionalized SWNTs soluble in organic solvents.

Covalent functionalization described above would significantly rupture the conjugation. So to avoid this limitation it is necessary to functionalize through non-covalent modification. The formation of noncovalent aggregates with surfactants or wrapping with polymers has shown themselves to be suitable methods to functionalize SWNTs with out effecting its electronic structure. In the search for nondestructive purification methods, it has been shown that nanotubes can be transferred to the aqueous phase in the presence of surface-active benzylal-konium chloride [135-137]. It is believed that the nanotubes are in the hydrophobic interiors of the corresponding micelles, which results in stable dispersions. When the hydrophobic part of an amphiphile contains aromatic group, an especially strong

interaction results, because effective stacking interactions can then form with the graphitic sidewalls of the SWNTs. This effect was demonstrated in the aggregation with N-succinimidyl-1-pyrenebutanoate [138]. In these aggregates, the succinimidyl group could be substituted with amino groups from proteins such as ferritin or streptavidin, which caused immobilization of the biopolymers on the tubes. This effect could be interesting for the development of biosensors, because the electronic properties of the tubes can be combined with the recognition properties of the immobilized biosystems.

Polymers have also been used in the formation of supramolecular complexes of SWNTs. Thus, the suspension of purified tubes in the presence of polymers such as poly (mphenylene- co-2,5-dioctoxy-p-phenylenevinylene) (PmPV, 2), in organic solvents such as $CHCl_3$, leads to the polymer wrapping around the tubes [139-141]. The properties of these supramolecular compounds are markedly different from those of the individual components. For example, the SWNT/PmPV complex exhibits conductivity eight-times higher than that of the pure polymer, without any restriction of its luminescence properties. The wrapping of SWNTs with polymers that bear polar side-chains, such as polyvinylpyrrolidone (PVP) or polystyrenesulfonate (PSS), leads to stable solutions of the corresponding SWNT/polymer complexes in water [142]. The bundles are again broken up by complex formation in this case. The thermodynamic driving force for complex formation is the need to avoid unfavorable interactions between the apolar tube walls and the solvent water.

We felt that it would be worthwhile to functionalize graphene to utilize graphene's outstanding physical properties for preparing composite materials, as well as in other practical applications which require preparation of uniform mixtures of graphene with many different organic, inorganic, and polymeric materials.

We have carried out functionalization of graphene by employing both covalent and non-covalent means. Covalent functionalization has been carried out through the following three independent routes. (a) amidation [143] (b) organosilane and organotin coating [144, 145] (c) acidification. Amidation makes graphene soluble in organic solvents like THF, CCl_4 and DCM, where as silane or tin coating gives stable dispersions in non polar solvents such as CCl_4. Acidification of graphene produces aqueous graphene solution which one stable for several months. While non-covalent functionalization of graphene attained through (a) wrapping with PEG [146-147] (b) π-π interaction [148] and wrapping with surfactants (c). In these three routes wrapping with PEG and surfactants solubilize graphene in water where as π-π interaction with 1-pyrenebutanoic acid succinimidyl ester (PYBS) gives stable dispersion of graphene in DMF.

2.4 Decoration of graphene by metal nanoparticles

Nanomaterials [149] and especially metal nanoparticles (NPs) [150] have emerged as a new class of compounds that are particularly interesting for materials science due to their unique electronic, optical, magnetic and catalytic properties. Importantly, these features differ from those of the bulk materials [151] and depend on the size and shape of the NP [152]. Current issues in NP research focus on the synthesis of NPs of noble metals such as Au, Ag, Pt [153], on studies of their properties [154] and on their applications in several areas from chemistry [155] to physics [156] to material sciences [157] to biology and medicine [158]. Impressive results have been attained with semiconductor NPs [159]. Of particular interest are new synthetic strategies to control the shape and the dimensionality of the NPs [159-160]. Intensive research has been devoted to the study of shape-dependence of

the fascinating properties and their applications [161]. Other classes of nanoparticles are intensively studied, such as iron/platinum (FePt), cobalt/platinum (CoPt) [162], magnetic nanoparticles [163] that exhibit novel optical and electrical properties [164].

Due to their large chemically active surface and stability at high temperatures carbon nanotubes (CNTs) have been used as a support material for the dispersion and stabilization of metal and semiconductor nanoparticles (NPs).The combination of the two classes of material (CNTs and NPs) may lead to a successful integration of the properties of the two components in the new hybrid materials that present important features for catalysis and nanotechnology [165]. The CNT surface serves as a template where NPs are absorbed or, when bearing functional groups, CNTs may be linked through organic fragments [166], to metal or semiconductor NPs—either ‘‘naked’’ or stabilized by a protecting monolayer. The first report on decorating CNTs with metal clusters dates back to 1994. Ajayan and coworkers [167] described the use of single walled carbon nanotubes (SWNTs) as a support material for dispersing ruthenium NPs that act as catalysts in heterogeneous catalysis. Following this promising work, hybrid composites were developed with either metal or semiconductor NPs.

Composites of CNTs with NPs can be achieved through two main pathways. Naked NPs are grown and/or deposited directly onto the CNT surface. In an alternative approach, NPs are pre-formed and connected to CNTs using covalent linking through organic fragments. Salts of noble metals are commonly used as precursors of NPs, which are obtained by a reduction process. If this process occurs in the presence of CNTs, the NPs can be deposited onto the CNT walls mostly through van der Waals interactions, which in some cases seem to be sufficiently strong to guarantee meaningful adhesion. Various methods—

application of heat, light, and reducing agents—have been utilized to perform the metal cation reduction. Precious and noble metals (Pt, Au, Pd,Ag, Rh and Ru) as well as Ni [168,169] have been used extensively in the literature. These metals are commonly used in heterogeneous catalytic reactions and their properties can be enhanced when CNTs are employed as support materials [165].

Applications of these hybrid materials as functional components in supercapacitors, gas sensors, biosensors, hydrogen storage have been reported [168]. Chen and coworkers [170] addressed its interest to a variety of metals and described a method for the growth of Pt, Ag, Au, Pd and Cu NPs and fibers [171] onto multiwalled carbon nanotubes (MWNTs). The metal cations were initially dispersed onto the nanotube surfaces and then reduced under hydrogen stream while heating. Besides acting as a supporting material, CNTs, very likely, play the role of templates in tailoring the size of metal particles.

Metal NPs can be linked to the CNT surface via covalent or weaker bonds. Therefore, the NPs are prepared and modified with suitable functional groups for the connection to the CNT surface. These linkers can be of two types: (1) the functional groups may be used to form covalent bonds with functional groups present on the CNT surface or (2) the linker simply sticks to the CNT surface through weak intermolecular interactions such as π-π stacking, hydrophobic or electrostatic attractions. Haddon and collaborators [171] first reported that oxidation of SWNTs and subsequent reaction with aliphatic amines, to give amides; leads to soluble functionalized SWNTs. Au NPs were connected to oxidized SWNTs using amino thiols or bifunctional thiols, which act as linkers for Au colloids [173]. Hydrophobic interactions between the ligands forming the monolayer that passivate the metal surface have been used to immobilize the metal NPs onto CNTs. Acetone molecules

adsorbed on CNTs can interact hydrophobically with Au nanoclusters covered with a monolayer of octanethiols [174]. These systems may become important for exploring and creating a rich variety of molecular nanostructures for device applications. A simple procedure has been reported to produce a composite material where MWNTs and SWNTs were decorated with Au NPs protected by a monolayer of dodecanethiol molecules simply by mixing dispersions of both components in dichloromethane [175]. It is important to point out that the nanoparticle protective monolayer imparts solubility properties to the new composite. The resulting Au–CNT system shows strong electronic coupling, which suggests interesting physicochemical properties. Transient absorption spectra analysis, following photoexcitation, suggests that the Au NPs function as electron acceptors, receiving additional electron density from MWNTs or SWNTs.

Pyrene molecules, bearing a long aliphatic chain terminated by a thiol group, can connect CNTs to Au NPs via π-π staking of the pyrene moiety to the CNT surface as shown in Fig 2.4.1 [176]. Spectroscopic experiments on the composite material show that the pyrene fluorescence is completely quenched and the Raman spectrum of the CNT is enhanced. These results imply a charge transfer character between CNTs and Au NPs—mediated by the linker. Electron transfer processes between donor groups and CNTs have also been observed to occur on SWNT–Zn porphyrin hybrid materials [177, 178].

Carbon nanotubes have been widely studied to form metal hybrid composites, which can find several applications in catalysis, nanoelectronics, optics, nanobiotechnology, etc. We thought that the newly discovered graphene would be promising candidate to form metal hybrid materials because of its interesting properties such as good thermal conductivity, high surface area and stability at high tepertaures. We have decorated graphene with

platinum and silver nanoparticles through polyol reduction method using chloroplatinic acid and silver nitrate as metal salts.

2.5. Electrochemical properties of graphene and graphene as supercapacitor material

Different carbon structures have been studied as electrode materials [179]. Electrodes made from various carbon materials (partially graphitized glassy carbon, activated carbon, and graphite fibers) are widely used in important ectrochemical applications [1-181], for example, fuel cells [182]. Several workers have focused on understanding the factors that govern electron-transfer kinetics on carbon electrodes. The surface structure of the solid carbon electrodes directing electron transfer (ET) reactions in electrochemistry has been well recognized, and it is found that the creation of specific surface structures, through pretreatments such as plasma activation [183] can drive the ET faster. The surface preparation and hence, the final surface structure is often found to be critical to the performance of the electrodes, its stability and reproducibility of results. The surface modification effects are also sensitive to the reaction that is being conducted at the electrodes [184]. Thus, different reactions should be considered when addressing the role of the electrode surface on the ET mechanism.

The oxidation of potassium ferrocyanide has served as a benchmark in investigating electrochemistry at different carbon electrodes [180]. The electrochemical oxidation generates ferricyanide, and the redox couple $Fe(CN)_6^{4-}$ /$Fe(CN)_6^{3-}$ is close to an ideal system with quasi-reversibility, especially on electrodes (such as carbon) where there is minimum bonding interaction between the electrode material and the cations in solution. The

importance of this redox couple in electrochemistry also stems from its role in instrument calibration, determination of diffusion coefficients and the electrochemical area of the electrode. This reaction on most electrodes precludes any effect of surface adsorption (oxide layer formation) on the ET kinetics and hence provides a straightforward correlation of the surface structure and reaction rates.

Here we report on the electrochemical study of graphene electrodes made from three different graphene samples named CG, EG and DG. Cyclic voltammetry was used in 1M KCl containing 100 mM potassium ferrocyanide to obtain information on electron transfer rate from the faradaic reaction of the redox species.

Electrochemical supercapacitors are passive and static electrical energy storage devices for applications requiring high power density such as energy back-up systems, consumer portable devices and electrical/hybrid automobiles [185,186]. Electrochemical supercapacitors store significantly higher amount of energy than conventional capacitors but less than that of batteries, and are similar in construction to conventional capacitors except that the metal electrodes are replaced by a highly porous electrode. The dielectric film separating the two electrodes is porous and the cell contains a suitable electrolyte such as aqueous (aq.) H_2SO_4. Energy is stored in supercapacitors due to the formation of a electrical double layer at the interface of the electrode (electrical double layer capacitors, EDLCs) or due to electron transfer between the electrolyte and the electrode through fast Faradiac redox reactions (psuedocapacitors). In the latter type of supercapacitors, the amount of charge stored is proportional to the voltage. Porous carbon materials such as activated carbon [187,188] xerogels [189] carbon nanotubes [190–193] mesoporous carbon [194] and carbide-derived carbons [195] have been investigated for use as electrodes in EDLCs. In the last few

years, there has been great interest in graphene, which constitutes an entirely new class of carbon. Electrical characterization of single-layer graphene has been reported [12].

We have investigated the use of graphene as electrode material in electrochemical supercapacitors. For this purpose, we have employed graphene prepared by different methods and compared their supercapacitor behaviour with aq. H_2SO_4 as the electrolyte. Furthermore, we have explored the use of ionic liquids as electrolytes. Thus, by employing the ionic liquid, N-butyl-N-methylpyrrolidinium bis(trifluoromethanesulfonyl)imide ($PYR_{14}TFSI$), we have been able to extend the operating voltage up to 3.5 V compared to 1 V normally obtained with aq. H_2SO_4 [15]

3. EXPERIMENTAL AND RELATED ASPECTS

3.1 Synthesis and characterization of graphenes

Synthesis of EG

The first method to prepare EG involved the thermal exfoliation of graphitic oxide. Graphitic oxide (GO) was prepared according to the Staudenmaier method [82, 83]. A 250 ml reaction flask containing a magnetic stir bar was charged with sulfuric acid (10 ml) and nitric acid (5 ml) and cooled by immersion in an ice bath. The acid mixture was stirred and allowed to cool for 15 min, and graphite (0.5 g) was added under vigorous stirring to avoid agglomeration. After the graphite powder was well dispersed, potassium chlorate (5.5 g) was added slowly over 15 min to avoid sudden increases in temperature. The reaction flask was loosely capped to allow evolution of gas from the reaction mixture and stirred for 96 h at room temperature. On completion of the reaction, the mixture was poured into 0.5 L of deionized water and filtered. The GO was redispersed and washed in a 5% solution of HCl. The filtrate was tested with barium chloride for the presence of sulphate ions. The HCl wash was repeated until this test was negative. The GO was then washed repeatedly with deionized water until the pH of the filtrate was neutral. The GO slurry was dried in vacuum at 60°C.

Graphite oxide (0.2 g), prepared as described above where the oxidation step was carried out for 4 days, was placed in an alumina boat and inserted into a 1.3 m long quartz tube that was sealed at one end. The other end of the quartz tube was fixed to a two holed rubber stopper. An argon (Ar) inlet was inserted through one of the holes of the rubber stopper, and the outlet was fixed through the other hole. The sample was purged with Ar for 10 min, and then the quartz tube was quickly inserted into a tube furnace preheated to 1050ºC and held in the furnace for 10 minutes.

Synthesis of DG

DG was prepared by graphitization of nanodiamond powder (particle size 4-6 nm, Tokyo Diamond Tools, Tokyo, Japan) in an inert argon atmosphere [79]. The mean size and the size distribution of the diamond particles checked by transmission electron microscopy were in good agreement with the reported ones (catalogue specifications). In order to avoid contamination with magnetic impurities, we treated nanodiamond particles by soaking in concentrated HCl before use. 50 mg of pristine nanodiamond powder placed in a graphite tube having diameter 0.35 cm, was heat treated in furnace in a helium atmosphere, at 1650°C for 3 hrs.

Synthesis of CG

CG was prepared by the pyrolysis of camphor over nickel particles under a reducing atmosphere [80]. The reaction was carried out in a two-stage furnace and camphor was slowly sublimed (170°C) by heating from the first furnace to the second furnace held at 770°C where the micron sized nickel particles were placed.

Synthesis of SG

SG was prepared by arc discharge of SiC rod in H_2 atmosphere [81]. The procedure is as follows. A graphite rod 11 mm in diameter was drilled with a hole (7.5 mm in diameter and 10 mm in depth), into which a SiC rod, 7.5 mm in diameter and 40 mm in length, was inserted and acted as the consumed anode. A graphite rod was used as the cathode. Pure hydrogen gas (250 torr) was sealed in the chamber to act as the discharge atmosphere. During discharge, 25 A (30 V) DC electric current was supplied and the distance between the tips of the electrodes was about 1 mm.

Synthesis of HG

To prepare HG, direct current (DC) arc discharge evaporation experiments were carried out in a stainless steel chamber that was filled with hydrogen and helium or methane and helium mixtures at different proportions, with out using any catalyst. The mixing ratios of gases are summarized in Table 2.1.1. In typical experiment a graphite rod (6 mm diameter and 50 mm long) was used as an anode and as cathode, a pure graphite rod (having diameter of 13 mm and 60 mm length) was used. The purity of the graphite rod was 99.998%. The experimental set up was shown in Fig 1. The discharge current was typically 100 A, and the voltage, about 38 V. The arc was maintained by continuously translating the cathode to keep a constant distance (2 mm) between it and the anode. Typical synthesis time was 10 min. Soot materials with web like appearance were formed on the inner walls of the reaction chamber and around the cathode after the evaporation. This material was characterized by employing different techniques.

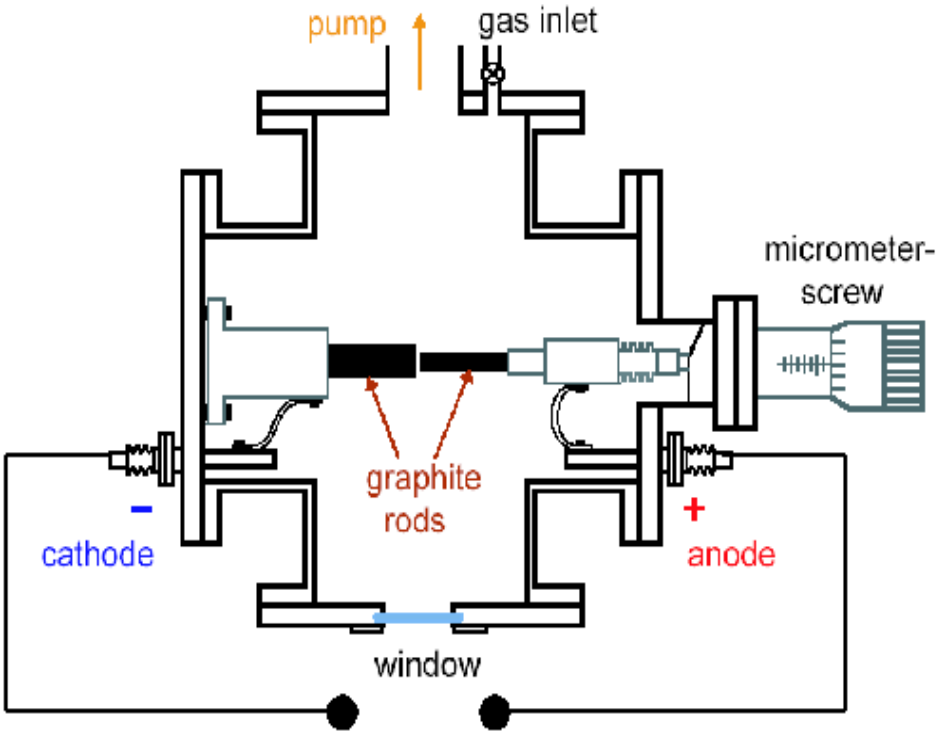

Fig 1: Schematic representation of arc-discharge apparatus

Table 2.1.1 The mixing ratio of gases taken in arc-discharge chamber

Sample name	Mixing ratio
AG 1	H_2 (70 torr) + He (500 torr)
AG 2	H_2 (100 torr) + He (600 torr)
AG 3	H_2 (200 torr) + He (500 torr)
AG 4	CH_4 (300 torr) + He (300 torr)

Characterization Techniques

X-ray diffraction (XRD): X-ray diffraction patterns of the samples were recorded in the θ-2θ Bragg-Bretano geometry with a Siemens D5005 diffractometer using Cu Kα (λ=0.151418nm) radiation.

Field emission scanning electron microscope (FESEM): FESEM images were recorded with a FEI NOVA NANOSEM 600.

UV absorption spectroscopy*:* UV absorption measurements were carried out at room temperature with a Perkin-Elmer model Lambda 900 UV/Vis/NIR spectrometer.

Raman spectroscopy*:* Raman spectra were recorded at different locations of the sample using Jobin Yvon LabRam HR spectrometer with 514 nm Ar laser.

Transmission electron microscopy (TEM): TEM images were obtained with a JEOL JEM 3010 instrument fitted with a Gatan CCD camera operating at an accelerating voltage of 300 kV. The samples were prepared by dispersing the product in CCl_4. A drop of the suspension was then put on a holey carbon coated Cu grid and allowed to evaporate.

Thermogravimetric analysis (TGA): Thermogravimetric analysis of the samples was carried out in a flowing oxygen atmosphere with a heating rate of 10°C per minute using a Mettler-Toledo-TG-850 apparatus

Atomic force microscopy (AFM): AFM measurements were performed using CP 2 atomic force microscope. The sample preparation is as follows. An 8 ml scintillation vial containing a magnetic stir bar was loaded with 1 mg of graphene and 3.0 ml of 1-methyl-2-pyrrolidinone (NMP) as the dispersion medium. The mixture was ultra sonicated for half an hour. After allowing the suspension to sit at room temperature for 1 h, an aliquot (0.5 ml) was taken and added to a 1.5 ml flex tube for centrifugation. The samples were centrifuged for nine cycles at 10,000 RPM for 5 min each. The sedimented material was discarded after each cycle, finally yielding a light-brown suspension. The suspension was spin-coated at 5,000 RPM onto freshly cleaved, highly oriented pyrolytic graphite.

3.2 Surface area of graphenes and uptake of H_2 and CO_2 by graphene

We have prepared graphene samples by four different methods, namely exfoliation of graphitic oxide (EG) [78], conversion of nanodiamond (DG) [80] arc evaporation of graphite rod (AG) [81] and mechanical exfoliation of graphitic oxide [121].

We have measured the adsorption of H_2 and N_2 by the various graphene samples at 1 atm and 77 K by employing a QuantaChrome Autosorb-1 instrument. Using the same instrument CO_2 uptake experiments were performed at 1 atm and 195 K.

We have carried out high pressure hydrogen adsorption experiments using a home-built adsorption set-up as reported by Gundiah *et al* [106]. The experiments were performed at 300 K and 100 bar using ultra high pure hydrogen (99.99%), with an impurity (e.g. moisture and nitrogen) content of less than 10 ppm. The graphene samples were accurately weighed (in excess of 100 mgs) and taken in the sample cell. The sample cell was evacuated

to 10^{-5} Torr and heated for 12 h at 125°C in order to degas the sample before the adsorption study.

3.3 Functionalization and solubilization of graphene

Amidation

To solubilize graphene samples (EG and DG) in non-polar solvents, amidation has been carried out. The procedure is as follows. In the first step, conc. nitric acid (2 ml), conc. sulfuric acid (2 ml) and water (16 ml) was added to graphene (50 mg) and subsequently heated in a microwave oven for 10 minutes under hydrothermal conditions. Further, the sample was heated at 100 °C for 12 hours. The product was washed with distilled water and centrifuged repeatedly to remove traces of acid. This yielded graphene that was functionalized with –OH and –COOH groups. The acid treated graphene was refluxed with excess $SOCl_2$ for 12 hours and the unreacted $SOCl_2$ was removed under vacuum. The product was treated with dodecylamine (5 ml) under solvothermal conditions at 100 °C.

Organosilane and organotin coating

We have used hexadecyltrimethoxysilane (HDTMS) and dibutyldimethoxytin (DBDT) [144, 145] for the covalent modification of graphene. The reaction was carried out as follows. Dry pristine graphene (1 mg), subjected to acid treatment, and was placed in a round-bottom flask, to which 15 ml of toluene was added. This mixture was sonicated for 15 minutes and the organosilane or organ tin reagent added to the mixture (1:1 molar ratio) in a nitrogen atmosphere. The reaction mixture was stirred and maintained at 55 °C over night. The product was washed with dry toluene and dried.

Acidification

In order to solubilize graphene in water using acidification, EG (5 mg) was stirred with (1:1) mixture of conc. nitric acid (2ml) and sulfuric acid (4 ml) at room temperature for 2 days. This gave some water-soluble graphene in addition to an insoluble fraction.

Wrapping with PEG

To prepare polyethylene glycol (PEG)-functionalized EG, the mixture of mild acid treated graphene (3 mg), excess of PEG (6 ml) and conc. HCl (2 ml) was heated in microwave oven for 10 minutes. The resulting product was further heated at 100°C for 12 hours.

Functionalization through π-π interaction

Non-covalent fictionalization by the interaction of 1-pyrenebutanoic acid succinimidyl ester (PYBS) [148] with graphene was carried out in dimethylformamide (DMF) at different temperatures in the 150-300 °C range. Typically, 5 ml of 12 mM PYBS solution in dry DMF was added to 1 mg graphene and the mixture was ultra-sonicated for 15 minutes at room temperature. To obtain stable dispersions for several days, the mixture of graphene and PYBS was heated in sealed tube at 150 °C, 180 °C, 200 °C and 300 °C for 3 hours.

Wrapping with surfactants

To get dispersions of graphene in water, we prepared surfactant solutions having different concentrations and checked for dispersibility. The procedure is as follows. 1.5 mM, 3 mM, 6 mM and 9 mM solutions of CTAB (Cetyl trimethyl ammonium bromide) were prepared in distilled water and to 5 ml of each of these solutions 1 mg graphene was added. These solutions were ultra-sonicated for 15 minutes and kept for observation. Similar

to CTAB, 1 mM, 2 mM and 4 mM, solutions of IGPAL (polyoxyehylene-40-nonylphenyl) and 10 mM, 20 mM, 40 mM, solutions of SDS (sodium hexadecyl sulfate) were prepared. To 5 ml of each of these solutions 1 mg graphene was added and ultra-sonicated for 15 minutes.

3.4 Decoration of graphene by metal nanoparticles

To decorate platinum nanoparticles [196,197] on graphene, graphene was treated with chloroplatinic acid in the presence of polyol reducing agent. The procedure is as follows. Graphene (1 mg), prepared by exfoliation of graphite oxide, was placed in hydrothermal bomb, to which 1 ml of 10 mM chloroplatinic acid ($HPtCl_4$) and 1 ml of ethylene glycol were added. This mixture was heated in a domestic microwave oven for 15 minutes. The resulting suspension was centrifuged and sedimented material was thoroughly washed with distilled water to remove any loosely adsorbed naoparticles and ethylene glycol. The same experiment was repeated with 5 mM chloroplatinic acid, remaining other conditions as same.

To decorate silver nanoparticles on graphene, the mixture of graphene (1mg), 1 ml of 5mM $AgNO_3$ solution, and 1 ml of ethylene glycol was heated in microwave oven for 15 minutes. The resulting samples were characterized by Transmission electron microscopy.

3.5 Electrochemical properties of graphene and graphene as supercapacitor material

Electrochemical measurements were performed using a PG262A potentiostat/ galvanostat, (Technoscience Ltd, Bangalore, India). Voltammetric properties of graphenes were investigated using a three electrode electrochemical cell containing a graphene paste electrode, platinum foil as the counter electrode and calomel as the reference electrode using

1M KCl solution containing 100 mM potassium ferrocyanide. All graphene paste electrodes were prepared using mineral oil as a binder (25 wt %) [198].

Graphene-based supercapacitor cells were fabricated following Conway [185]. The measurements were carried out with a two-electrode configuration, the mass of each electrode being 5 mg and the ionic liquid, N-butyl-N-methylpyrrolidinium bis (trifluoromethanesulfonyl)imide ($PYR_{14}TFSI$) was dried at 80°C under vacuum for a day prior to the experiment. The fabrication and characterization of cell was done at 60°C in a mBraun glove box keeping the oxygen and water levels at less that 0.1 ppm. We have performed cyclic voltammetry to characterize the two-electrode supercapacitor cells with the different graphenes. The specific capacitance is given by the following equation: $C_{CV} = 2(i_+ - i_-)/(m \times \text{scan rate})$, where i_+ and i_- are maximum current in the positive scan and negative scan respectively and m is the mass of electrode. The energy density is given as $E= CV^2$, where C is the capacitance taking into account both the electrode masses and V is the operational voltage.

4. RESULTS AND DISCUSSION

4.1 Synthesis and characterization of graphenes

We prepared graphene by employing different independent routes including arc evaporation of graphite rod which one newly developed by us. To know the quality of these samples, we have used different characterization techniques such as TEM, XRD, AFM, Raman spectroscopy and TGA. Results concluded from above characterizations are summarized below.

TEM analysis

In Figs 1, 2, 3 and 4 we show typical TEM images of the different graphene samples, CG, EG, DG and HG respectively.

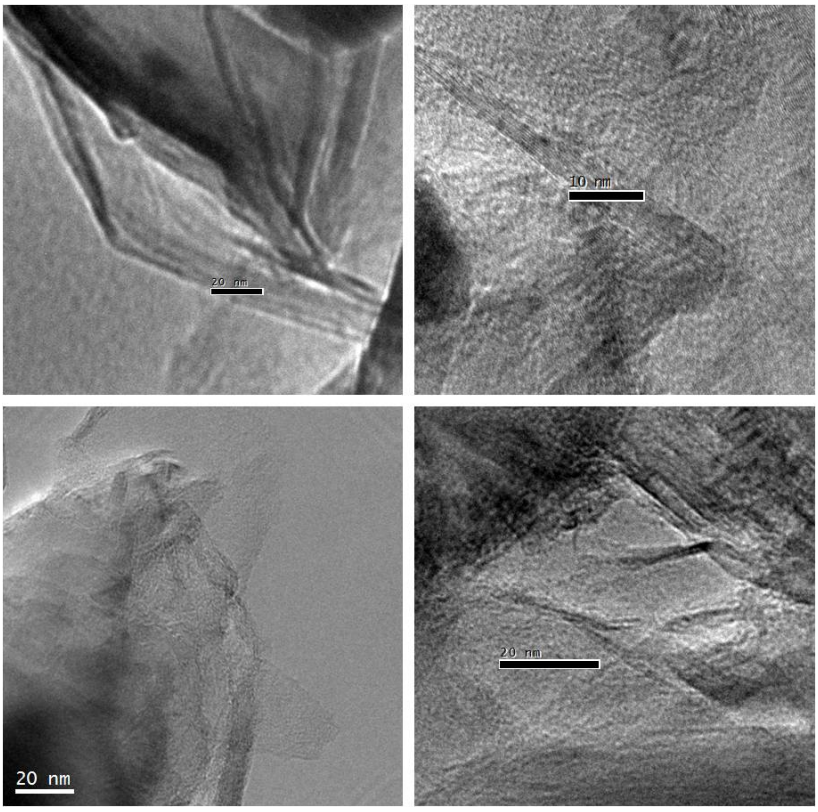

Fig 1: TEM images of graphene obtained from reductive pyrolysis of camphor (CG)

Large crystalline sheets are observed in the case of CG, while disordered graphene sheets are seen in EG as can be seen from in Figs 1 and 2.

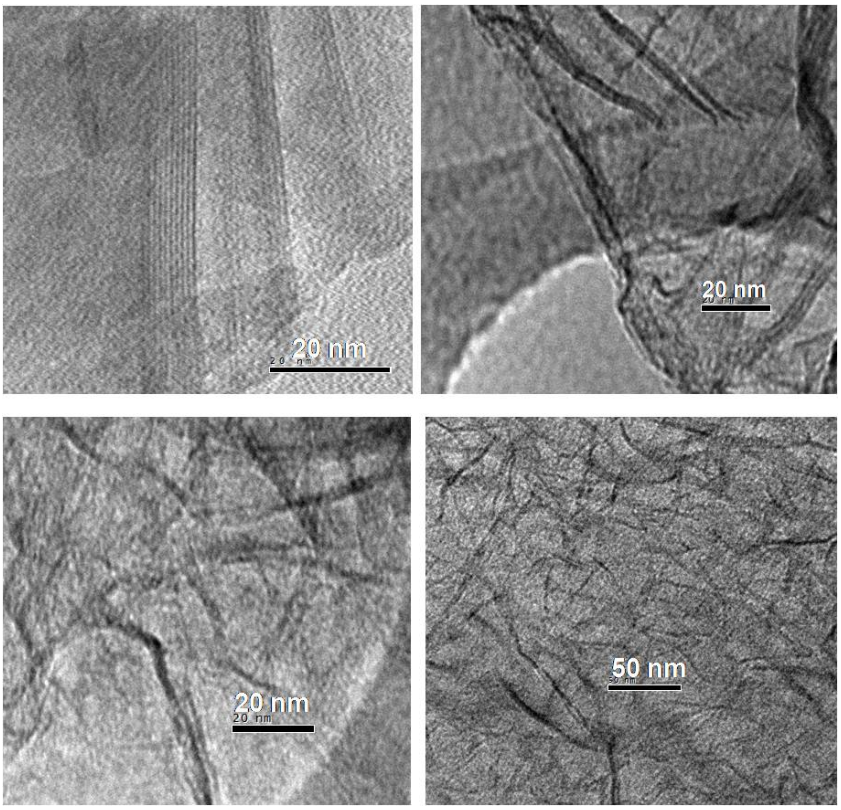

Fig 2: TEM images of graphene obtained from thermal exfoliation of graphitic oxide (EG)

Small particles with diameters in the 3-20 nm range along with onion-like nanoparticles are found in the TEM image of DG [Fig 3]. TEM images of HG samples, prepared at different conditions show few layer graphene including onion like particles. HG 3 shows completely graphene sheets with no onions, while other samples (HG 2, HG3, and HG 4) show both sheets and onions. TEM images of HG samples showed in Fig 4.

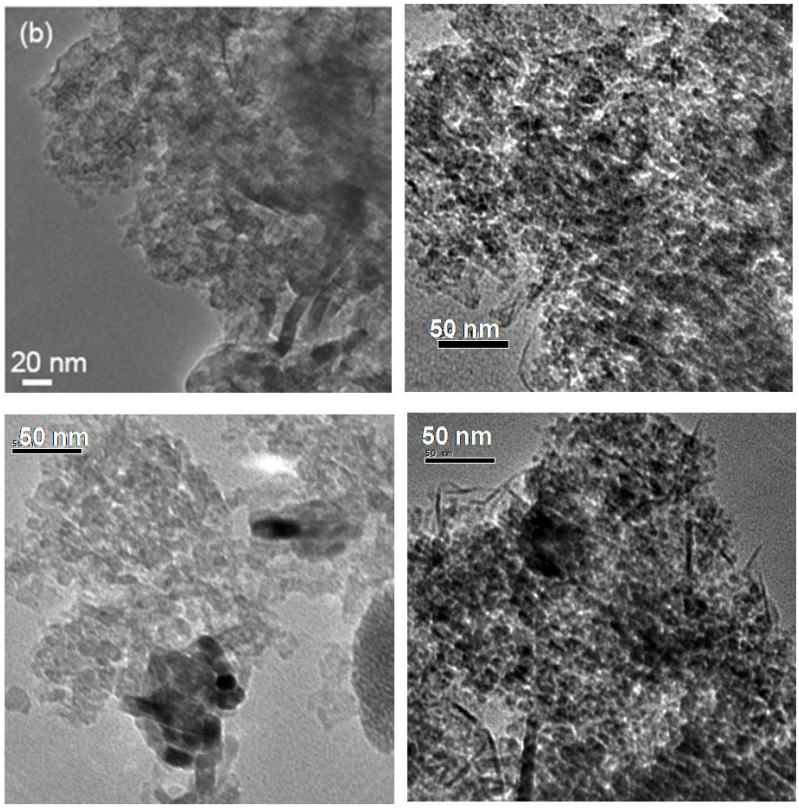

Fig 3: TEM images of graphene obtained from thermal conversion of nanodiamond (DG)

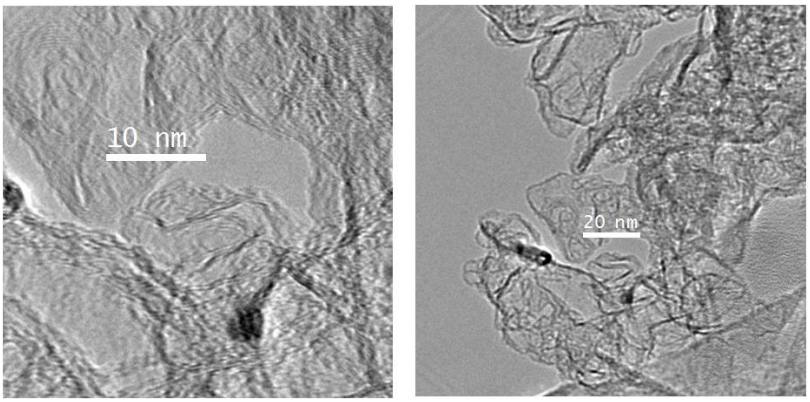

HG 1

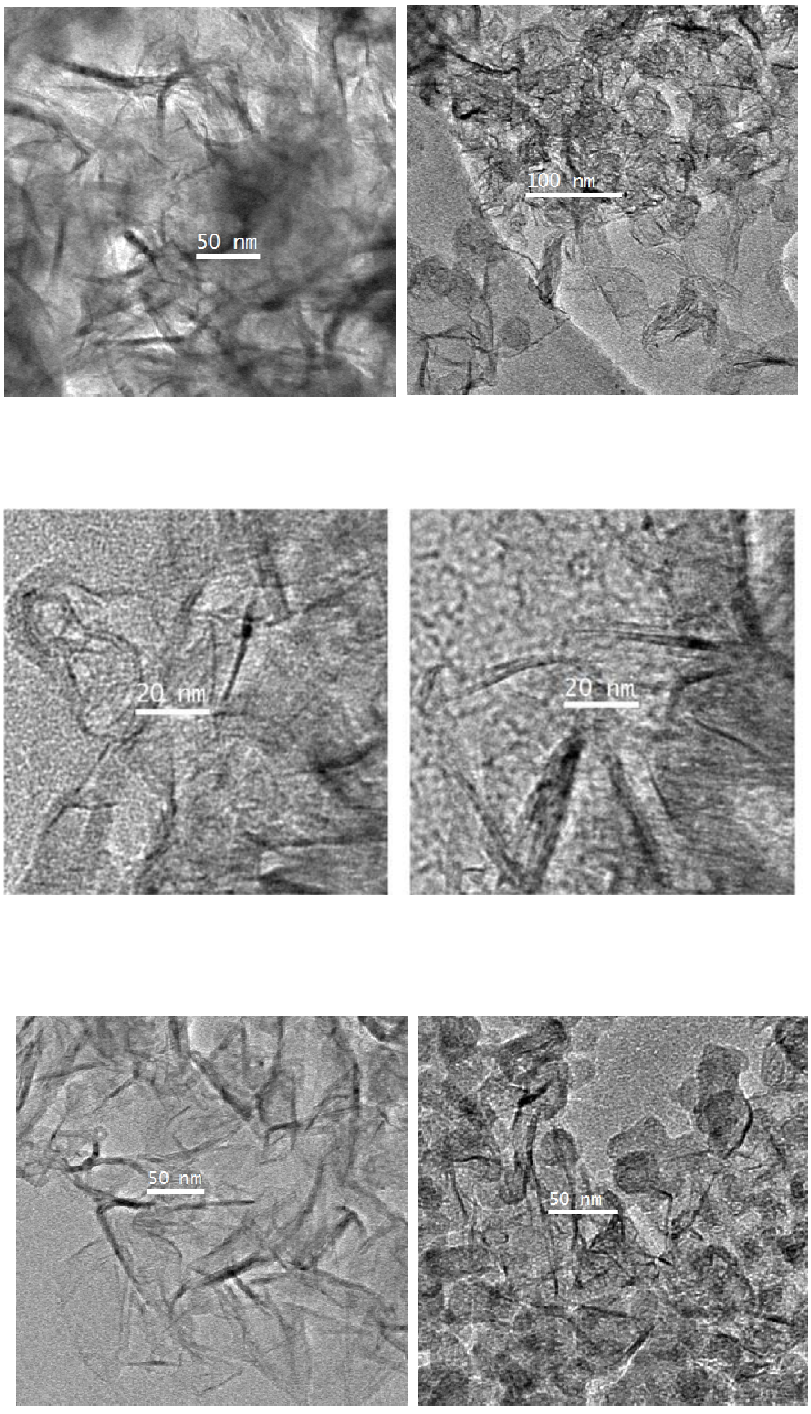

Fig 4: TEM images of graphene obtained by arc-discharge of graphite rod (HG)

X- ray diffraction

The XRD patterns of CG, EG and DG are shown in Fig 5. The sharp graphitic reflection in powder x-ray diffraction pattern of CG shows that it comprises of large number of layers. EG shows broad peaks in the XRD pattern. The XRD pattern of DG reveals that it contains reflections corresponding to both small and large graphitic particles. By fitting the (002) reflection, one can obtain the average number of layers using the Scherrer formula. In Table 1 we showed number of layers obtained from fitting of (002) reflection for different graphene samples. Lorentzian fit for the (002) reflection from various EG and DG samples prepared by us shown in Figs 6 and 7 respectively. CG primarily consists of number layers around 33 and 51. The number of layers in EG is found to be 3 and 16 while in DG it is 6 and 87.

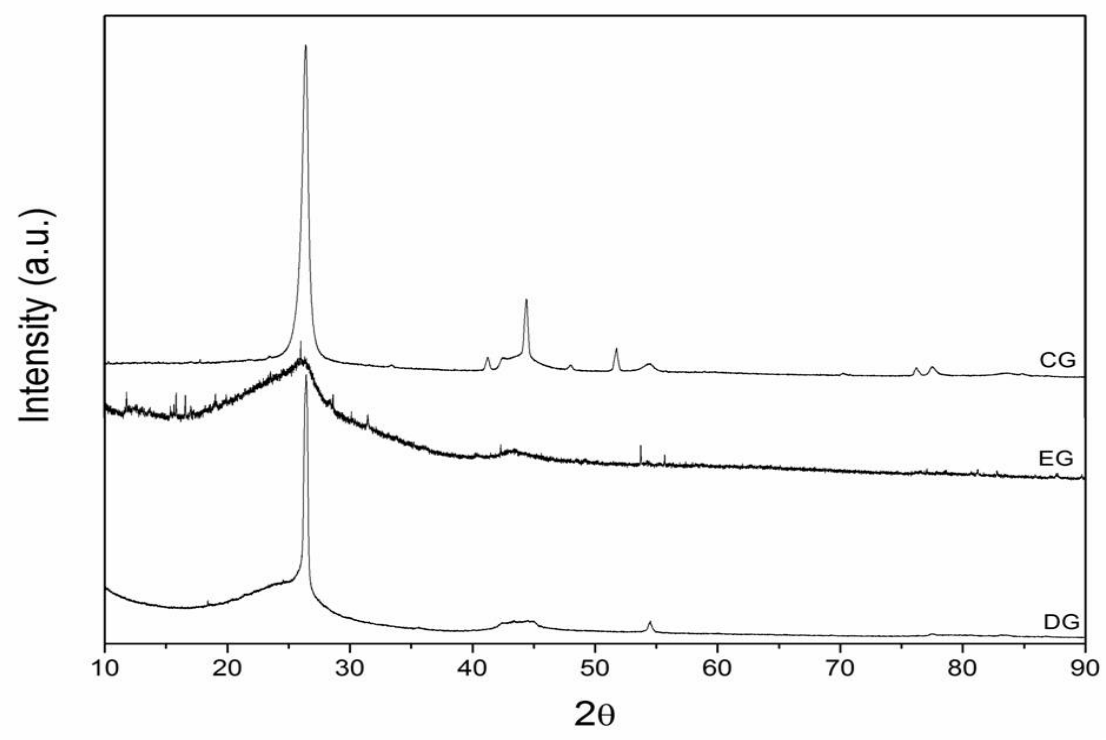

Fig 5: X-ray diffraction patterns of the CG, EG and DG

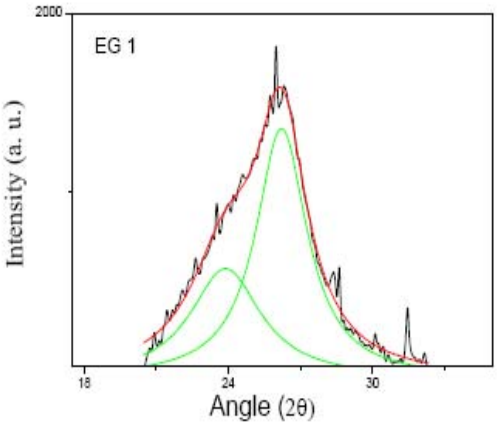

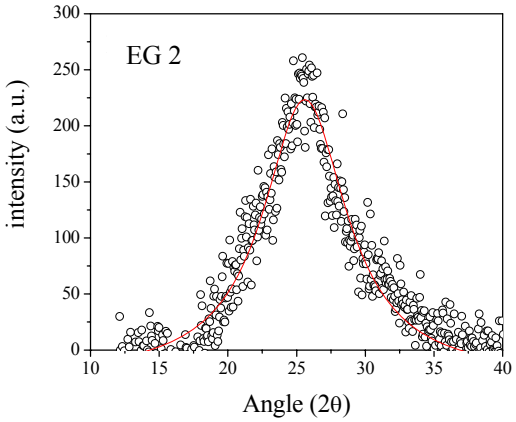

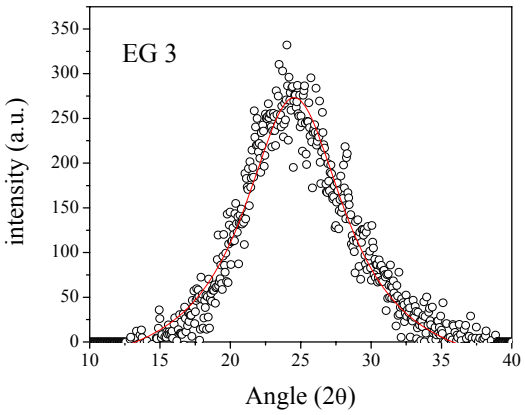

Fig 6: Lorentzian fit for the (002) reflection from EG

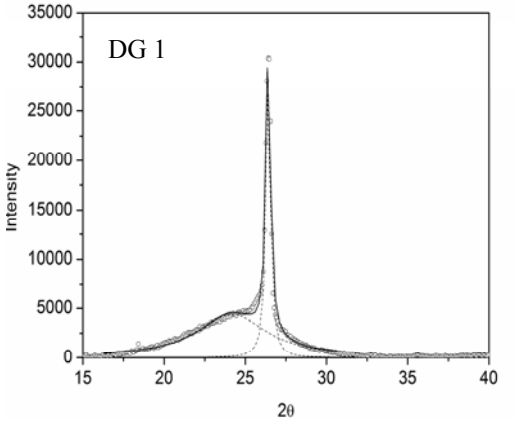

Angle (2θ)

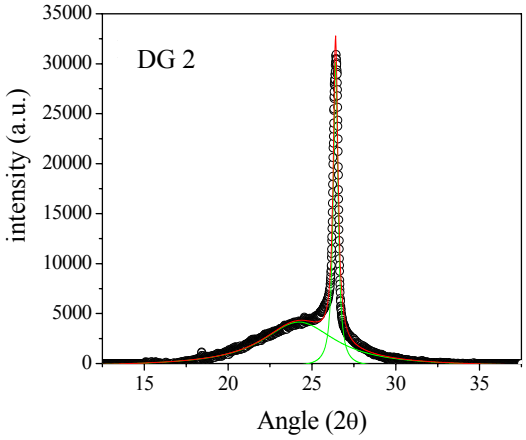

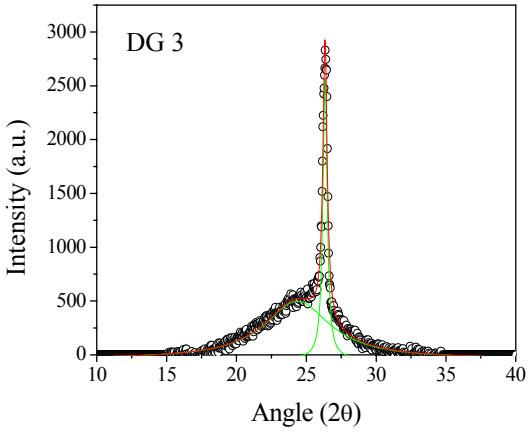

Fig 7: Lorentzian fit for the (002) reflection from DG

Table 1: Number of layers obtained from (002) reflection for graphene samples

Sample name	(002) narrow position (deg)	(002) broad position (deg)	Number of layers
CG	26.1	26.4	33,57
EG 1	23.7	26.1	3,16
EG 2	24.5		6
EG 3	24.6		4
DG 1	24.4	26.3	6, 87
DG 2	24.1	26.1	10, 66
DG 3	24.2	26.3	9, 51

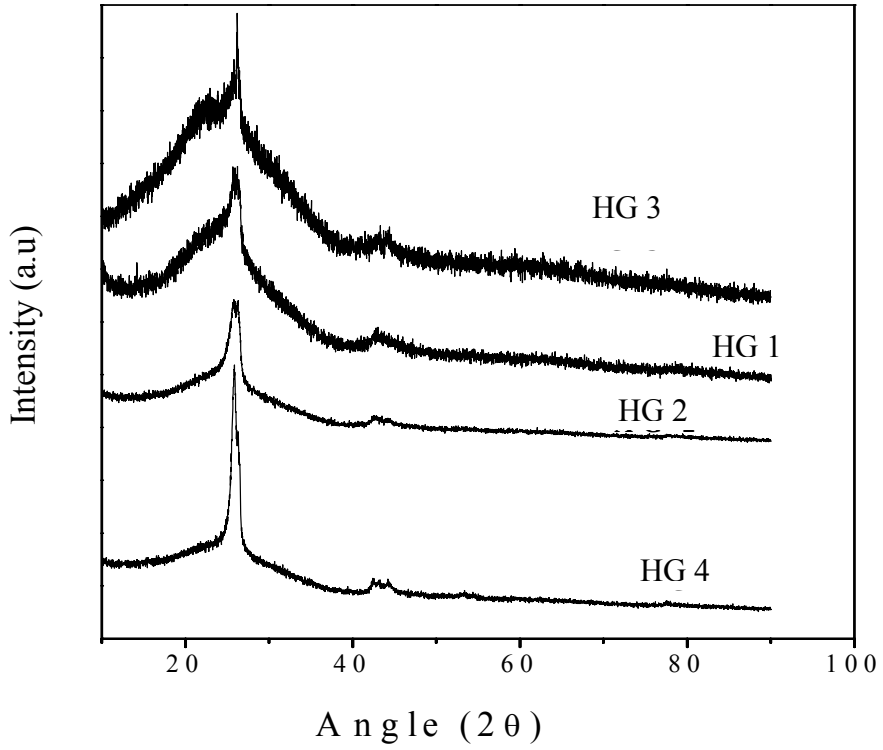

Figure 8: X-ray diffractograms of HG samples

Figure 8 shows the X-ray diffractograms of graphene samples prepared by arc-discharge method. The samples HG 1, HG 3 show very broad peaks at the graphite (002), (100) and (101) positions, where graphite (100) and (101) peaks merge into a single broad peak around 45°. Samples HG 2, HG 4 show the existence of a very broad peak and a relatively sharp peak at the graphite (002) position around 25°, in addition to a broad peak at 42°–44° corresponding to the graphite peaks (100) and (101). From (002) fitting the number of layers, in these samples found to be around 3 and 18. Results are summarized in Table 2. Fitted curves of (002) reflection from different HG samples shown in Fig 9.

Table 2: Number of layers in different HG samples Obtained from (002) reflection

Sample name	(002) narrow position (deg)	(002) broad position (deg)	Number of layers
HG 1	23.12	26.1	3, 13
HG 2	23.2	26	3,14
HG 3	22.52	26.5	2, 12
HG 4	22.5	25.6	3,18

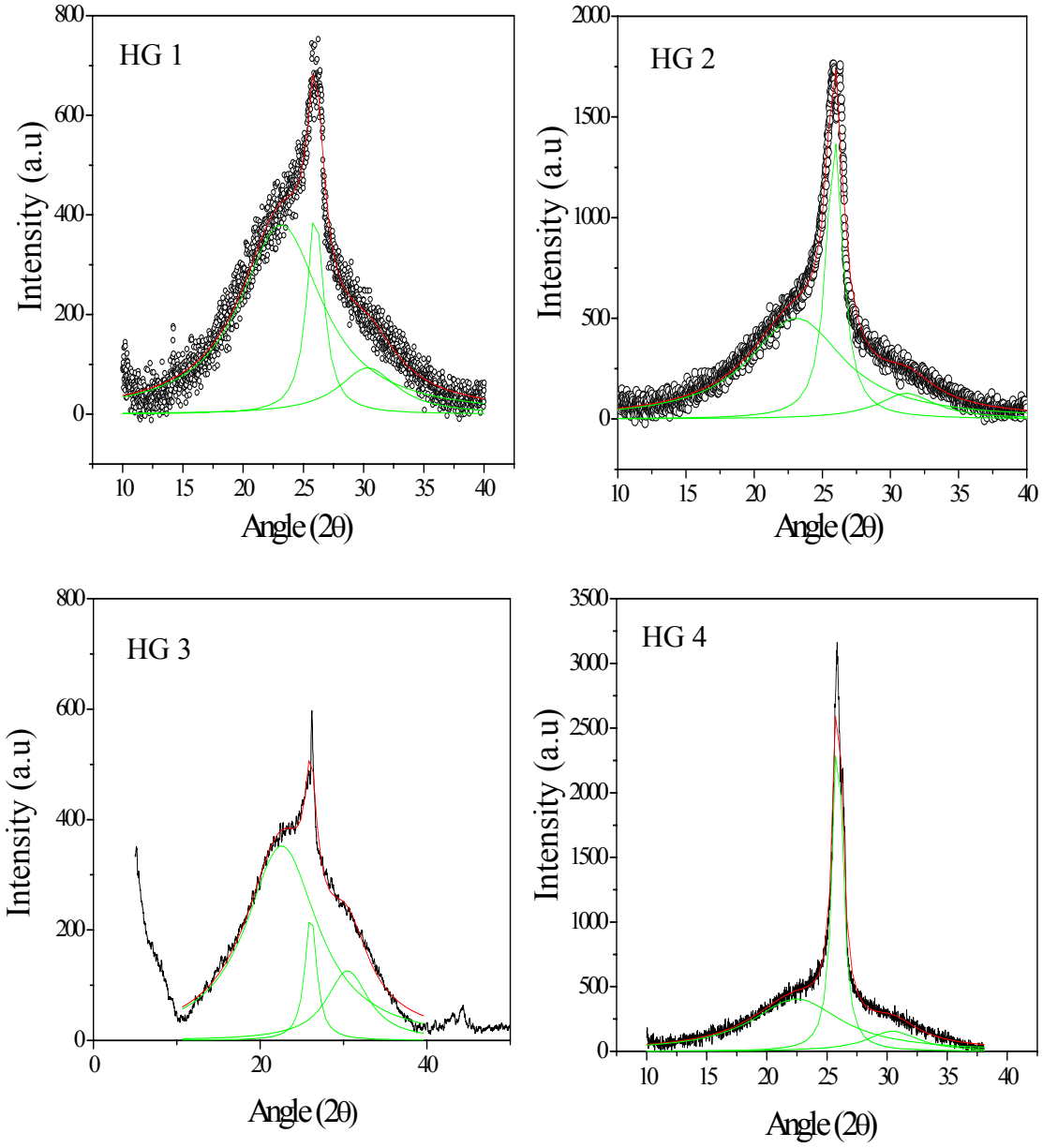

Fig 9: Lorentzian fit for the (002) reflection from different HG samples

AFM analysis

We have carried out extensive AFM studies at different locations of CG, EG and DG. We show typical AFM images of these graphenes in Figs 10, 11 and 12. AFM cross-section height profile analysis indicates that the CG sample consists of greater than 20 layers while EG and DG possess of 3 to 6 graphene layers

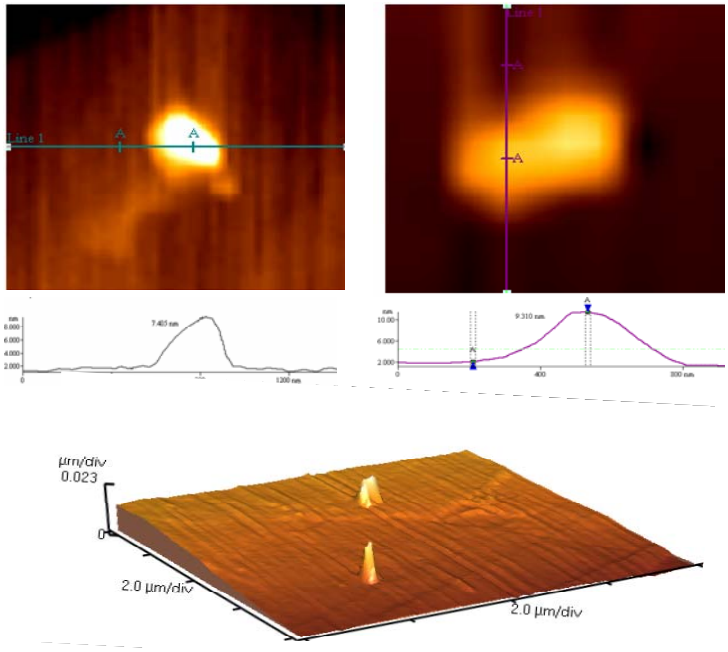

Fig 10: AFM image of CG

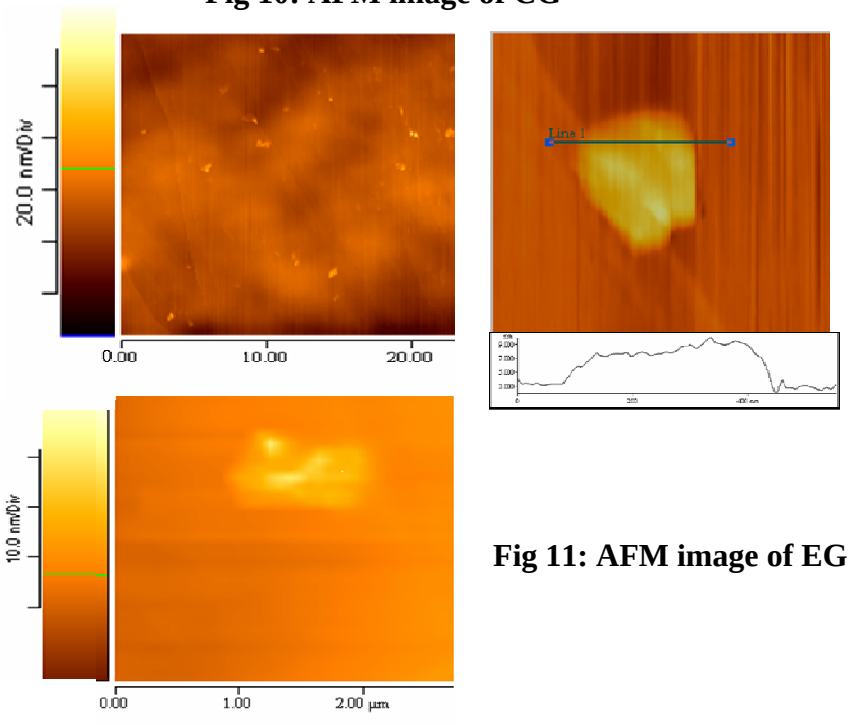

Fig 11: AFM image of EG

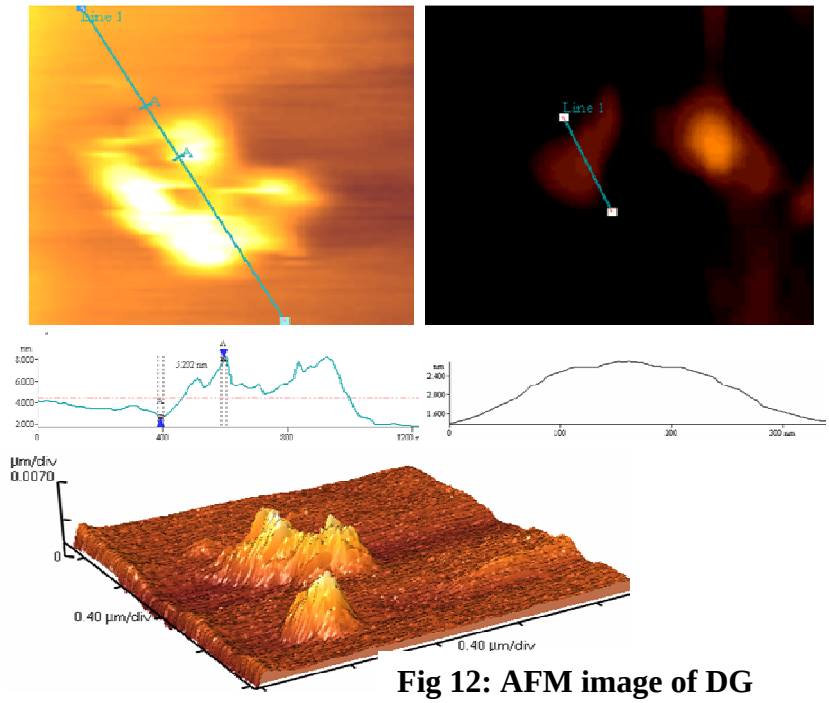

Fig 12: AFM image of DG

Raman spectroscopy

Raman spectroscopy is most useful tool to characterize graphene [199-201]. A single layer graphene shows the well-known G-band around 1560 cm^{-1} and a band around 1620 cm^{-1} (D′). The D′ band is defect induced and not found in graphite. The D-band around 1350 cm^{-1} arising from disorder is very weak in a single layer graphene and increases in intensity with the number of layers. The 2D band (~2600 cm^{-1}) which appears in single layer graphene is also sensitive to the number of layers and shows greater structure (often a doublet) with increase in the number of layers. In Fig 13, we show typical Raman spectra for

the graphene samples (EG, DG and CG) taken at two different locations and in Table 3 Raman band positions are summarized.

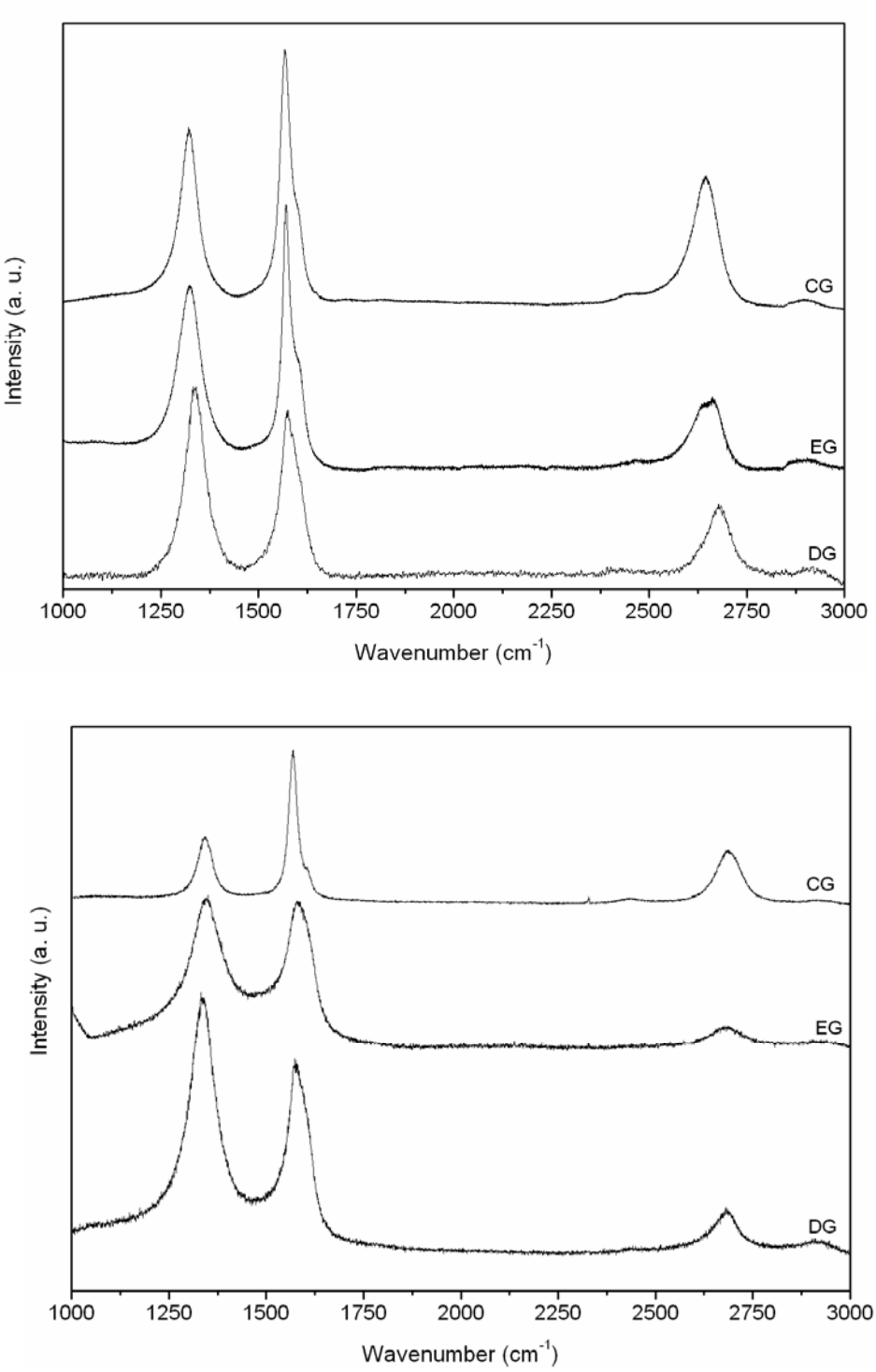

Fig 13: Raman spectra of graphene samples taken at two different locations

Table 3: Raman band positions of CG, EG and DG samples

Sample	D	G	D’	2D	D + G
CG	a 1321 b 1342	1567 1569	1604 1605	2647 2687	2919 2920
EG	a 1324 b 1352	1569 1574	1605 1608	2652 2705	2908 2926
DG	a 1332 b 1330	1576 1576	1606 1608	2678 2682	2909 2905

Raman spectra of HG samples taken at different locations have shown in Fig 14 and band positions given in Table 4.

Table 4: Raman band positions of HG samples

Sample	D	G	D’	2D	D + G
HG 1	a 1329 b 1328	1560 1560	1597 1597	2665 2660	2920 2923
HG 2	a 1324 b 1352	1566 1567	1590 1589	2665 2660	2921 2923
HG 3	a 1337 b 1339	1573 1573	1603 1602	2690 2691	2926 2929
HG 4	a 1335 b 1336	1566 1565	1597 1597	2684 2684	2928 2929

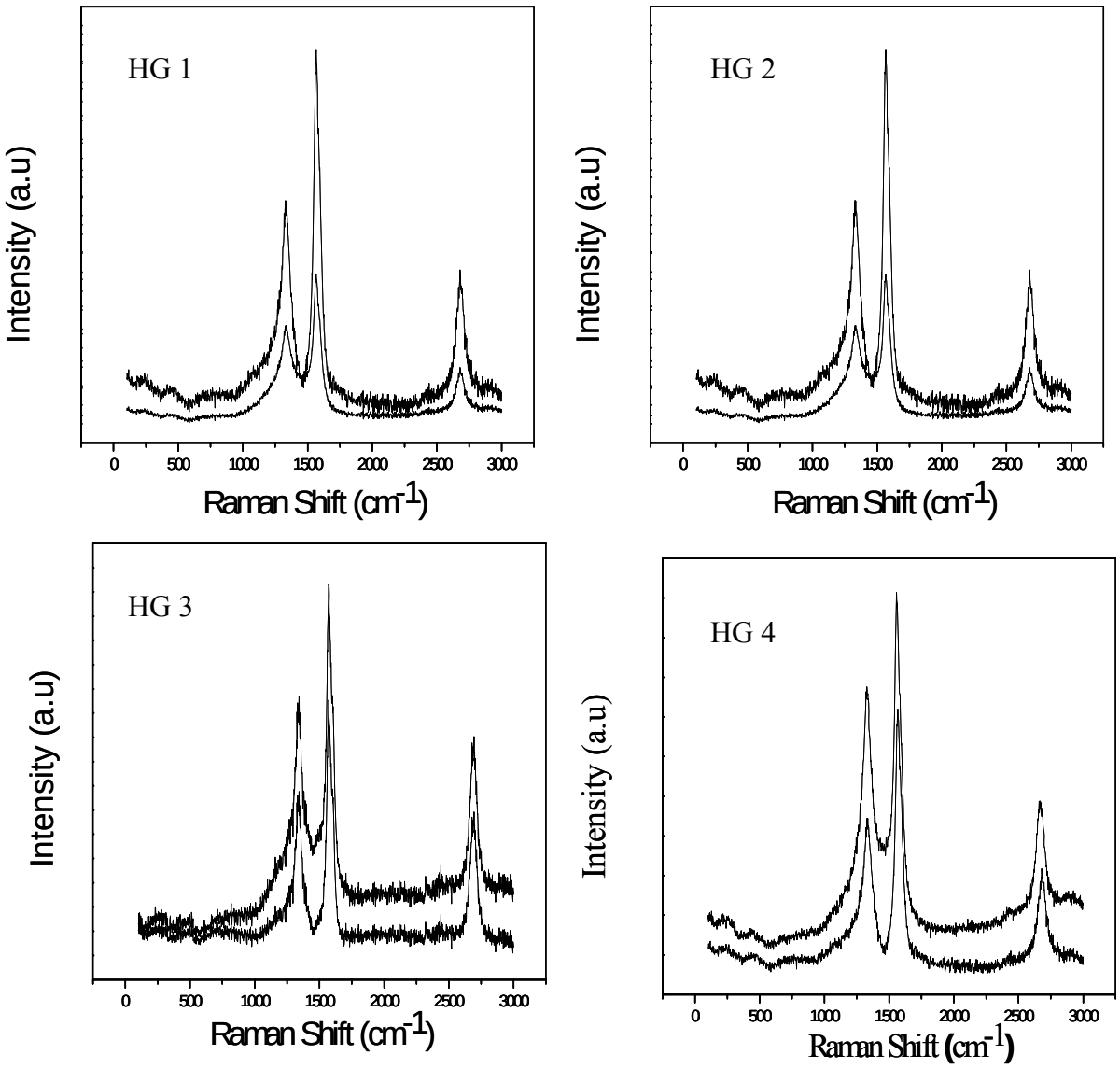

Fig 14: Raman spectra of HG samples taken at two different locations

We have calculated the in-plane crystallite size, L_a from the spectra taken at various locations of the graphene samples by employing the ratio, $L= 4.4 (I_D/I_G)$ [2, 3] [Table 5]. In-plane crystallite size, L_a of graphene samples follows the following order CG> HG> EG> DG.

Sample	**I_G/I_D**	**Crystallite size (nm)**
CG	2.4, 2.8	10, 12
EG	1.0, 1.4	4, 6
DG	0.8, 1.1	4, 5
HG 1	1.6, 1.5	7, 7
HG 2	1.8, 1.65	6, 7
HG 3	1.8, 2	6, 8
HG 4	1.98,1.97	8, 9

Table 5: In-plane crystallite size, L_a of graphene samples

TGA

Fig 15 we show the thermogravimetric analysis curves of CG, EG and DG. CG undergoes sharp oxidation around 730°C while DG gets oxidized at 700°C. EG exhibits the lowest oxidation temperature of ~520°C, exhibiting a sharp mass loss at this temperature followed by gradual mass loss. The low oxidation temperature of EG is ascribed due to the presence of functional groups while the other graphenes consist of pure carbon and more crystalline in nature as observed in the x-ray diffraction patterns.

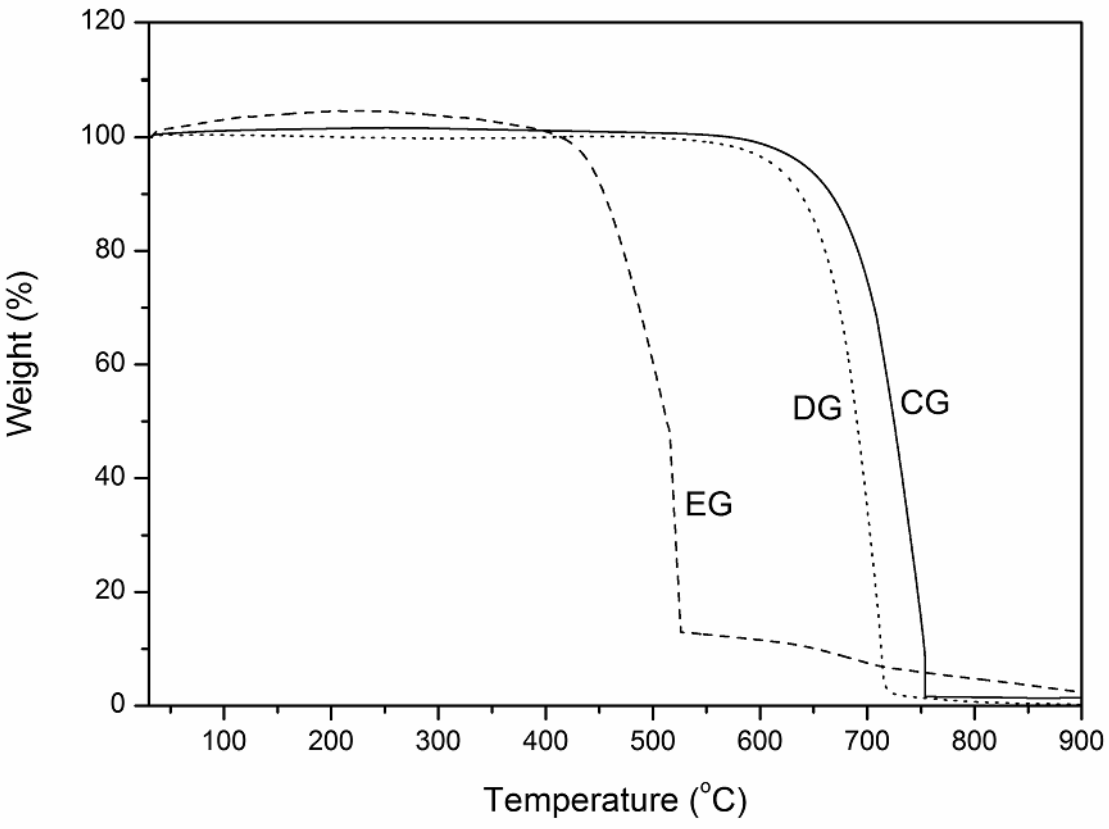

Fig 15: Thermogravimetric analysis of the different graphenes

4.2 Surface areas and uptake of H_2 and CO_2 by graphene samples

Surface areas

We have prepared several graphene samples (EG 1, EG 2, EG 3, EG 4, and EG 5) by the exfoliation of graphitic oxide by following the literature procedure [78]. These samples possess Brunauer-Emmett-Teller (BET) surface areas in the range of 639 -1550 m^2/g. We have also treated the graphene sample, EG 3, with hydrogen at 1000°C for 4 hours to obtain EG 3-H_2, and with a 1:1 mixture of concentrated nitric and sulfuric acids at 100°C under hydrothermal conditions to obtain EG 3-COOH. One sample of graphene, EG 5, was prepared by mechanical exfoliation of graphitic oxide in water, followed by the treatment with hydrazine [2]. The surface area of EG 3-COOH was the lowest (34 m^2/g) while that of EG 3-H_2 was 1258 m^2/g. The surface area values of different graphene samples EG 1, EG 2, EG 3, EG 4, EG 5, including acid treated (EG 3-COOH) and hydrogen treated (EG 3-H_2), are summarized in Table 6. Nitrogen adsorption isotherms of EG 1, EG 2, EG 3, EG 4, EG3-COOH and EG3-H_2 have shown in Fig 16.

Sample	Surface area (m^2/g)
EG 1	1550
EG 2	871
EG 3	639
EG 4	925
EG 5	700
EG 3 H_2treated	1258
EG 3 COOH	34

Table 6: BET Surface area values of EG samples

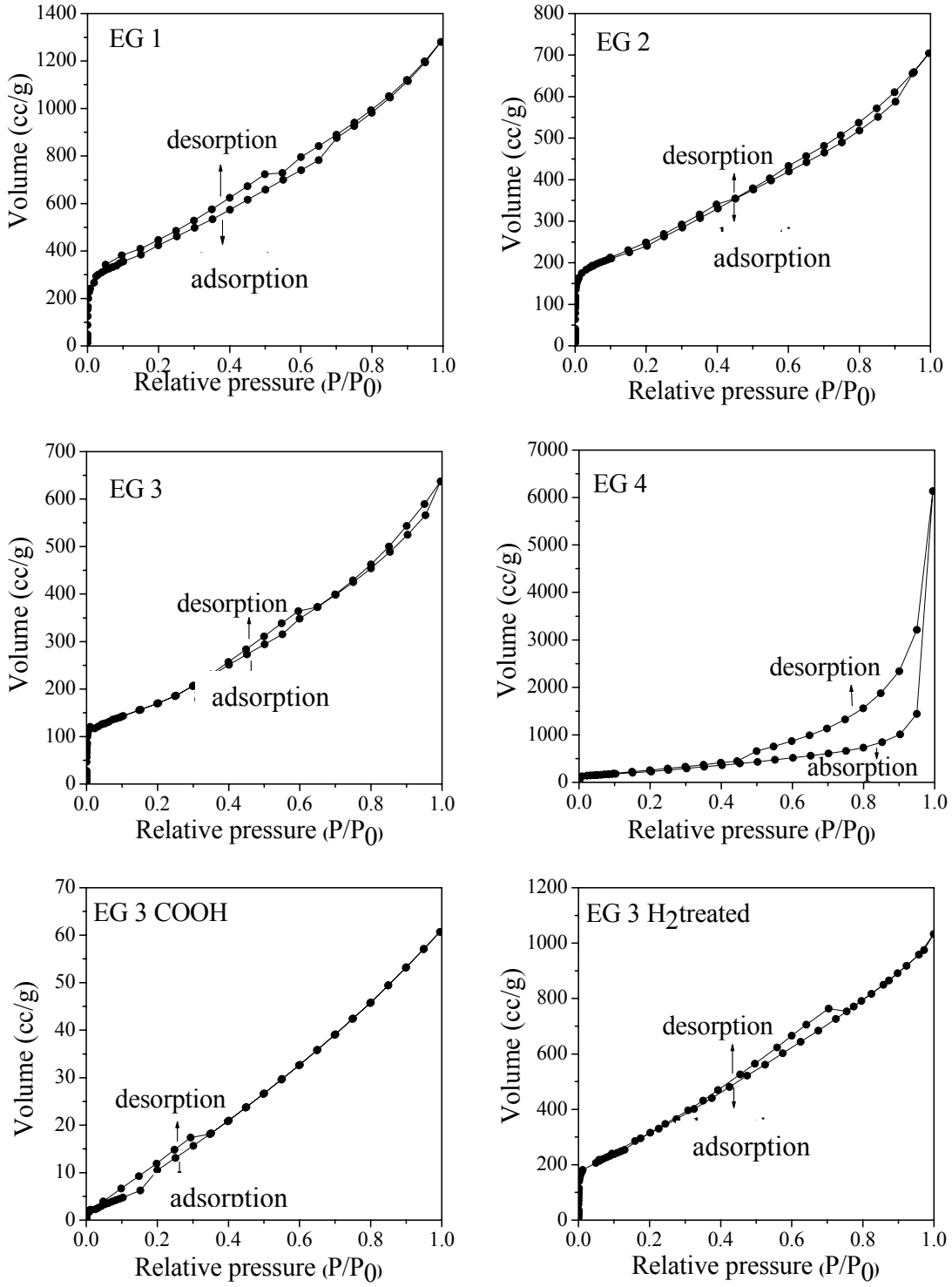

Fig 16: Nitrogen adsorption and desorption curves of EG samples

We have also prepared graphene samples (DG 1, DG 2, DG 3, DG 4 DG 5 and DG 6) by the transformation of nanodiamond [80]. These samples have surface areas in the range 280-1013 m^2/g and contain 8-10 graphene layers. The surface areas of the graphene samples depend on the number of layers, the surface area of single-layer graphene being ~2600 m^2/g [6]. In Table 7, we show the surface area values of all DG samples. The BET surface area plots of DG 1, DG 2, DG3 and DG 4 are shown in Fig 17.

Table 7: BET Surface area values of DG samples

Sample name	Surface area (m^2/g) (1 atm, 77 K)
DG 1	908
DG 2	785
DG 3	520
DG 4	839
DG 5	1013
DG 6	280

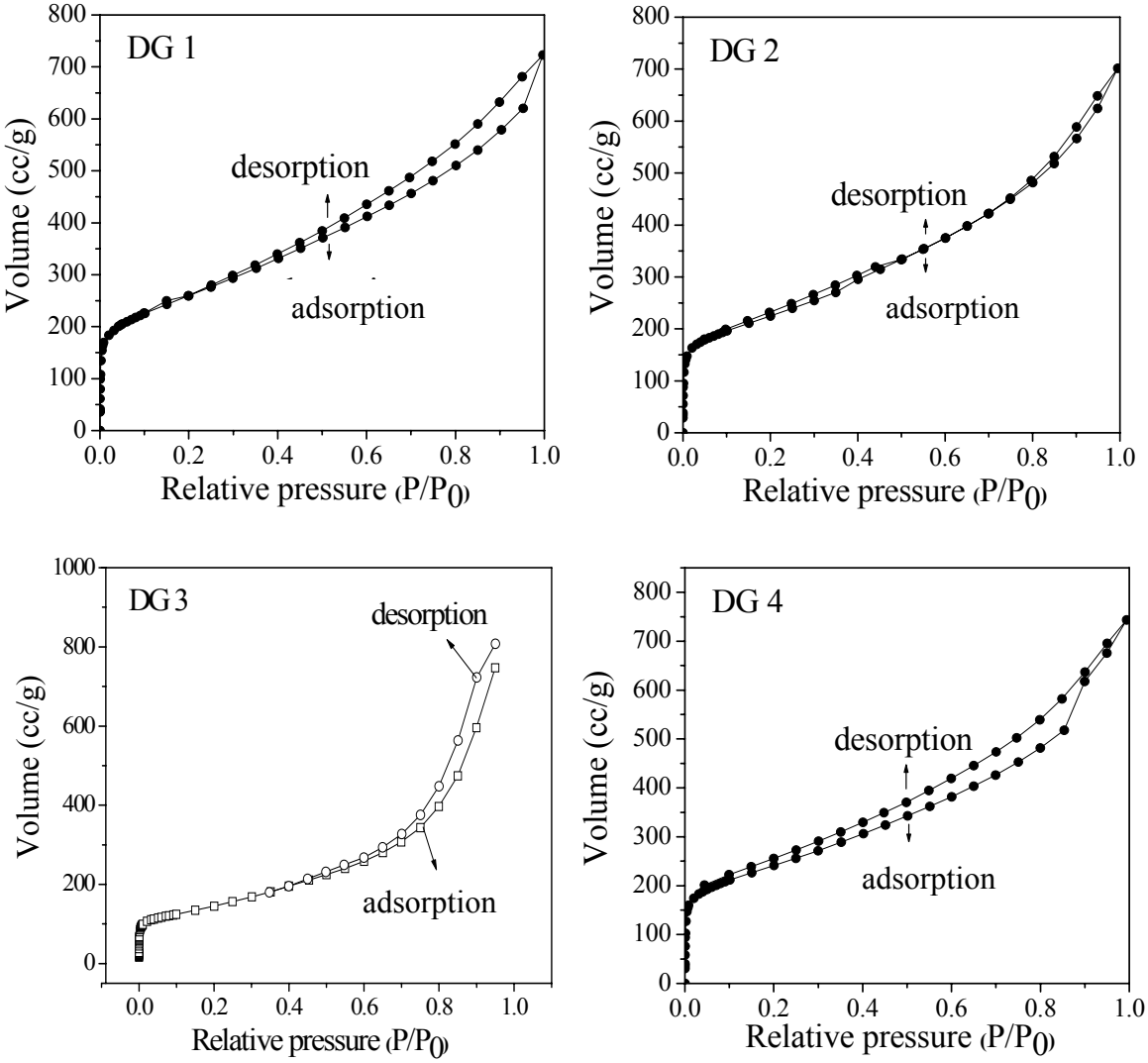

Fig 17: Nitrogen adsorption and desorption curves of DG samples

We prepared graphene by employing arc-discharge using graphite rod as consumed anode [81]. Arc discharge chamber filled with a mixture of hydrogen and helium or methane and helium mixtures at different proportions. These samples show surface area in

the range of 270-680 m^2/g. Among these samples HG 1 shows highest value around 680 m^2/g, next HG 3 comes showing around 480 m^2/g.

HG 2, HG 4 show quite low values around 270, 281 respectively. We have shown BET surface area plots in Fig 18

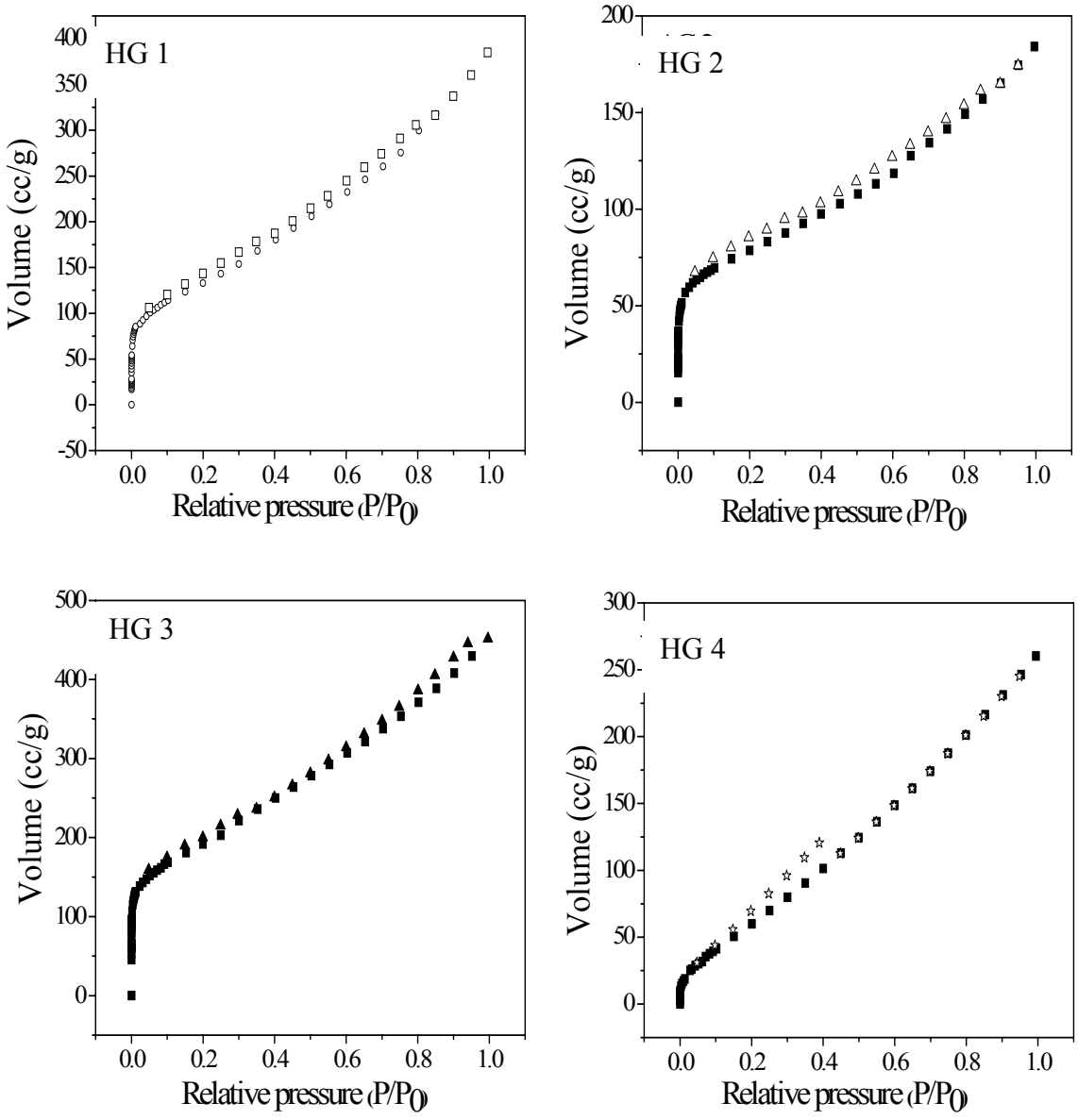

Fig 18: Nitrogen adsorption and desorption curves of HG samples

Hydrogen uptake

We have measured the adsorption of H_2 by the various graphene samples at 1 atm and 77 K by employing a Quanta Chrome Autosorb-1 instrument. In Table 8, we have given H_2 uptake values of EG samples. In Fig. 19, we show typical adsorption and desorption curves of EG 1, EG 2, EG 3 and EG 4 samples. In EG samples, EG 1 showed highest H_2 uptake around 1.7 wt %.

Table 8: H_2 uptake values of EG samples

Sample name	H_2 adsorption (wt %) (1 atm, 77 K)	H_2 adsorption (wt %) (high pressure) (100 atm, 298 K)
EG 1	1.7	
EG 2	1.131	2.07
EG 3	0.62	1.9
EG 4	1.38	3.1
EG 5	0.86	
EG 3 H_2 treated	1.07	2.13
EG 3 COOH	0.05	

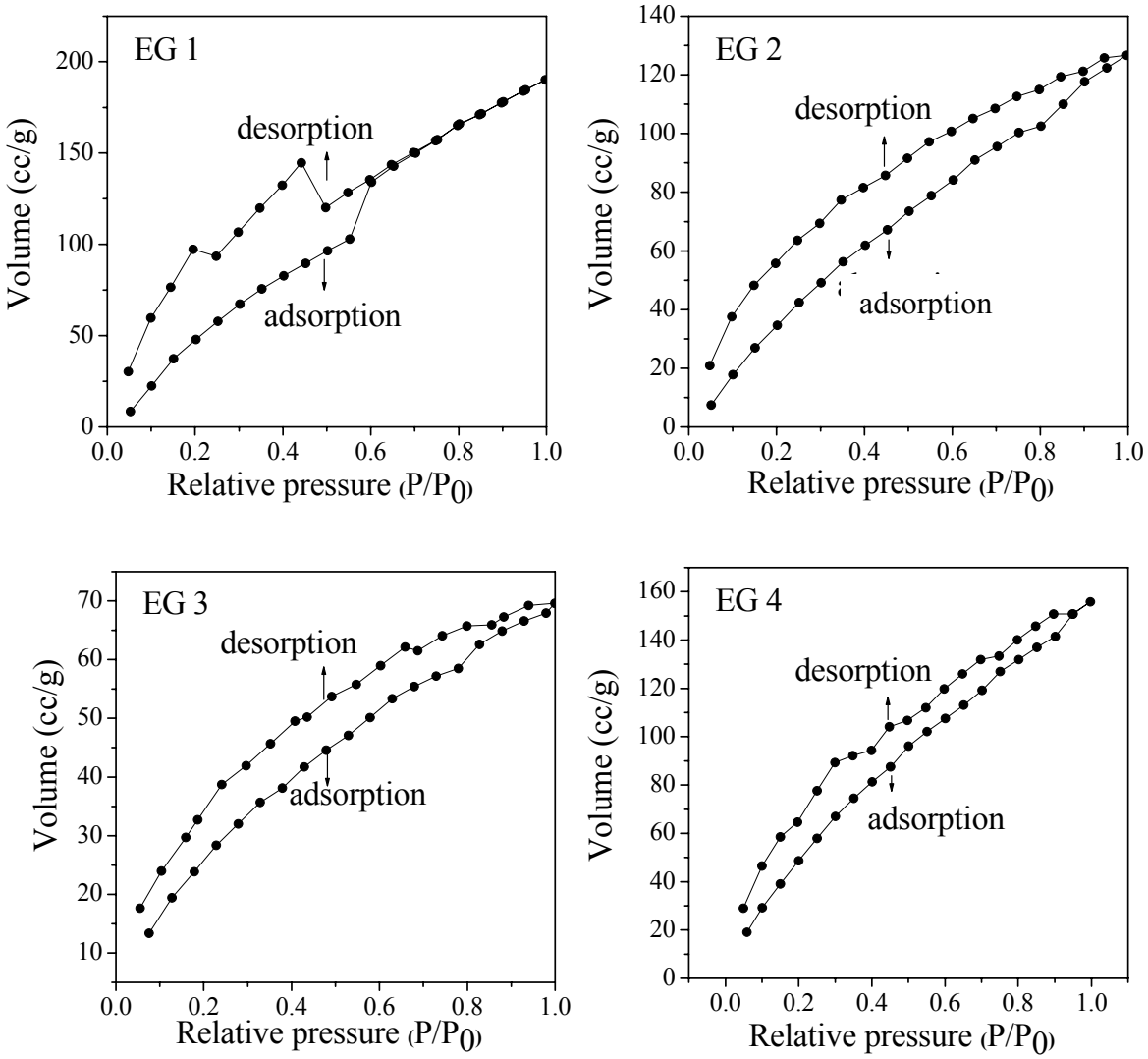

Fig 19: H_2 uptake curves of EG samples

DG samples have shown H_2 uptake in the range of 0.32-1.21 wt % at 1 atm and 77 K. Among all DG samples DG 5 sample show highest uptake around 1.21 wt % at 1 atm and 77 K. DG 2 sample is found to exhibit an uptake of 2.5 wt % at 100 atm and 298 K. Adsorption and desorption curves of DG samples are shown in Fig 20 and up take values are summarized in Table 9

Table 9: H_2 uptake values of DG

Sample name	**H_2 adsorption (wt %) (1 atm, 77 K)**	**H_2 adsorption (wt %) (high pressure) (100 atm, 298 K)**
DG 1	1.16	
DG2	1.02	
DG 3	0.68	2.5
DG 4	1.11	
DG5	1.21	

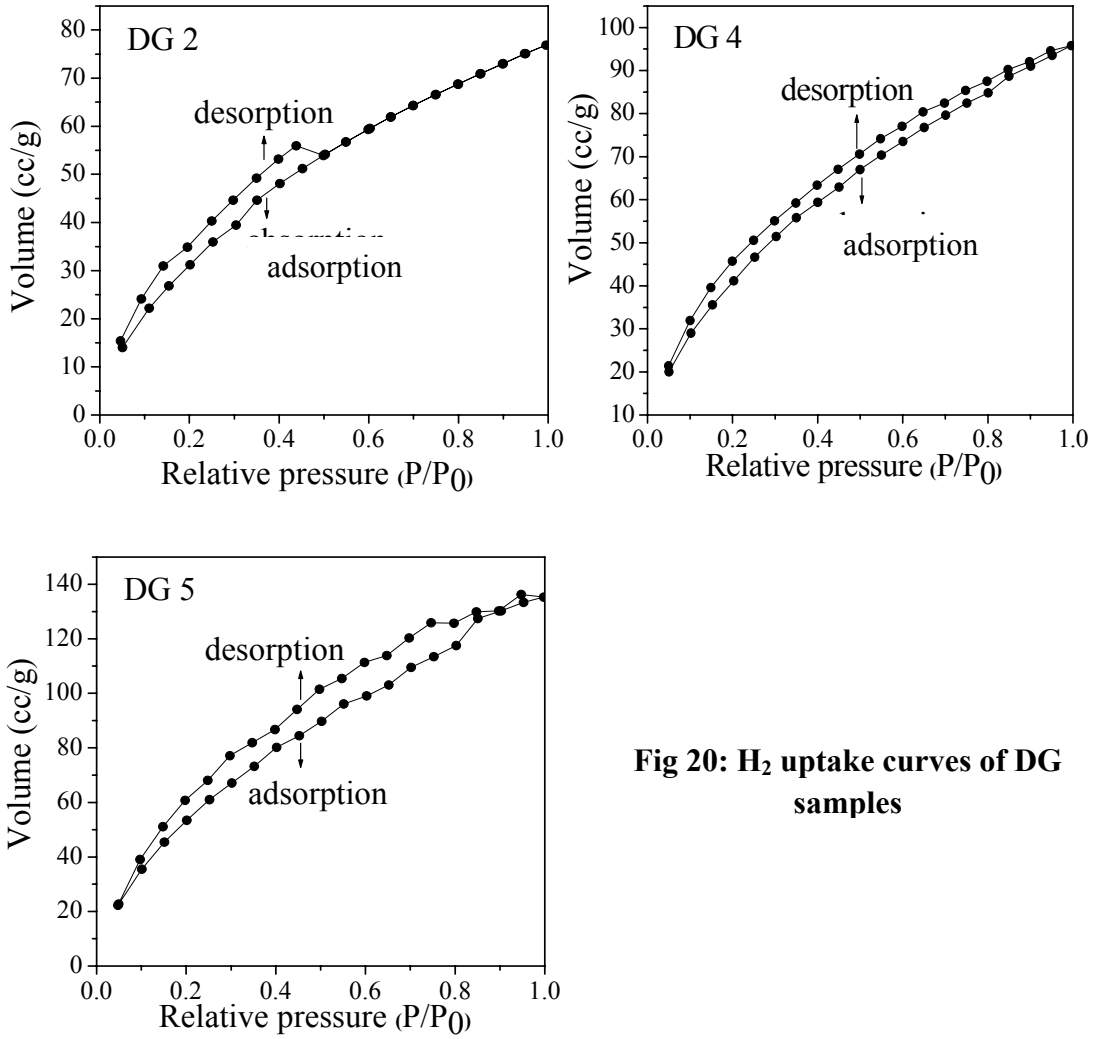

Fig 20: H_2 uptake curves of DG samples

By using a home-built adsorption set-up [16] we have carried high pressure hydrogen adsorption measurements. We find EG 4 (with 1.4 wt % uptake at 1 atm and 77 K) exhibits a hydrogen uptake of 3.1 wt % at 100 bar pressure and 298 K. DG 2 shows around 2.5 wt % and EG 3 H_2 shows close to 2 wt %. These values of the H_2 uptake at high pressure

are comparable to those of single-walled nanotubes [106]. High pressure hydrogen uptake curves of EG 4, DG 2 and EG 3 H_2 samples are given in Fig 21.

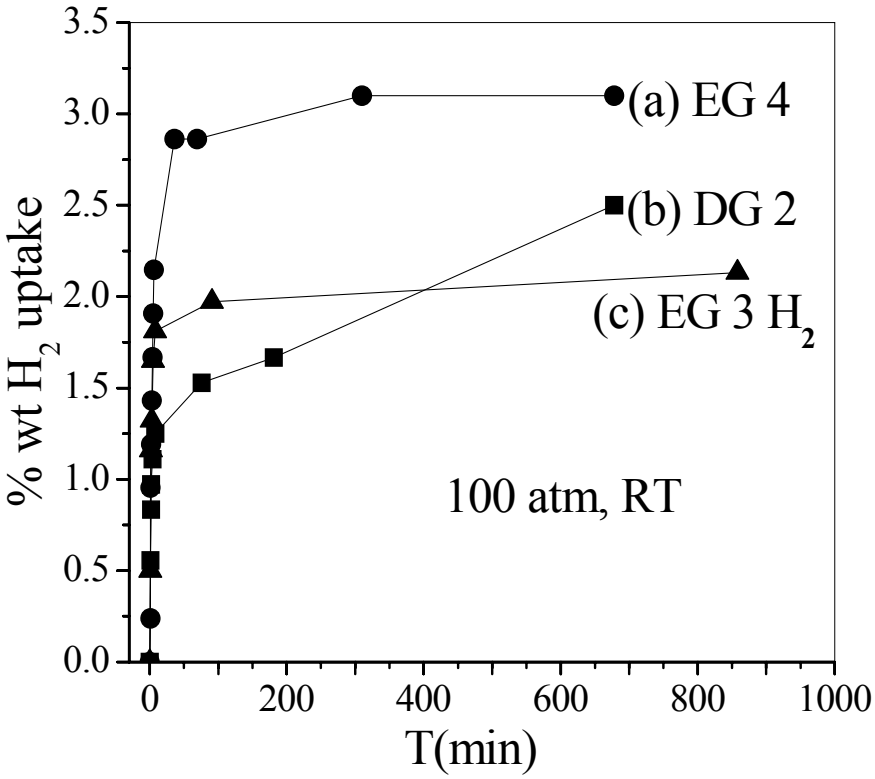

Fig 21: High pressure H_2 uptake curves of graphene samples

Among all discharge samples HG 1 comes out be best, it shows 1.01 wt % at low pressure (1 atm and 77 K) and 2.0 wt % at high pressure (100 atm and 300 K). HG 3 and HG 2 show around 0.63 and 0.227 wt % respectively. Fig 22 shows H_2 uptake plots of discharge samples.

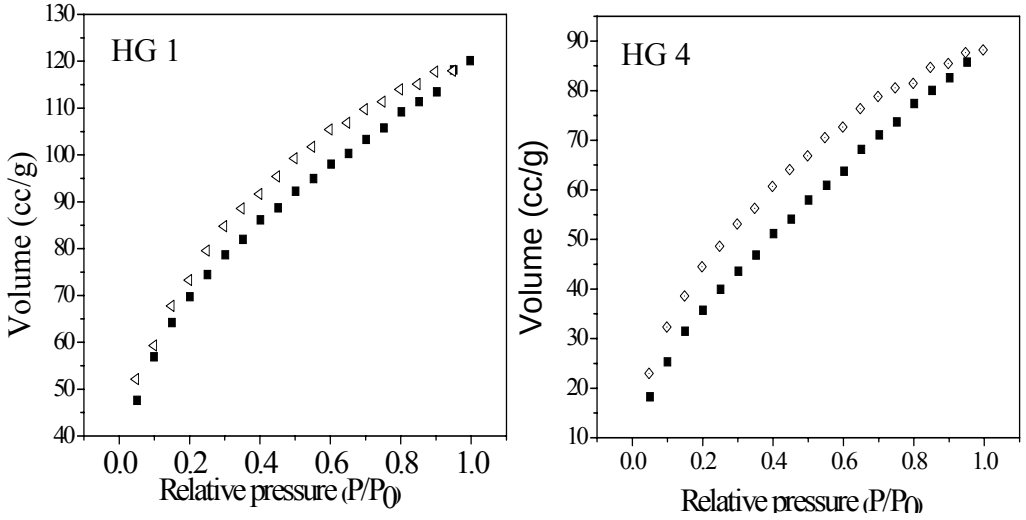

Fig 22: H_2 adsorption and desorption curves of HG samples

The values of H_2 uptake by the various graphene samples prepared by us vary linearly with the surface area as shown by Fig 23. By extrapolation of the plot in Fig 23, to the surface area of single-layer graphene, we estimate its hydrogen uptake at 1 atm and 77 K to be around 3 wt% which is impressive.

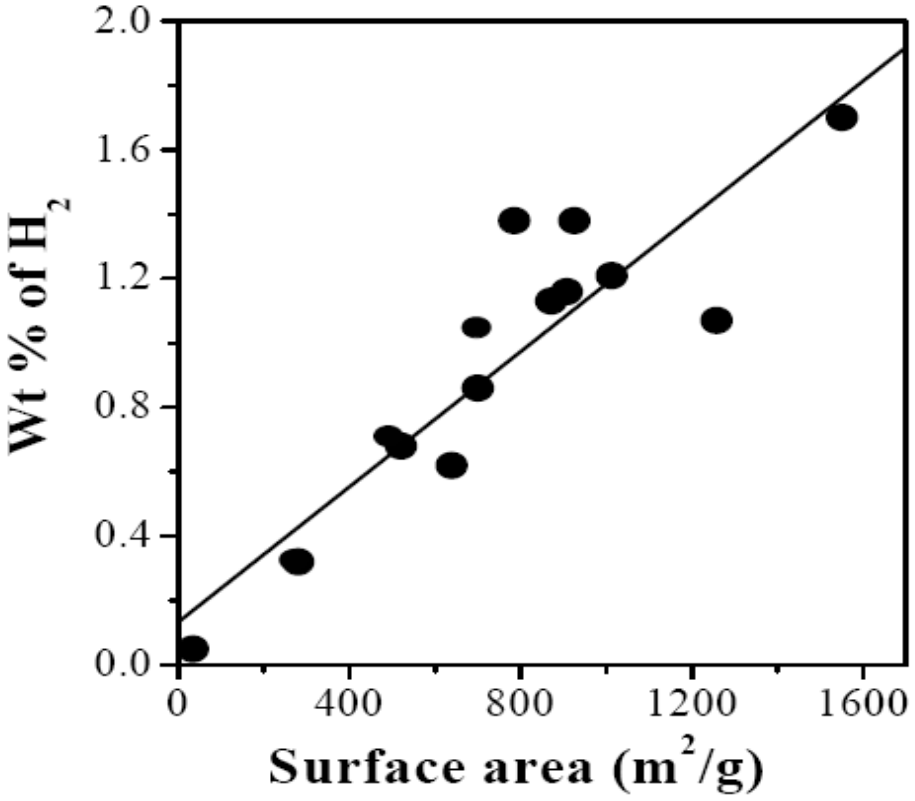

Fig 23: Linear relationship between the BET surface area and the wt% of hydrogen uptake at 1 atm pressure and 77 K temperature

Though the graphene samples examined by us exhibit lower hydrogen uptake compared to the 6.0 wt% target of Department of Energy (USA), there is significant scope for further improvements, by producing samples with smaller number of layers and significantly higher surface areas. It is possible that single layer graphene will exhibit 5-6 wt % of H_2 uptake at 100 atm and 298 K.

CO_2 uptake

We have studied the uptake of CO_2 at 1 atm and 195 K by using several samples of graphene prepared by us. Fig. 24, Fig 25 and Fig 26 show CO_2 adsorption and desorption curves of EG, DG and HG samples respectively. The EG samples show CO_2 uptake in the range of 21-34 wt %. EG 1 and EG 4 show similar values close to 34 wt %. EG 2 and EG 3 show around 20 wt % and 26 wt % respectively. It is possible that the small values of CO_2 uptake can occur in graphene samples containing large size particulates.

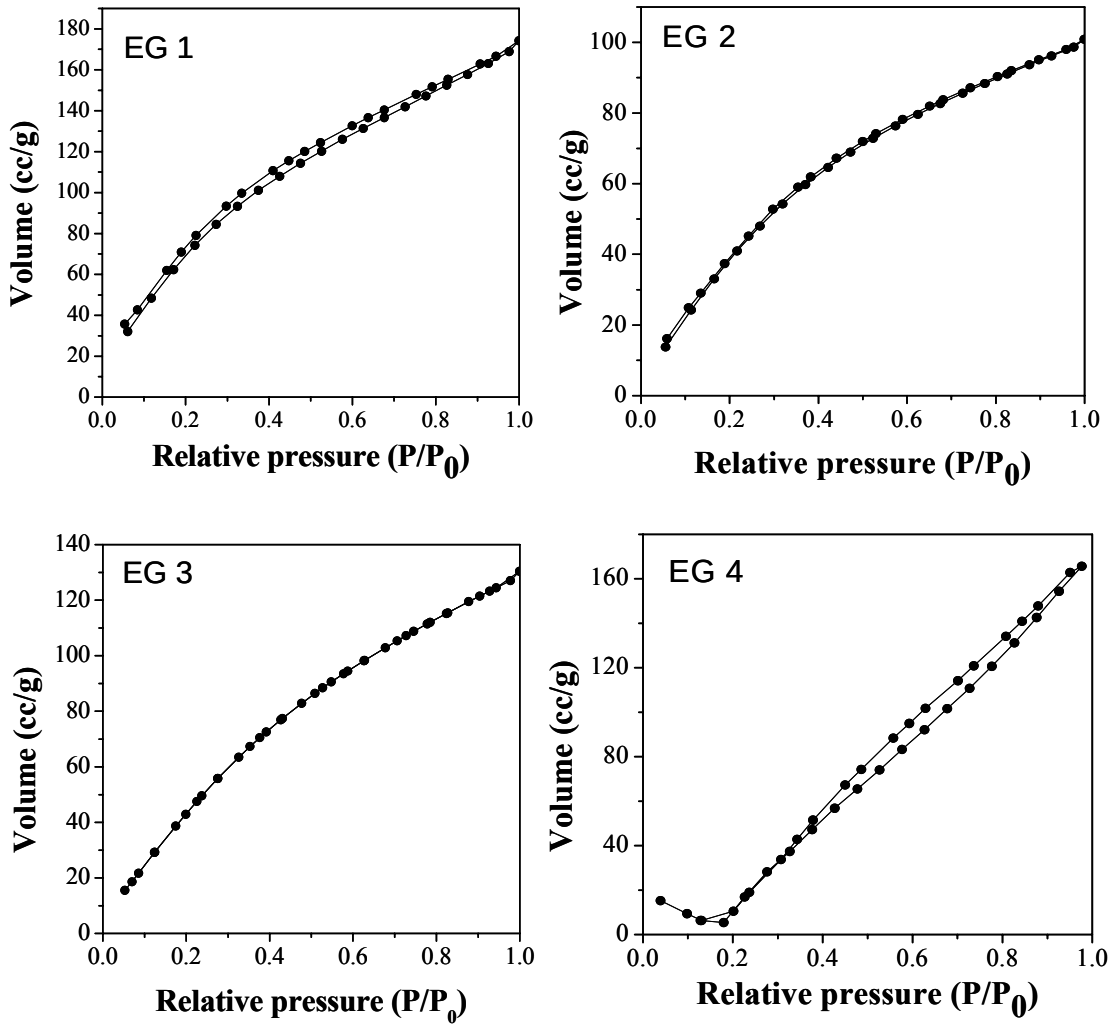

Fig 24: CO_2 adsorption and desorption curves of EG samples

The DG samples show somewhat variable values of CO_2 uptake in the range 10-38 wt %. In DG samples DG 5 show highest value close to 37 wt % while DG 4, DG 2, DG 6 exhibit 32, 9.5, 9.5 wt % respectively.

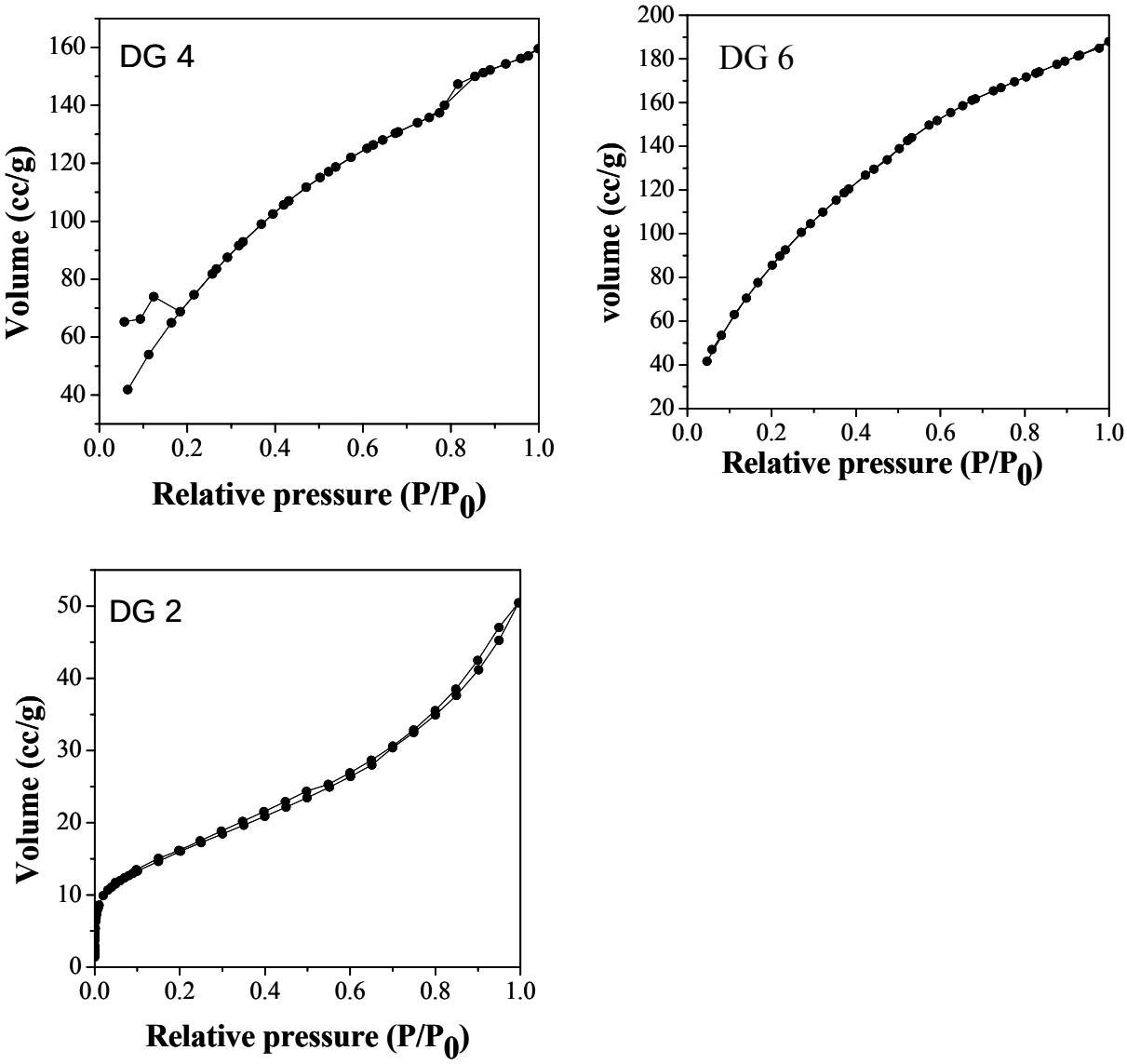

Fig 25: CO_2 adsorption and desorption curves of DG samples

When compare with EG and DG, the HG samples show quite low CO_2 uptake in the range of 10-17 wt %. HG 1 shows 16.8 wt %, where as HG 2 and HG 3 exhibit 10.6 wt % and 11.9 wt %.

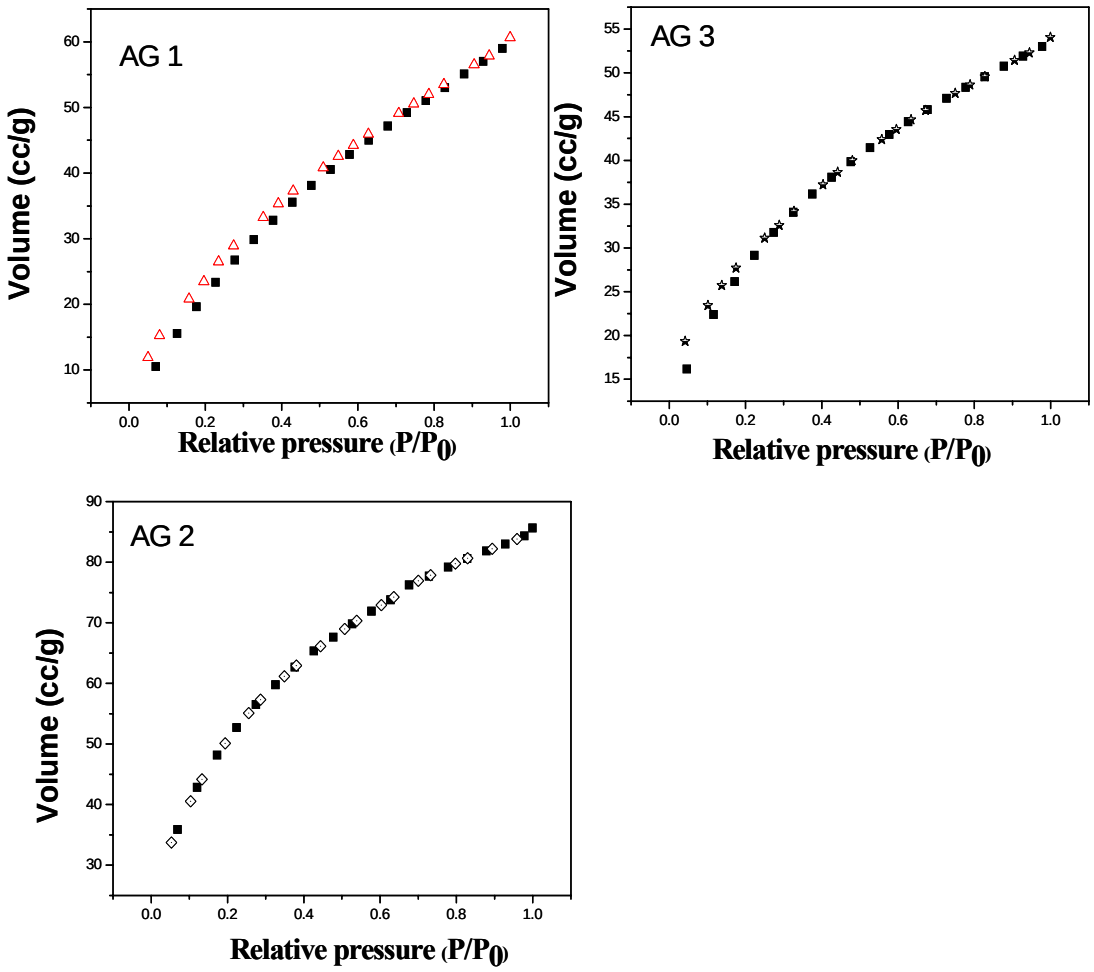

Fig 26: CO_2 adsorption and desorption curves of HG samples

4.3 Functionalization and solubilization of graphene

Amidation

By carrying out the amidation reaction similar to that reported for carbon nanotubes, we have obtained dispersions of EG in various non-polar solvents. The results are similar to those reported by Haddon and co-workers [143]. In Fig. 27, we show photographs of the dispersions of amide-functionalized EG in dichloromethane, carbon tetrachloride and tetrahydrofuran. In Fig. 28, we show photographs of similar dispersions prepared with DG. The product dodecylamido graphene has solubility of 0.5 mg/ml and stable up to 6 hrs. It should be noted, however, that DG requires hasher acid treatment and over longer periods to enable to carry out further functionalization.

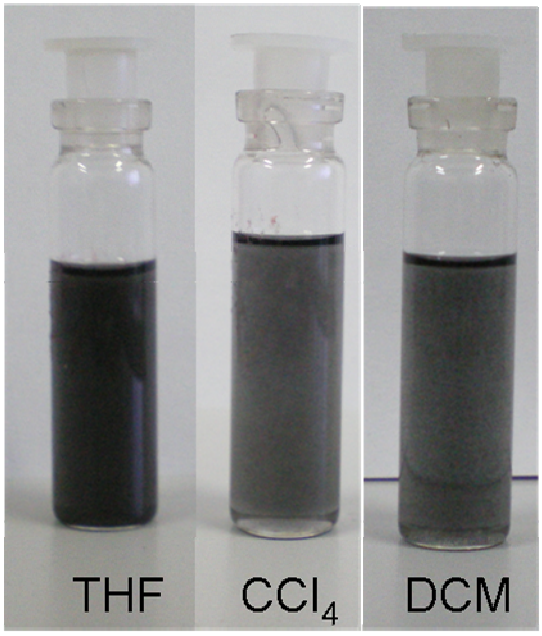

Fig. 27: Amide functionalized-EG in THF, CCl_4 and DCM

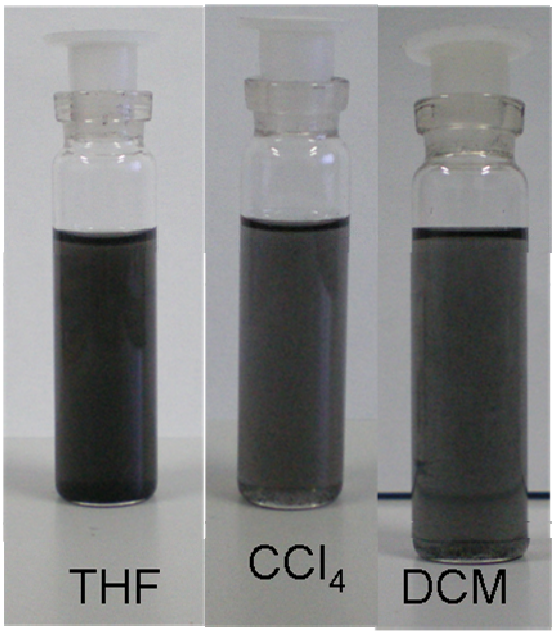

Fig. 28: Amide functionalized-DG in THF, CCl_4 and DCM

In Fig. 29, we show the infrared spectra of EG at various stages of the solubilization process. After acid treatment, EG show a carbonyl stretching band at 1710 cm^{-1} due to the carboxyl groups. On functionalization with dodecylamine, the C=O stretching band shifts to 1650 cm^{-1} due to the formation of amide band, in addition to C-H and N-H stretching bands around 2800 and 3300 cm^{-1} respectively are observed.

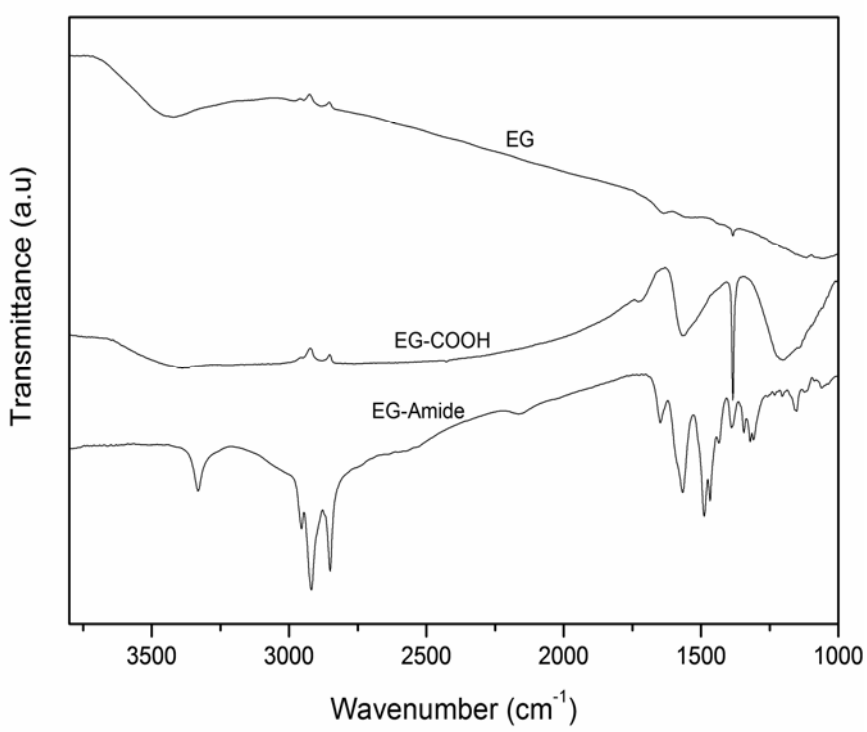

Fig. 29: Infrared spectra of pristine EG, acid treated EG (EG-COOH) and amide functionalized EG (EG-amide).

Organosilane and organotin coating

We have accomplished covalent functionalization of EG and DG graphene samples by reaction with hexadecyltrimethoxysilane (HDTMS) and dibutyldimethoxytin (DBDT) [144,145]. The functionalized samples were characterized by IR spectroscopy. The functionalized samples were dispersible in CCl_4 and the dispersions were stable for 6 hrs or more. In Figures 30, 31, we show photographs of the dispersions of organosilane and organotin functionalized graphenes.

Fig. 30: Organosilane coated EG and DG

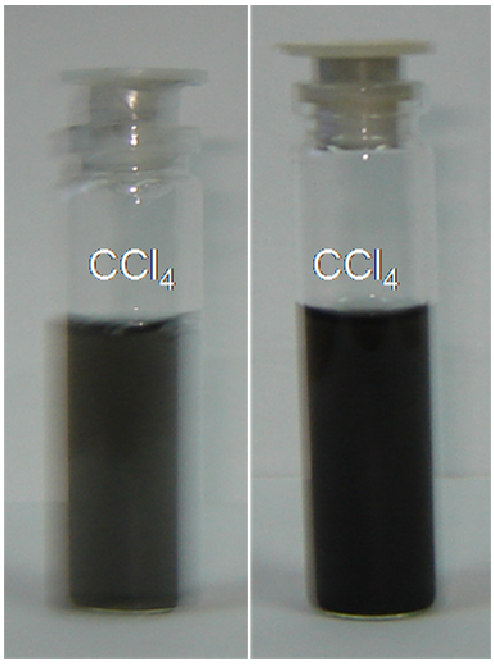

Fig. 31: Organotin coated EG and DG

The IR spectrum of the sample functionalized with HDTMS shows the Si-O vibration band at 1100 cm^{-1} along with the bands due to alkyl groups at around 2950 cm^{-1} [Figs 32 (a) and 33(a)]. The sample functionalized with dibutyldimethoxytin shows the presence of Sn-O band at 500-600 cm^{-1} and alkyl bands at 2850 and 2950 cm^{-1} [Figs 32 (b) and 33 (b)]. It clearly indicates the formation of organo silane and organo tin coating on graphene surface

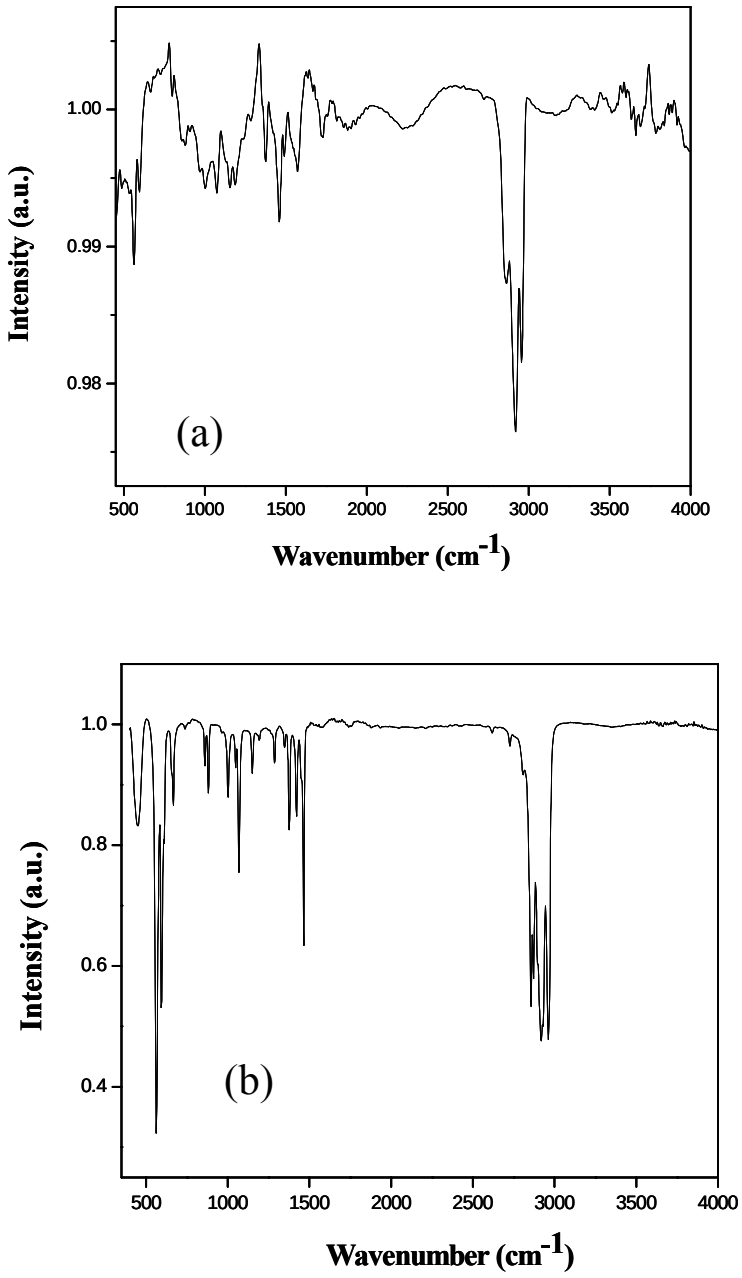

Fig. 32: IR spectra of EG functionalized by the (a) organosilane and (b) organotin reagents

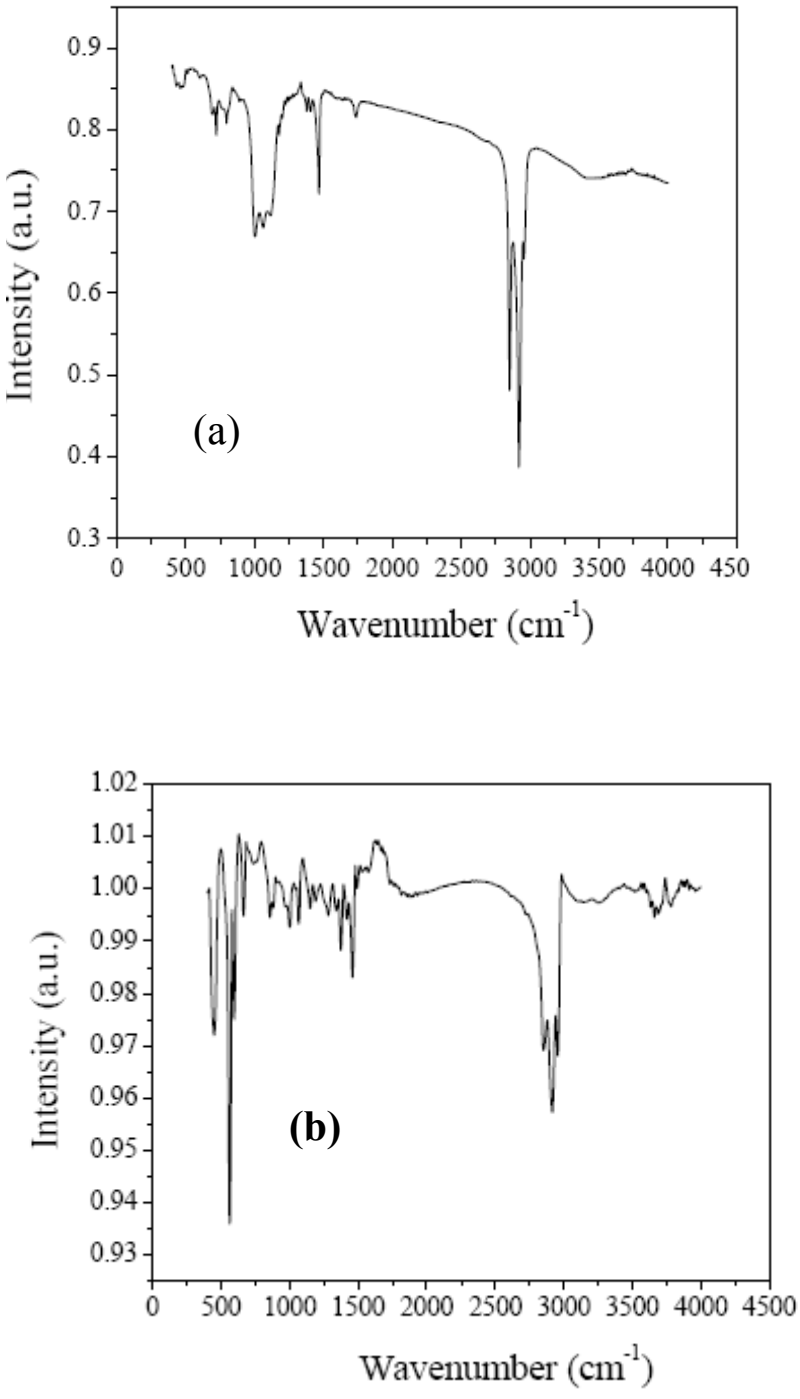

Fig. 33: IR spectra of DG functionalized by the (a) organosilane and (b) organotin

Acidification

As-prepared EG shows evidence for the presence of carbonyl and hydroxyl groups on the surface. After further treatment of EG with nitric and sulphuric acid mixture, we obtain a water solution of EG, along with the insoluble portion of the sample which settles down. The infrared (IR) spectrum of the soluble part obtained after drying shows a prominent band due to carbonyl group in addition to a broad band due to –OH groups is observed as shown in Fig. 34

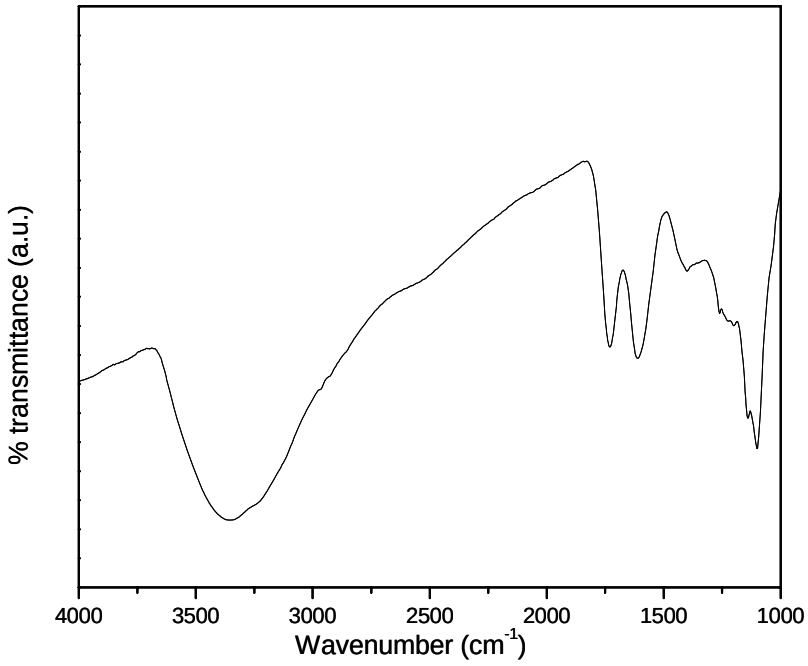

Fig 34: Infrared spectrum of water-soluble EG.

The Raman spectrum of the water-soluble EG shown in Fig. 35 (a) exhibits the characteristic G, D and 2D bands and shows that L_a of the sample is 4 on an average (as calculated from the intensity ratio of the D and G bands). In Fig. 35 (b), we show the photograph of the water-soluble graphene.

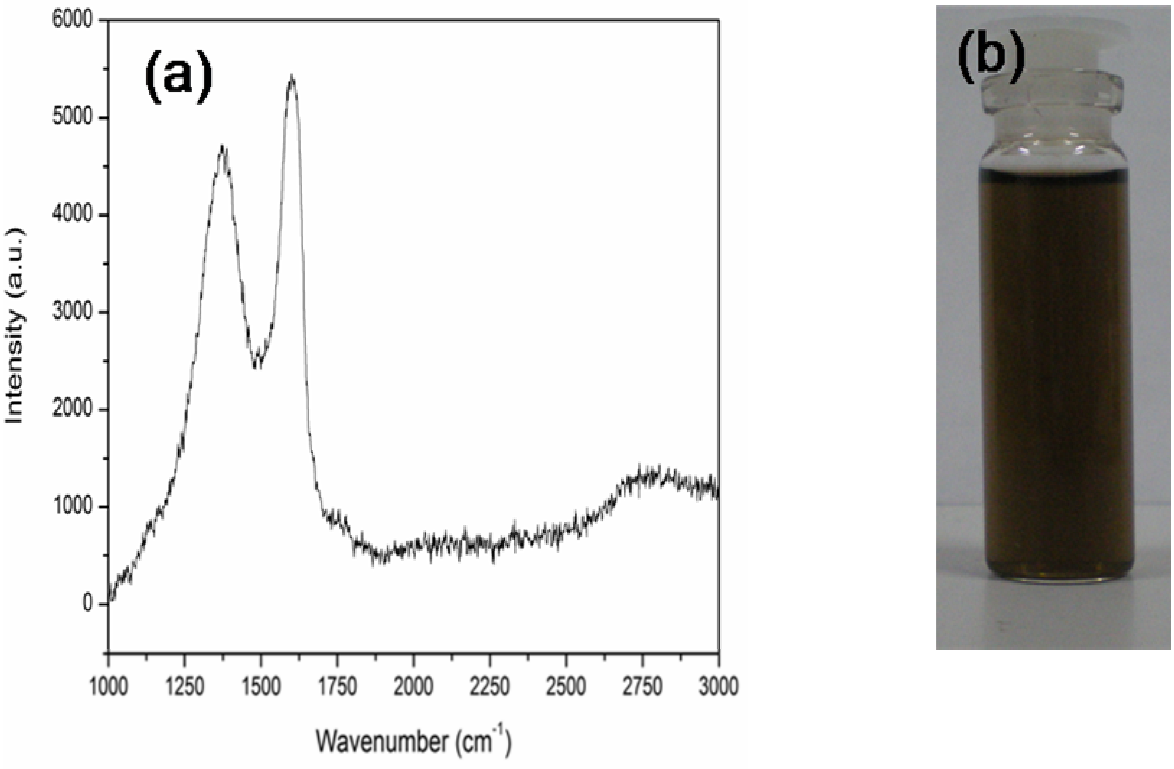

Fig. 35 (a) Raman spectrum and (b) Photograph of water-soluble EG

Wrapping with PEG

The water-insoluble EG when treated with polyethylene glycol (PEG) yielded water-dispersible graphene. In Fig. 36 (a), we show a photograph of the water-dispersion of PEG-treated graphene. IR spectra of PEG functionalized graphene is shown in Fig. 36 (b).

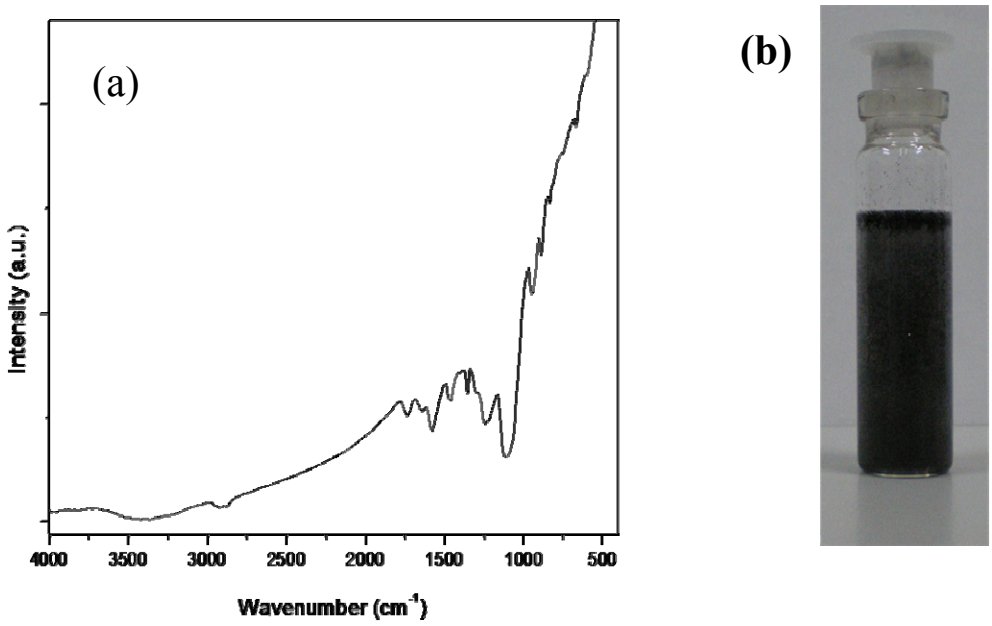

Fig 36 (a) IR spectrum and (b) water dispersion of PEG functionalized graphene

Functionalization through π-π interactions

We have been able to accomplish the solubilization of both EG and DG in DMF by reacting with PYBS [148]. It was necessary to heat the EG sample with PYBS at 200 °C, and the DG sample at 300 °C to obtain the dispersions which were stable for several days. Samples prepared at low temperatures were stable only up to 2-3 hrs. In case of Electronic absorption spectra of the PYBS-graphene dispersions show the pyrene bands with changes in the relative intensities because of π-π interactions (see Fig 37). In Figures 38 and 39 we show the photographs of dispersions EG and DG in DMF respectively.

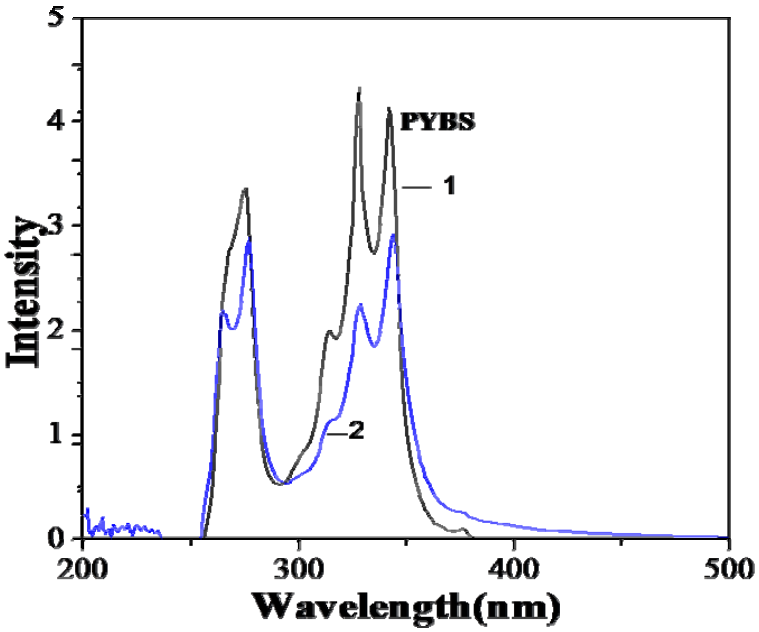

Fig 37: UV absorption spectra of PYBS and PYBS treated EG

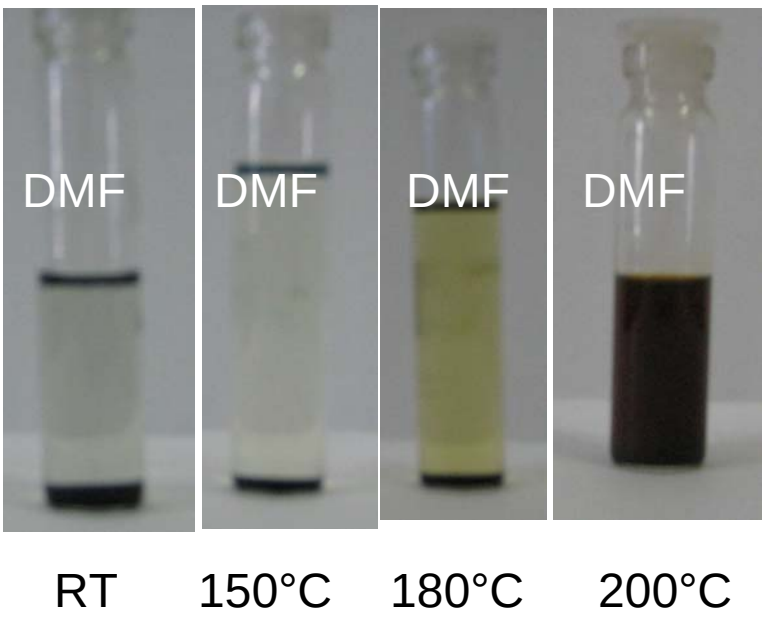

Fig 38: Photographs of DMF dispersions of PYBS treated EG at different temperatures after seven days

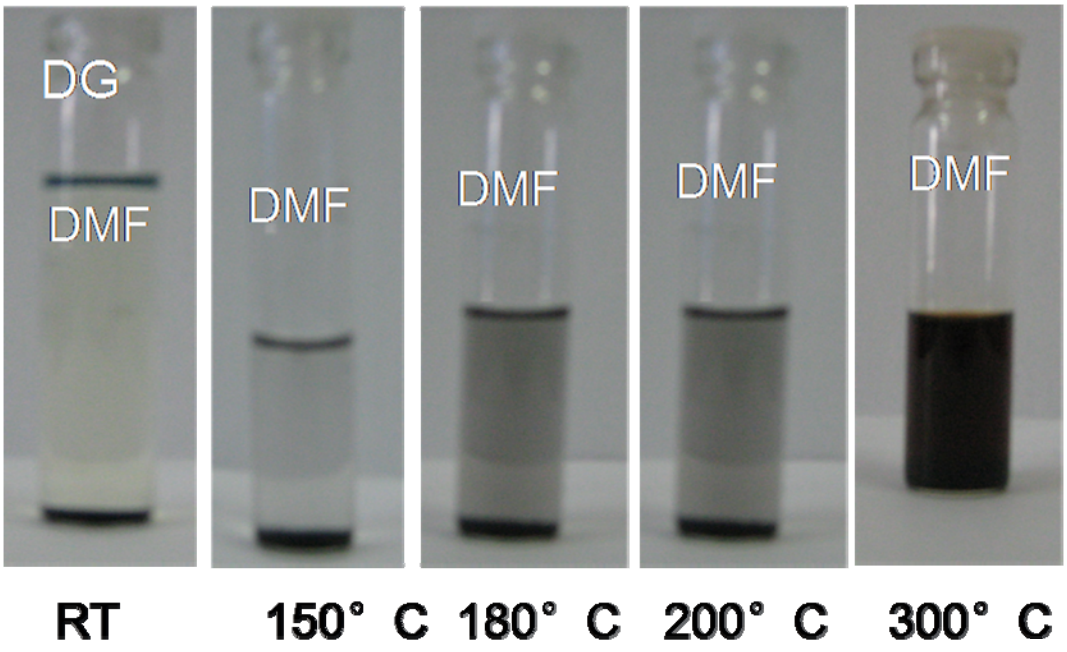

Fig 39: Photographs of DMF dispersions of PYBS treated DG at different temperatures after seven days.

Wrapping with surfactants

Non-covalent functionalization of graphene was accomplished by wrapping with different concentrations of surfactants such as CTAB, SDS and IGP. In the case of CTAB, the best dispersions for EG and DG in water were obtained at 6 mM and 9 mM respectively. Photographs of EG and DG dispersions in CTAB are shown in Figure 40. SDS gave good dispersions in water at 20 mM for EG and at 10 mM for DG. The best results were obtained with IGP which gave stable dispersions of EG and DG at a low concentration of 1 mM. The photographs of the dispersions in SDS and IGP are shown in Fig 41 and Fig 42 respectively. Raman spectra of these dispersions shows the characteristic D, G and 2D bands of graphene [see Figs 43, 44 and 45]. In case of EG the obtained dispersions were quite stable up to 7 days, where as the dispersions obtained with DG were stable up to only 2 days.

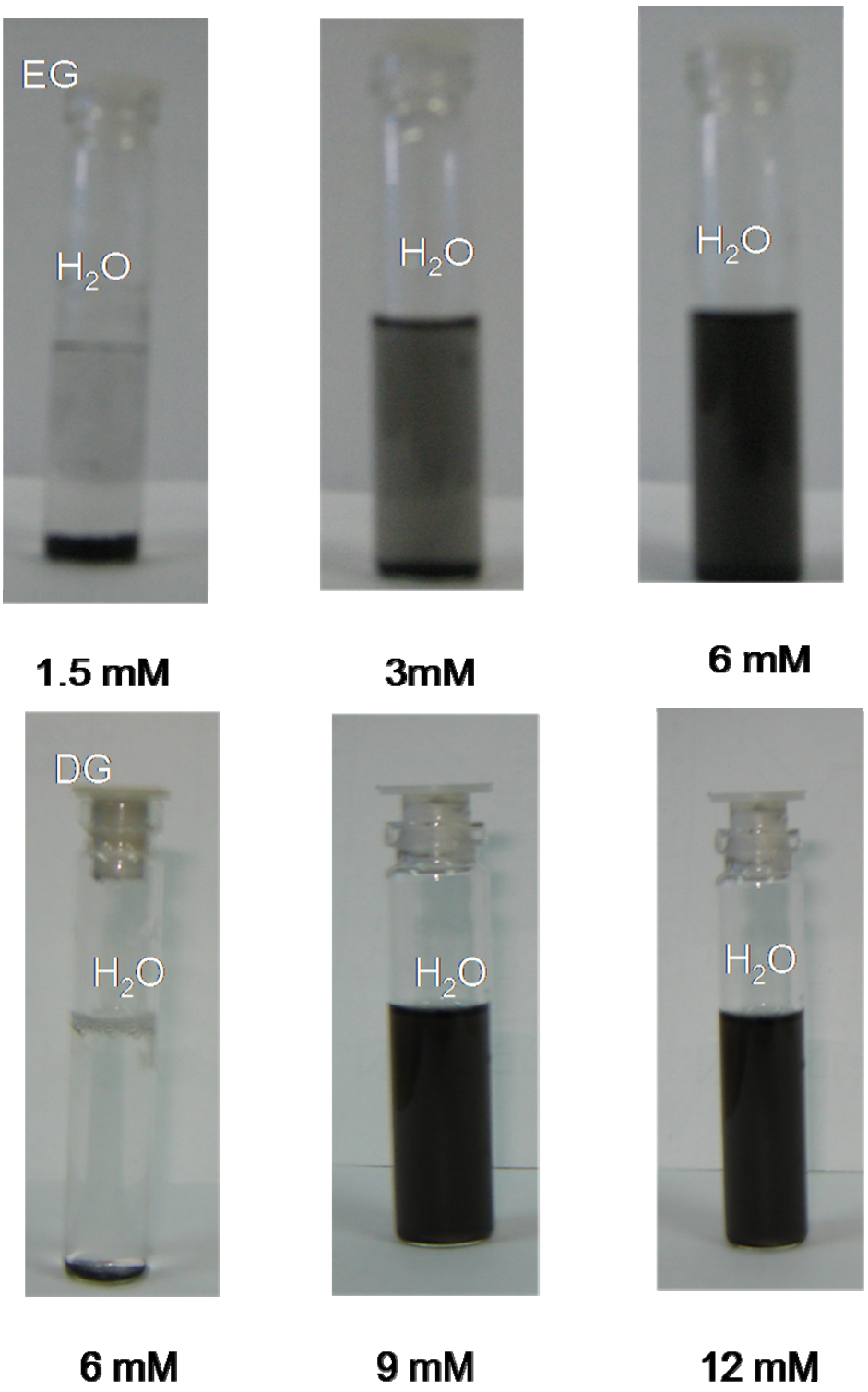

Figure 40: Photographs of water dispersions of EG and DG treated with CTAB at different concentrations

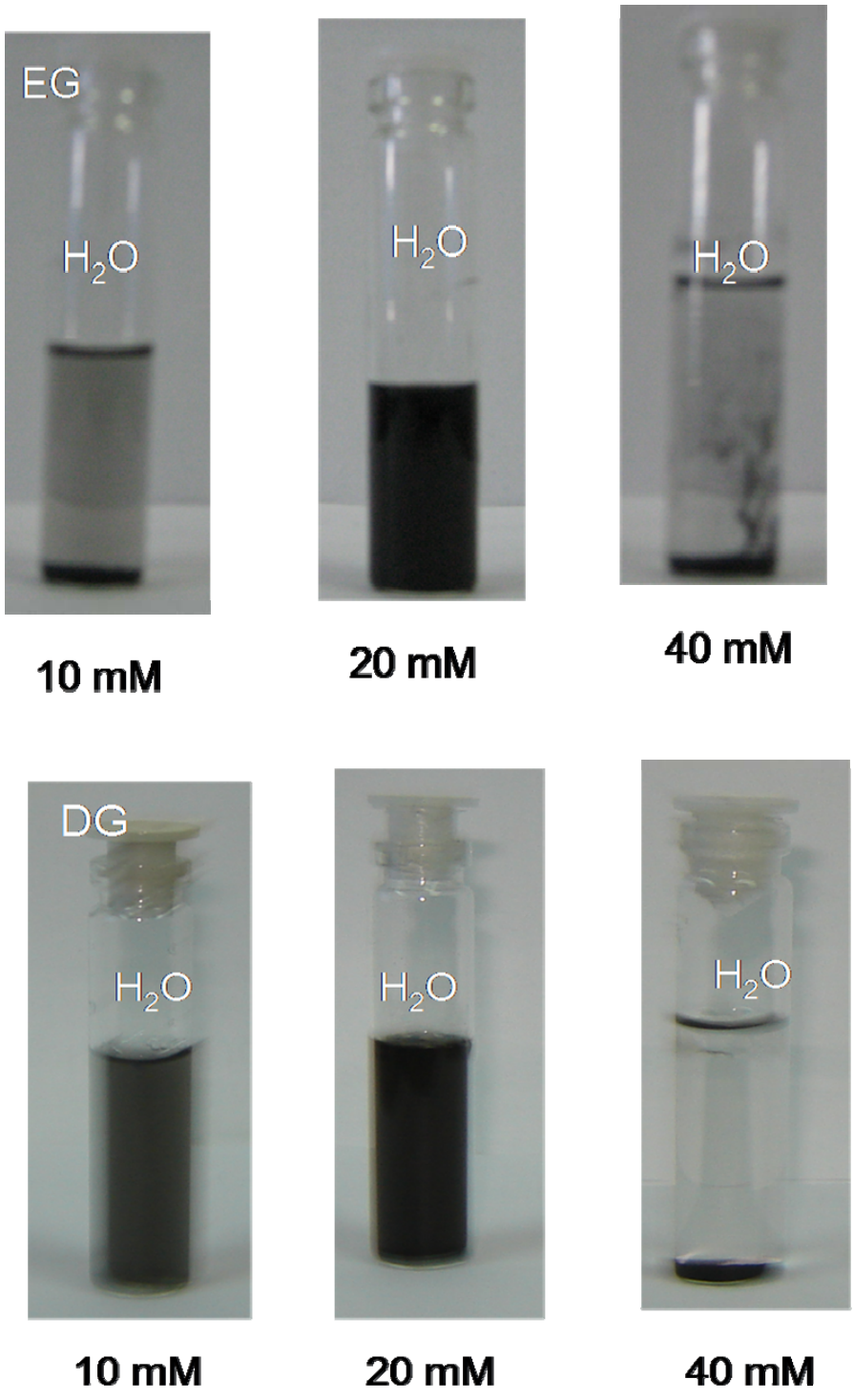

Figure 41: Photographs of water dispersions Of EG and DG treated with SDS at different concentrations

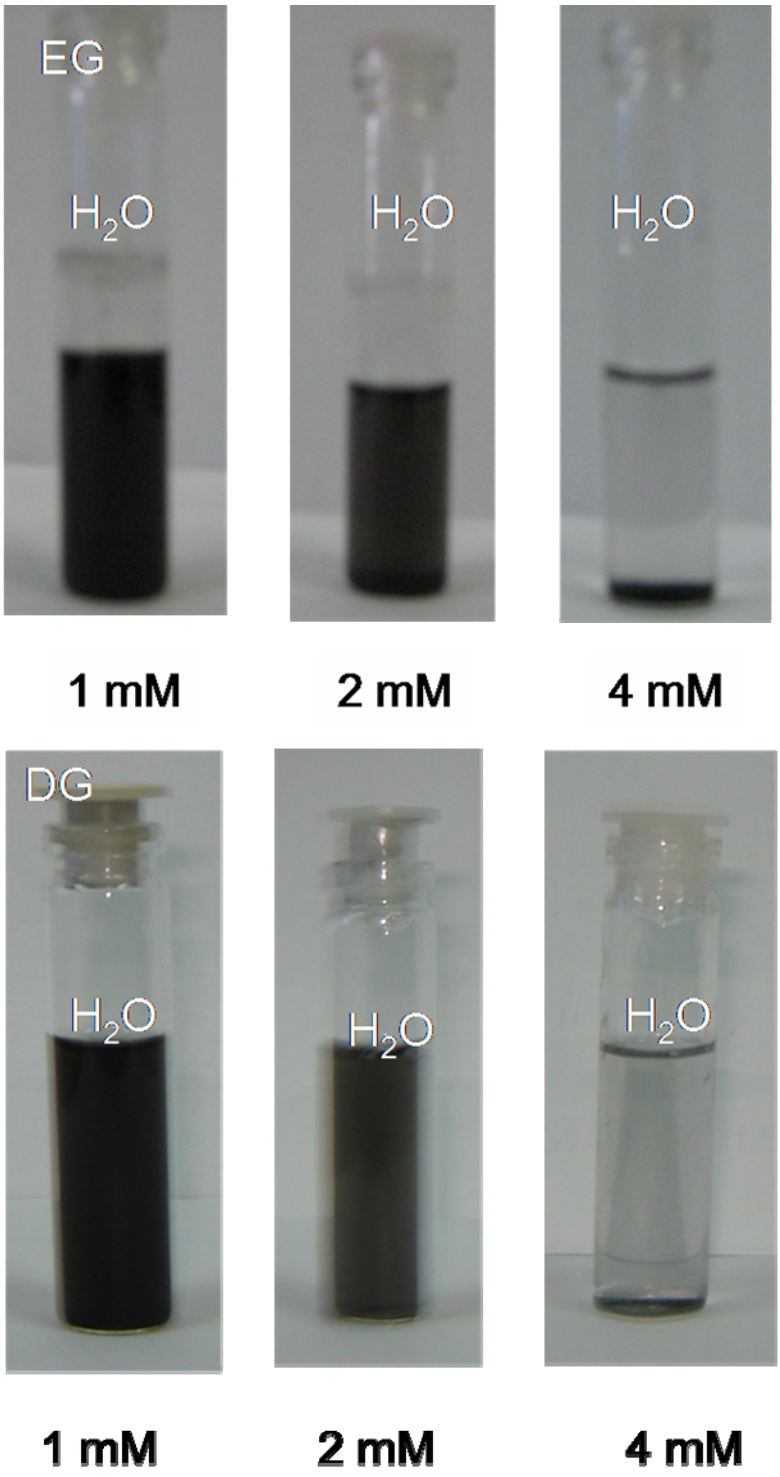

Figure 42: Photographs of water dispersions Of EG and DG treated with IGP at different concentrations

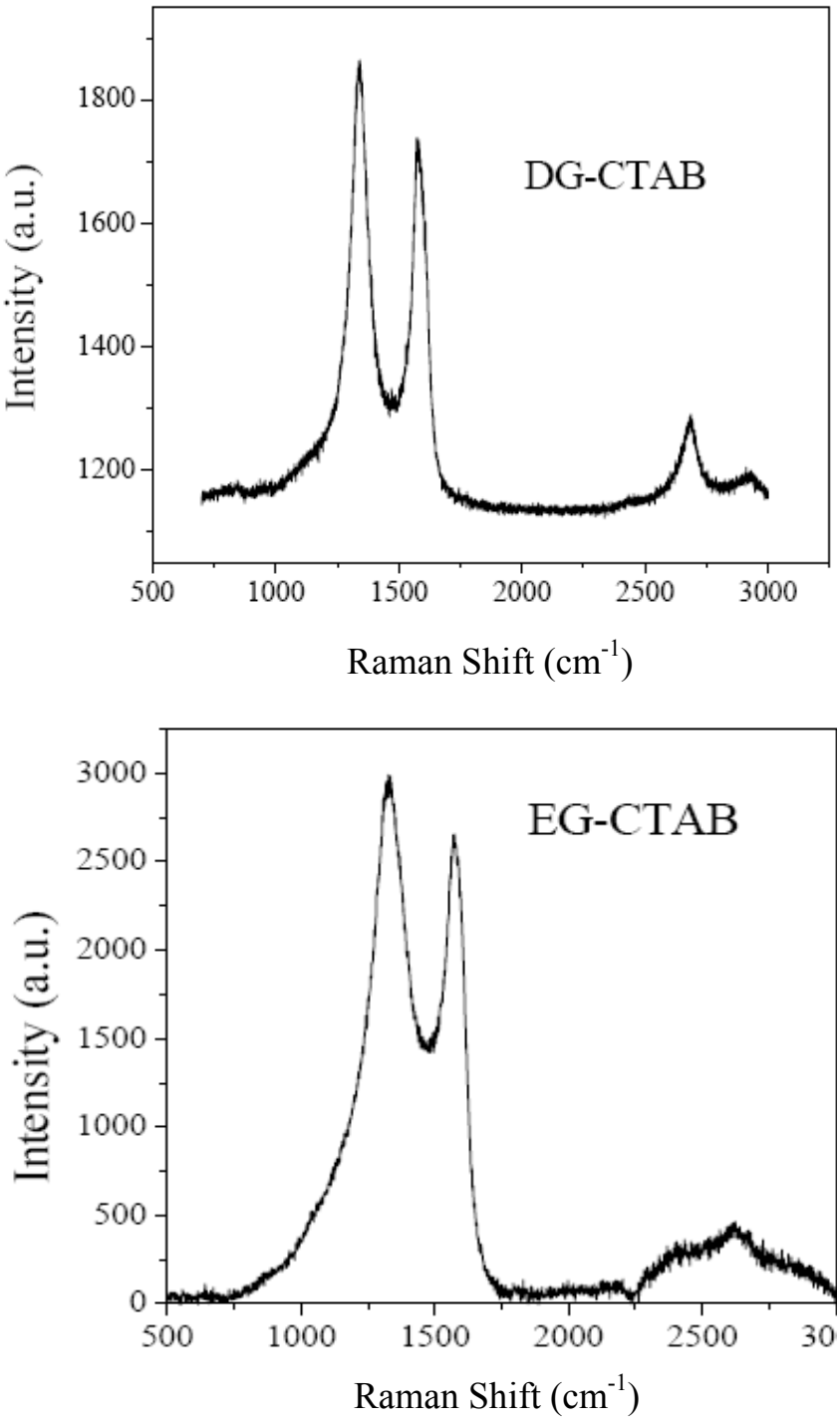

Fig 43: Raman spectra obtained from water dispersions of EG and DG treated with CTAB

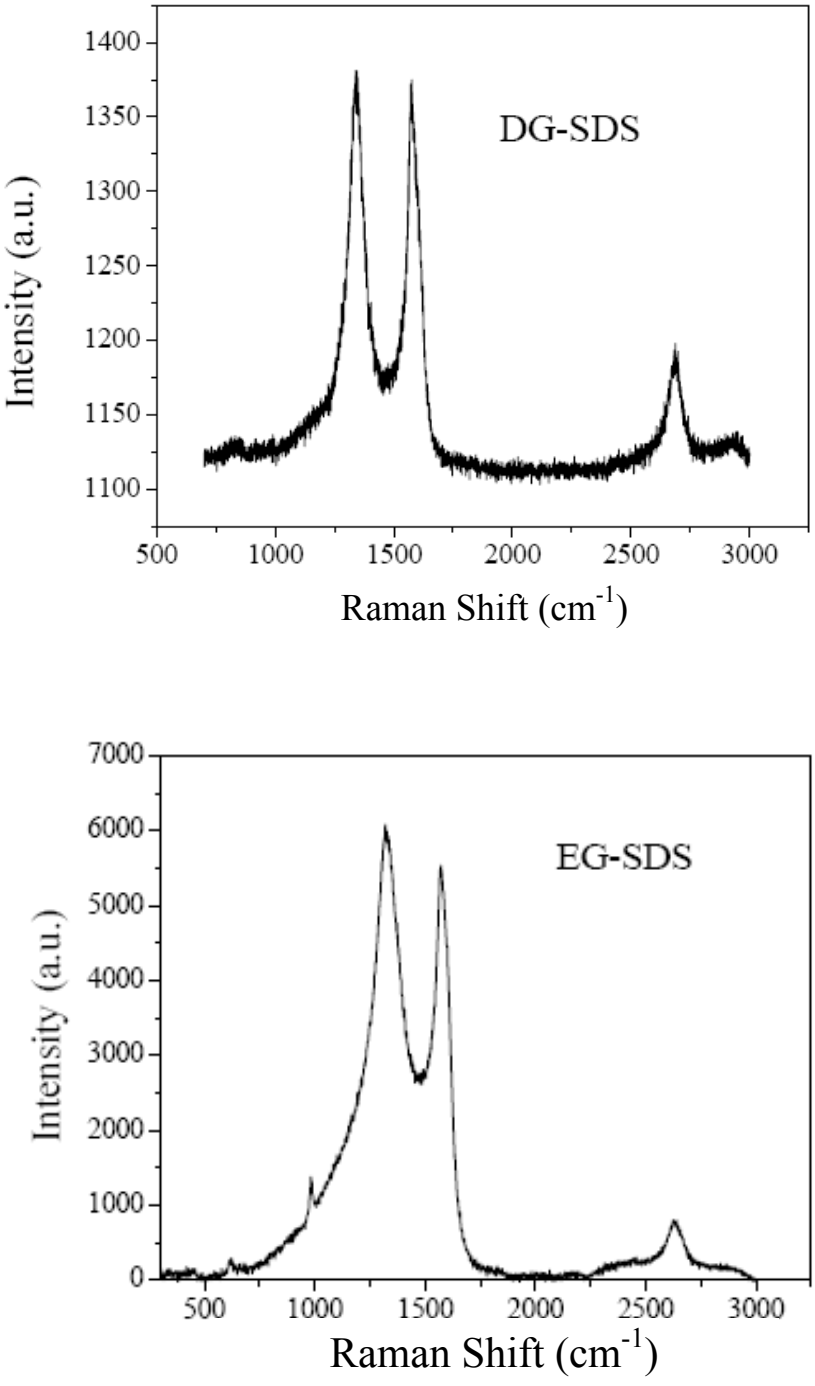

Fig 44: Raman spectra obtained from water dispersions of DG and EG treated with SDS

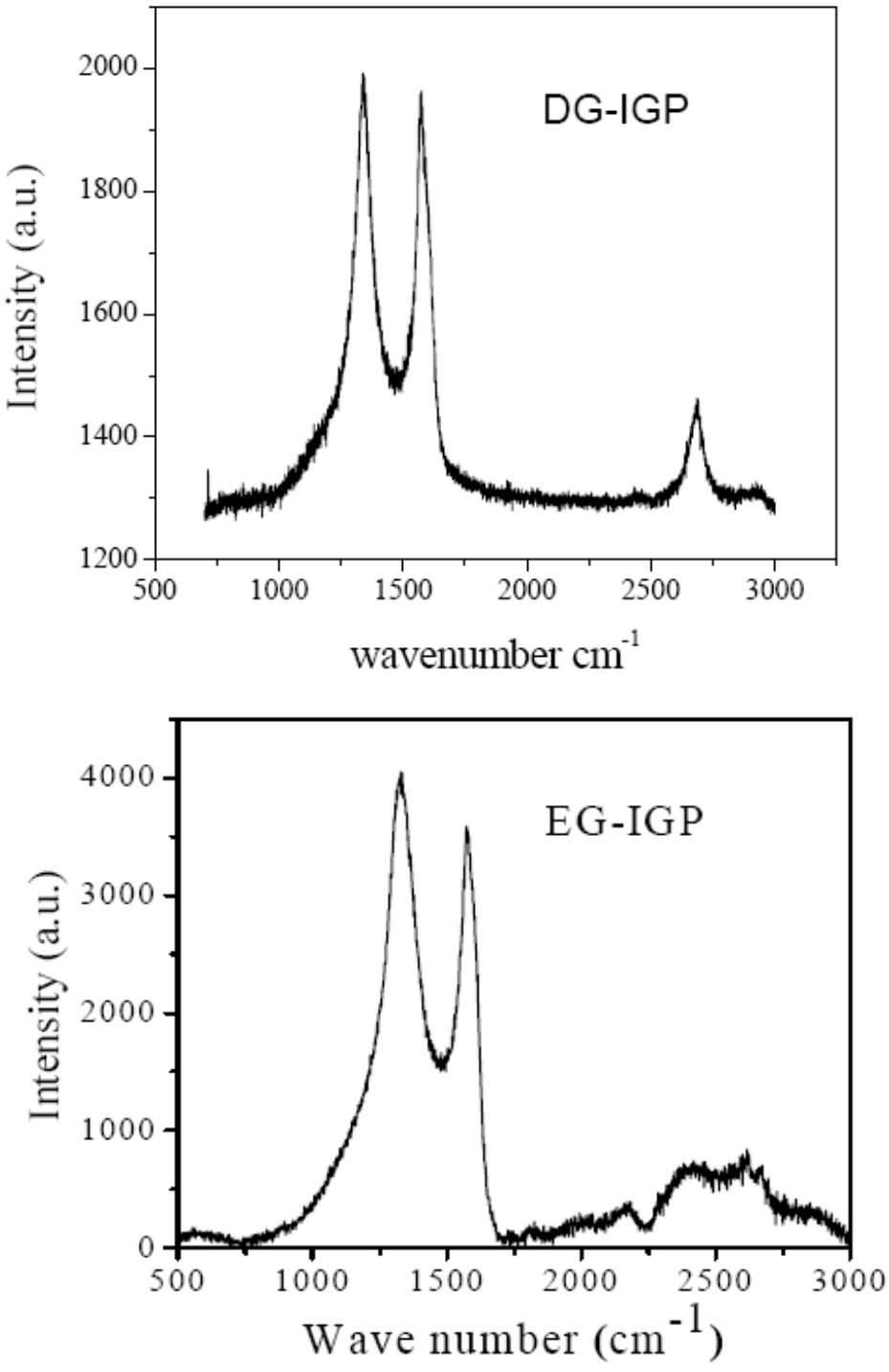

Fig 45: Raman spectra obtained from water dispersions of DG and EG treated with IGP

4.4 Decoration of graphene by metal nanoparticles

We have decorated graphene with platinum and silver nanoparticles by polyol reduction method using chloroplatinic acid and silver nitrate as metal salts. TEM images show the size of decorated platinum [Fig 46] particles is around 10 nm while silver is around 5 nm [Fig 47].

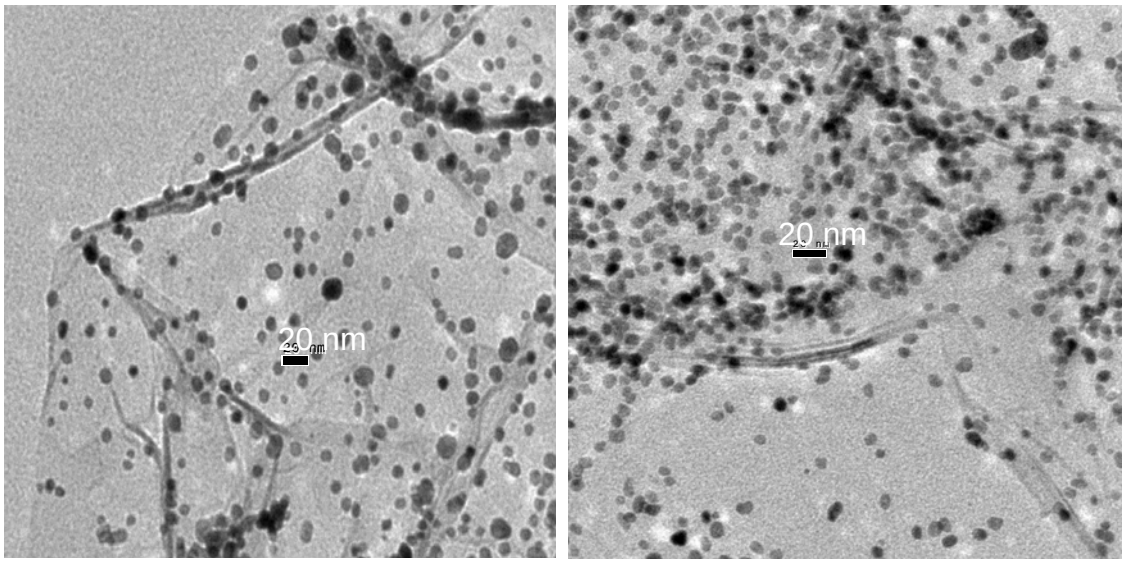

Fig 46: Graphene decorated with platinum nanoparticles

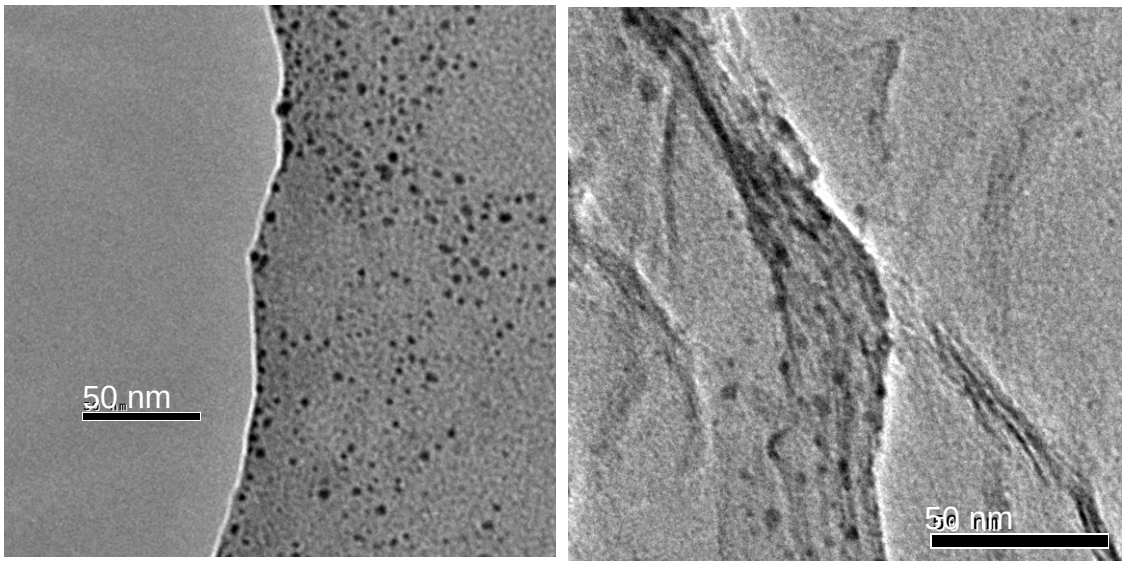

Fig 47: Graphene decorated with silver nanoparticles

4.5 Electrochemical properties of graphene and graphene as supercapacitor material

We have investigated the electrochemical properties of the CG, EG and DG using the redox reactions with potassium ferrocyanide. The peak to peak separation is known to be significantly depends on the microstructure of the carbon electrode used. [202]. A small peak to peak separation (~ 70 mV) is achieved when the edges of graphite are exposed to the electrolyte while it is significantly larger (even close to 1 V) when the basal planes are involved. In Fig 48, we show typical cyclic voltammograms of the redox reaction of 100 mM potassium ferrocyanide (in 1 M KCl) carried out using working electrodes of different graphenes. While the peak to

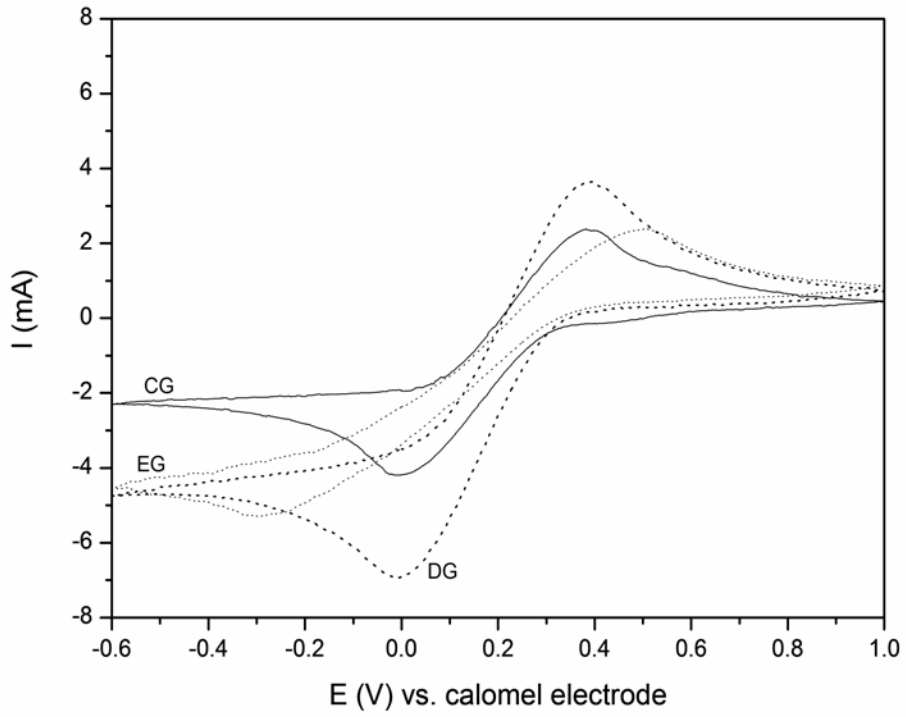

Fig 48: Cyclic voltammograms of the different graphene electrodes (at a scan rate of 20 mV/s) for 100mM $K_4Fe(CN)_6$ in 1M KCl.

peak separation depends on the scan rate, and it is found to be the largest in the case of EG. DG and CG exhibit similar peak separations. The behavior of EG is similar to that of basal plane in graphite. On the other hand, DG and CG exhibit slightly better kinetics.

We fabricated supercapacitors cells using an ionic liquid, N-butyl-N-methylpyrrolidinium bis(trifluoromethanesulfonyl)imide ($PYR_{14}TFSI$) as the electrolyte has a large potential window. In Fig 49 we show typical CVs of graphene-$PYR_{14}TFSI$ supercapacitors obtained at a scan rate of 100 mV/s. Specific capacitance values of 75 F/g and 40 F/g were obtained with EG and DG respectively. The specific capacitance depends significantly on the scan rate as the ionic liquid is highly viscous [Fig 50]. The maximum value of energy density stored in these capacitors are 31.9 and 17.0 $Whkg^{-1}$ respectively for EG and DG. These are some of the highest values reported to date and are comparable to those of microporous carbons reported by Balducci et al [203].

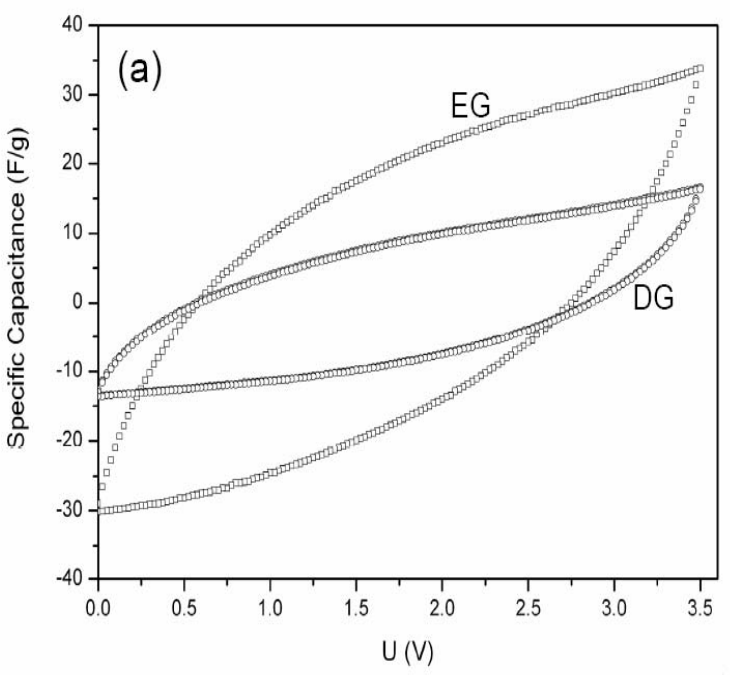

Fig 49: Voltammetry characteristics of a capacitor built from graphene electrodes (5 mg each) at a scan rate of 100 mV/s using ionic liquid

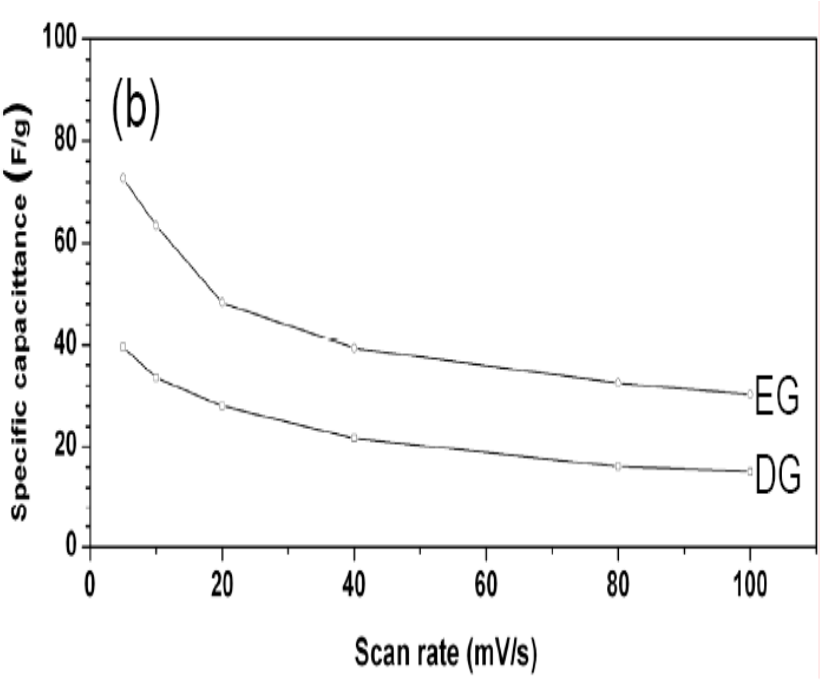

Fig 50: Specific capacitance as a function of scan rate using $PYR_{14}TFSI$.

5. CONCLUSIONS

In conclusion, graphene samples were prepared by different procedures and characterized, utilizing different techniques such as, X-ray diffraction (XRD), transmission electron microscopy (TEM), atomic force microscopy (AFM), Raman spectroscopy and thermogravimetric analysis (TGA). In terms of surface area, graphene prepared by the exfoliation of graphite oxide (EG) seems to be best but graphene prepared by arc-discharge of graphite has a smaller number of layers. Graphene prepared by conversion of nanodiamond (DG) is also satisfactory and has greater thermal stability than that EG. EG shows electrochemical redox behavior similar to that of the basal plane of graphite and can be used for fabrication of electrochemical supercapacitors.

Graphene samples prepared by different methods generally exhibit high surface areas. Graphenes prepared by exfoliation of graphitic oxide, arc evaporation of graphite rod and conversion of nanodiamond exhibit significant uptake of H_2 and CO_2. The H_2 uptake varies linearly with the surface area. While the maximum H_2 uptake, found by us at 100 atm and 298 K is 3.1 wt %, it should be possible to increase it by preparing better samples and by reducing the average number of graphene layers. Exfoliated graphene sample shows high CO_2 uptake up to 35 wt % at 1 atm and 195 K. Graphene has the potential of being a useful H_2 storage material and H_2 uptake studies of improved graphene samples should be pursued. Graphene may also be useful for preferentially by adsorbing CO_2.

We have been able to functionalize and solubilize graphene prepared by two methods in different media by employing both covalent and non-covalent modifications. Solubilization in non-polar solvents has been accomplished by through covalent functionalization using long-chain alkyl amine, organosilane and organotin reagents.

Solubilization in polar solvents such as DMF has been accomplished by means of π-π interaction between graphene and a pyrene derivative. Solubilization in water has been attained by using polyethylene glycol and different surfactants such as SDS, CTAB, and IGP.

We were able to decorate graphene by Pt and Ag in a single processing step through microwave-assisted polyol reduction of metal salts.

Studies of the electron transfer kinetics of the different graphene samples prepared by us shown that DG and CG exhibit better kinetics compared with EG, which behaves similar to the basal plane of graphite.

Graphene acts as a good electrode material for application in supercapacitors. The specific capacitance of the exfoliated graphene in the aqueous electrolyte is comparable to that obtained with activated carbons and superior to that of carbon nanotubes while value of the energy density of the graphene capacitors is one of the highest known to date. The supercapacitor characteristics are directly related to the quality of the graphene specifically the number of layers and the associated surface area. It should be possible to further improve the performance characteristics by modifying or improving the quality of the graphene samples.

6. REFERENCES

1. Fowler, W. A., Rev. Mod. Phys., 56, 149 **(1984).**

2. Pauling, L., The Nature of the Chemical Bond, Cornell University Press, Ithaca, NY, **(1960).**

3. Curl, R. F., Rev. Mod. Phys., 69, 691 **(1997).**

4. Kroto, H., Rev. Mod. Phys., 69, 703 **(1997).**

5. Smalley, R. E., Rev. Mod. Phys., 69, 723 **(1997).**

6. Iijima, S., Nature, 354, 56 **(1991).**

7. Wallace, P. R. The band theory of graphite. Phys. Rev., 71, 622 **(1947).**

8. McClure, J. W. Diamagnetism of graphite. Phys. Rev., 104, 666 **(1956).**

9. Slonczewski, J. C. & Weiss, P. R. Band structure of graphite. Phys. Rev., 109, 272 **(1958).**

10. Oshima, C., and Nagashima, A., J. Phys.: Condens. Matter, 9, 1 **(1997).**

11. Novoselov, K. S., et al., Proc. Natl. Acad. Sci. USA, 102, 10451 **(2005).**

12. Novoselov, K. S., et al., Science, 306, 666 **(2004).**

13. Partoens, B. & Peeters, F. M. From graphene to graphite: Electronic structure around the K point. Phys. Rev. B, 74, 075404 **(2006).**

14. Peierls, R. E. Bemerkungen u ber Umwandlungstemperaturen. Helv. Phys. Acta, 7, 81 **(1934).**

15. Peierls, R. E. Quelques proprietes typiques des corpses solides. Ann. Inst. Henri Poincare, 5, 177 **(1935).**

16. Landau, L. D. Zur Theorie der Phasenumwandlungen II. Phys. Z. Sowjetunion, 11, 26, **(1937).**

17. Landau, L. D. & Lifshitz, E. M. Statistical Physics Part I, Sections 137 and 138 (Pergamon, Oxford, **1980**).

18. Mermin, N. D. Crystalline order in two dimensions. Phys. Rev., 176, 250 **(1968).**

19. Berger, C. et al. Electronic confinement and coherence in patterned epitaxial graphene. Science, 312, 1191 **(2006).**

20. Ohta, T., Bostwick, A., Seyller, T., Horn, K. & Rotenberg, E. Controlling the electronic structure of bilayer graphene. Science, 313, 951 **(2006).**

21. Stankovich, S. et al. Graphene-based composite materials. Nature, 442, 282 **(2006).**

22 J. C. Meyer, A. K. Geim, M. I. Katsnelson, K. S. Novoselov, T. J. Booth, S. Roth Nature, 446, 60 **(2007).**

23. Born, M. & Huang, K. Dynamical Theory of Crystal Lattices (Clarendon, Oxford, **1954**).

24. Venables, J. A., Spiller, G. D. T. & Hanbucken, M. Nucleation and growth of thinfilms. Rep. Prog. Phys., 47, 399 **(1984).**

25. Zinkeallmang, M., Feldman, L. C., Grabow, M. H. Clustering on surfaces. Surf. Sci. Rep., 16, 377 **(1992).**

26. Evans, J. W., Thiel, P. A., Bartelt, M. C. Morphological evolution during epitaxial thin film growth: Formation of 2D islands and 3D mounds. Surf. Sci. Rep., 61, 1 **(2006).**

27. Nelson, D. R. & Peliti, L. Fluctuations in membranes with crystalline and hexatic order. J. Phys., 48, 1085 **(1987).**

28. Radzihovsky, L. & Le Doussal, P. Self-consistent theory of polymerized membranes. Phys. Rev. Lett., 69, 1209 **(1992).**

29. Nelson, D. R., Piran, T., Weinberg, S. Statistical Mechanics of Membranes and Surfaces (World Scientific, Singapore, **2004**).

30. Slonczewski, J. C., Weiss, P. R., Phys. Rev., 109, 272 **(1958).**

31. Semenoff, G. W., Phys. Rev. Lett., 53, 2449 **(1984).**

32. Haldane, F. D. M., Phys. Rev. Lett., 61, 2015 **(1988).**

33. Novoselov, K. S. et al. Two-dimensional gas of massless Dirac fermions in graphene. Nature, 438, 197 **(2005).**

34. Zhang, Y., Tan, J. W., Stormer, H. L. & Kim, P. Experimental observation of the quantum Hall eff ect and Berry's phase in graphene. Nature, 438, 201 **(2005).**

35. Schedin, F. et al. Detection of individual gas molecules by graphene sensors. Preprint at http://arxiv.org/abs/cond-mat/0610809 **(2006).**

36. Novoselev, K. S. et al. Room-temperature quantum Hall effect in graphene. Science, 315, 1379 **(2007).**

37. Semenoff, G. W. Condensed-matter simulation of a three-dimensional anomaly. Phys. Rev. Lett., 53, 2449 **(1984).**

38. Haldane, F. D. M. Model for a quantum hall effect without Landau levels: condensed-matter realization of the "parity anomaly". Phys. Rev. Lett., 61, 2015 **(1988).**

39. Zheng, Y. & Ando, T. Hall conductivity of a two-dimensional graphite system. Phys. Rev. B, 65, 245420 **(2002).**

40. Gusynin, V. P. & Sharapov, S. G. Unconventional integer quantum Hall effect in graphene. Preprint at khttp://xxx.lanl.gov/abs/cond-mat/0506575l **(2005).**

41. Peres, N. M. R., Guinea, F. & Neto, A. H. C. Electronic properties of twodimensional carbon. Preprint at khttp://xxx.lanl.gov/abs/cond-mat/0506709l **(2005).**

42. Ando, T., Nakaishi, T. & Saito, R. Berry's phase and absence of back scattering in carbon nanotubes. J. Phys. Soc. Jpn., 67, 2857 **(1998).**

43. Mikitik, G. P., Sharlai, Y. V. Manifestation of Berry's phase in metal physics. Phys. Rev. Lett., 82, 2147 **(1999).**

44. Berger, C. et al. Ultrathin epitaxial graphite: 2D electron gas properties and a route toward graphene-based nanoelectronics. J. Phys. Chem. B, 108, 19912 **(2004).**

45 Zhang, Y., Small, J. P., Pontius, W. V. & Kim, P. Fabrication and electric-fielddependent transport measurements of mesoscopic graphite devices. Appl. Phys. Lett., 86, 073104 **(2005).**

46. Zhang, Y., Small, J. P., Amori, E. S. & Kim, P. Electric field modulation of galvanomagnetic properties of mesoscopic graphite. Phys. Rev. Lett., 94, 176803 **(2005).**

47. Bunch, J. S., Yaish, Y., Brink, M., Bolotin, K. & McEuen, P. L. Coulomb oscillations and Hall effect in quasi-2D graphite quantum dots. Nano Lett., 5, 287 **(2005).**

48. S. Das Sarma, A. Pinczuk, Perspectives in Quantum Hall Effects (Wiley, New York, **1997).**

49. S. Q. Murphy et al., Physica E (Amsterdam) 6, 293 **(2000).**

50. G. Landwehr et al., Physica E (Amsterdam) 6, 713 **(2000).**

51. Novoselov, K. S., et al., Nat. Phys., 2, 177 **(2006).**

52. Cann, E., Falko, V. I., Phys. Rev. Lett., 96, 086805 **(2006).**

53. Partoens, B., and Peeters, F. M., Phys. Rev. B, 74, 075404, **(2006).**

54. Stankovich, S. et al. Stable aqueous dispersions of graphitic nanoplatelets via the reduction of exfoliated graphite oxide in the presence of poly (sodium 4- styrenesulfonate). J. Mater. Chem., 16, 155 **(2006).**

55. Kotov, N. A., Dekany, I., Fendler, J. H. Ultrathin graphite oxide-polyelectrolyte composites prepared by self-assembly. Transition between conductive and non-conductive states. Adv. Mater., 8, 637 **(1996).**

56. Du, X. S., Xiao, M., Meng, Y. Z. & Hay, A. S. Novel synthesis of conductive poly (arylene disulfide)/graphite nanocomposite. Synth. Met., 143, 129 **(2004).**

57. Liu, P., Gong, K. Synthesis of polyaniline-intercalated graphite oxide by an in situ oxidative polymerization reaction. Carbon, 37, 706 **(1999).**

58. Ounaies, Z., Park, C., Wise, K. E., Siochi, E. J. & Harrison, J. S. Electrical properties of single wall carbon nanotube reinforced polyimide composites. Compos. Sci. Technol., 63, 1637 **(2003).**

59. S. Stankovich, D. A. Dikin, G. H. B. Dommett, K. M. Kohlhaas, E. J. Zimney, E. A. Stach, R. D. Piner, S. T. Nguyen, R. S. Ruoff, 442, 282 **(2006).**

60. Chung, D. D. L. Electrical applications of carbon materials. J. Mater. Sci., 39, 2645 **(2004).**

61. D. A. Dikin, S. Stankovich, E. J. Zimney, R. D. Piner, G. H. B. Dommett, G. Evmenenko, S. T. Nguyen, R.S. Ruoff, Nature, 448, 457 **(2007).**

62. Moseley, P. T. Solid state gas sensors. Meas. Sci. Technol., 8, 223 **(1997).**

63. Capone, S. et al. Solid state gas sensors: State of the art and future activities. J. Optoelect. Adv. Mater., 5, 1335 **(2003).**

64. Kong, J. et al. Nanotube molecular wires as chemical sensors. Science, 287, 622 **(2000).**

65. Collins, P. G., Bradley, K., Ishigami, M., Zettl, A. Extreme oxygen sensitivity of electronic properties of carbon nanotubes. Science 287, 1801 **(2000).**

66. Dutta, P. & Horn, P. M. Low-frequency fluctuations in solids: 1/f noise. Rev. Mod. Phys., 53, 497, **(1981).**

67. F. Schedin, A. K. Geim, S. V. Morozov, E. W. Hill, P. blake, M. I. katsnelson, K. S. novoselov, nature materials, 6, 652, **(2007).**

68. Dresselhaus, M. S. & Dresselhaus, G. Intercalation compounds of graphite. Adv. Phys. 51, 1 **(2002).**

69. Granqvist, C. G. Sol. Energy Mater. Sol. Cells, 91, 1529 **(2007).**

70. Phillips, J. M.; Kwo, J., Thomas, G. A.; Carter, S. A., Cava, R. J., Hou, S. Y., Krajewski, J. J.; Marshall, J. H.; Peck, W. F.; Rapkine, D. H., van Dover, R. B., Appl. Phys. Lett., 65, 115 **(1994).**

71. Scott, J. C., Kaufman, J. H., Brock, P. J., DiPietro, R.; Salem, J., Goitia, J. A. J. Appl. Phys., 79, 2745 **(1996).**

72. Schlatmann, A. R.; Wilms Floet, D.; Hilberer, A.; Garten, F.; Smulders, P. J. M.; Klapwijk, T. M.; Hadziioannou, G. Appl. Phys. Lett., 69, 1764 **(1996).**

73. Wu, Z. C., Chen, Z. H., Du, X., Logan, J. M., Sippel, J., Nikolou, M., Kamaras, K., Reynolds, J. R., Tanner, D. B., Hebard, A. F., Rinzler, A. G., Science, 305, 1273 **(2004).**

(74). van de Lagemaat, J., Barnes, T. M., Rumbles, G., Shaheen, S. E., Coutts, T. J., Weeks, C., Levitsky, I., Peltola, J., Glatkowski, P., Appl. Phys. Lett., 88, 233503 **(2006).**

(75). C. Y. King, R., Roussel, F., Appl. Phys. A, 86, 159 **(2007).**

76. G. A. Olah, and Á. Molnár, Hydrocarbon Chemistry (Wiley-Interscience, Hoboken, NJ, USA, **2003**).

77. N. Watanabe, T. Nakajima, and H. Touhara, Graphite fluorides (Elsevier, Amsterdam, **1988**).

78. H. C. Schniepp, J. -L. Li, M. J. McAllister, H. Sai, M. Herrera-Alonso, D. H. Adamson, R. K. Prud'homme, R. Car, D. A. Saville and I. A. Aksay, J. Phys. Chem. B, 110, 8535 **(2006).**

79. P. R. Somani, S. P. Somani and M. Umeno, Chem. Phys. Lett., 430, 56 **(2006).**

80. O. E. Andersson, B. L. V. Prasad, H. Sato, T. Enoki, Y. Hishiyama, Y. Kaburagi, M. Yoshikawa and S. Bandow, Phys. Rev. B, 58, 16387 **(1998).**

81. Y. Li, S. Xie, W. Zhou, D. Tang, X. P. Zou, Z. Liu and G. Wang, Carbon, 39, 626 **(2001).**

82. Staudenmaier, L. Ber. Dtsch. Chem. Ges., 31, 1481 **(1898).**

83. Hummers, W., Offeman, R. E., J. Am. Chem. Soc., 80, 1339 **(1958).**

84. Klabunde, K., et al., J. Am. Chem. Soc., 118, 12465 **(1996).**

85. Klabunde, K., et al., J. Phys. Chem., 100, 12142 **(1996).**

86. Hornyak, G.L., C.J. Patrissi, and C.R. Martin., J. Phys. Chem. B, 101, 1548 **(1997).**

87. Leon, R., D. Margolese, P. Petroff, and G.D. Stucky, Phys. Rev. B, 52, 2285 **(1995).**

88. Blake, N.P., V.I. Srdanov, G.D. Stucky, and H. Metiu, J. Chem. Phys., 104, 8721 **(1996).**

89. Cao, G., M.E. Garcia, M. Alcala, L.F. Burgess, and T.E. Mallouk, J. Am. Chem. Soc. 114, 7574 **(1992).**

90. Dickinson, T.A., J. White, J.S. Kauer and D.R. Walt, Nature, 382, 697 **(1996).**

91. S. Satyapal, J. Petrovic, C. Read, G. Thomas, G. Ordaza, Catal. Today, 120, 246 **(2007).**

92. R. V. Siriwardane, M. S. Shen, E. P. Fisher, Energy Fuel, 17, 571 **(2003).**

93. R. V. Siriwardane, M. S. Shen, E. P. Fisher, J. A. Poston, Energy Fuel, 15, 279 **(2001).**

94. N. D. Hutson, Chem. Mater., 16, 4135 **(2004).**

95. Y. Zou, E. R. Alírio, Energy Convers. Manage, 43, 1865 **(2002).**

96. M. L. Gray, Y. Soong, K. J. Champagne, J. Baltrus, R. W. Stevens,P. Toochinda, S.

S. C. Chuang, Sep. Purif. Technol., 35, 31 **(2004).**

97. T. Filburn, J. J. Helble, R. A. Weiss, Ind. Eng. Chem. Res., 44, 1542 **(2005).**

98. S. Satyapal, T. Filburn, J. Trela, J. Strange, Energy Fuel, 15, 250 **(2001).**

99. O. Leal, C. Bolívar, C. Ovalles, J. Carcía, Y. Espidel, Inorg. Chim.Acta, 240,183 **(1995).**

100. N. Texier-Mandoki, J. Dentzer, T. Piquero, S. Saadallah, P. David, C. Vix-Guterl,

Carbon, 42, 2735 **(2004).**

101. J. B. Parra, C. O. Ania, A. Arenillas, F. Rubiera, J. M. Palacios, J. J. Pis, J. Alloys

Compd., 379, 280 **(2004).**

102. R. Zacharia, K. Y. Kim, S. W. Hwang and K. S. Nahm, Catal.Today, 120, 426 **(2007)**

103. H. Jin, Y. S. Lee and I. Hong, Catal. Today, 20, 399 **(2007).**

104. A. D. Lueking, R. T. Yang, N. M. Rodriguez, R. T. K. Baker, Langmuir, 20, 714

(2004).

104. A. D. Lueking, R. T. Yang, N. M. Rodriguez, R. T. K. Baker, Langmuir, 20, 714

(2004).

105. M. Marella and M. Tomaselli, Carbon, 44, 1404 **(2006).**

106. G. Gundiah, A. Govindaraj, N. Rajalakshmi, K. S. Dhathathreyan, C. N. R. Rao,

J. Mater. Chem., 13, 209 **(2003).**

107. B. Panella, M. Hirscher and S. Roth, Carbon, 43, 2209 **(2005).**

108. R. Dash, J. Chmiola, G. Yushin, Y. Gogotsi, G. Landisio, J. Singer, J. Fischer and S.

Kucheyev, Carbon, 44, 2489 **(2006).**

109. M. Shiraishi, T. Takenobu, H. Kataura and M. Ata, Appl. Phys. A, 78, 947 **(2004).**

120. B. Panella, M. Hirscher and B. Ludescher, Microporous Mesoporous Mater., 103, 230 **(2007).**

121. Stankovich, S., Dikin, D. A., Piner, R. D., Kohlhaas, K. A.; Kleinhammes, A., Jia, Y., Wu, Y., Nguyen, S. T., Ruoff, R. S. Carbon, 45, 1558 **(2007).**

122. Dujardin, E., Ebbesen, T. W.; Krishnan, A., Treacy, M. M. J., Adv. Mater., 10, 1472 **(1998).**

123. Chen, Y., Haddon, R. C., Fang, S., Rao, A. M., Eklund, P. C., Lee, W. H., Dickey, E. C., Grulke, E. A., Pendergrass, J. C., Chavan, A., Haley, B. E., Smalley, R. E., J. Mater. Res., 13, 2423 **(1998).**

124. Ebbesen, T. W., Cones and Tubes: Geometry in the Chemistry of Carbon. Acc. Chem. Res., 31, 558 **(1998).**

125. Liu, J., Rinzler, A. G., Dai, H., Hafner, J. H., Bradley, R. K., Boul, P. J., Lu, A., Iverson, T., Shelimov, K., Huffman, C. B., Rodriguez- Macias, F., Shon, Y.-S., Lee, T. R., Colbert, D. T., Smalley, R. E., Science, 280, 1253 **(1998).**

126. Mawhinney, D. B., Naumenko, V., Kuznetsova, A., Yates, J. T. J., Liu, J., Smalley, R. E., Chem. Phys. Lett., 324, 213 **(2000).**

127. Hu, H., Bhowmik, P., Zhao, B., Hamon, M. A., Itkis, M. E., Haddon, R. C., Chem. Phys. Lett., 345, 25 **(2001).**

128. Ausman, K. D., Piner, R., Lourie, O., Ruoff, R. S., Korobov, M., J. Phys. Chem. B, 104, 8911 **(2000).**

129. Monthioux, M., Smith, B. W., Burteaux, B., Claye, A., Fischer, J. E., Luzzi, D. E., Carbon, 39, 1251 **(2001).**

130. Itkis, M. E., Niyogi, S., Meng, M., Hamon, M., Hu, H., Haddon, R. C., Nano Lett., 2, 155 **(2002).**

131. Tohji, K., Takahashi, H., Shinoda, Y., Shimizu, N., Jeyadevan, B., Matsuoka, I., Saito, Y., Kasuya, A., Ito, S., Nishina, Y., J. Phys. Chem. B, 101, 1974 **(1997).**

132. Bandow, S., Asaka, S., Zhao, X., Ando, Y., Appl. Phys. A, 67, 23 **(1998)**.

133. Dujardin, E., Ebbesen, T. W., Krishnan, A., Treacy, M. M. J., Adv. Mater., 10, 611 **(1998).**

134. Dillon, A. C., Gennet, T., Jones, K. M., Alleman, J. L., Parilla, P. A., Heben, M. J., Adv. Mater., 11, 1354 **(1999).**

135. S. Bandow, A. M. Rao, K. A. Williams, A. Thess, R. E. Smalley, P. C. Eklund, J. Phys. Chem. B, 101, 8839 **(1997).**

136. G. S. Duesberg, M. Burghard, J. Muster, G. Philipp, S. Roth, Chem. Commun., 435, **(1998).**

137. V. Krstic, G. S. Duesberg, J. Muster, M. Burghard, S. Roth, Chem. Mater., 10, 2338 **(1998).**

138. R. J. Chen, Y. Zhang, D. Wang, H. Dai, J. Am. Chem. Soc., 123, 3838 **(2001).**

139. S. A. Curran, P. M. Ajayan, W. J. Blau, D. L. Carroll, J. N. Coleman, A. B. Dalton, A. P. Davey, A. Drury, B. McCarthy, S. Maier, A. Strevens, Adv. Mater., 10, 1091 **(1998).**

140. A. Star, J. F. Stoddart, D. Steuerman, M. Diehl, A. Boukai, E. W. Wong, X. Yang, S., W. Chung, H. Choi, J. R. Heath, Angew. Chem, 113, 1771 **(2001).**

141. J. N. Coleman, A. B. Dalton, S. Curran, A. Rubio, A. P. Davey, A.Drury, B. McCarthy, B. Lahr, P. M. Ajayan, S. Roth, R. C. Barklie, W. J. Blau, Adv. Mater., 12, 213 **(2000).**

142. M. J. O'Connell, P. Boul, L. M. Ericson, C. Huffman, Y. Wang, E. Haroz, C. Kuper, J. Tour, K. D. Ausman, R. E. Smalley, Chem. Phys. Lett., 342, 265 **(2001).**

143. S. Niyogi, E. Bekyarova, M. I. Itkis, J. L. McWilliams, M. A. Hamon and R. C. Haddon, J. Am. Chem. Soc., 128, 7720 **(2006).**

144. P. Asuri, S. S. Karajanagi, J. S. Dordick, and R. S. Kane, J. Am. Chem. Soc., 128, 1046 **(2006).**

145. Y. Zhang, Y. Shen, D. Han, Z. Wang, J. Song and L. Niu, J. Mater. Chem., 16, 4592 **(2006).**

146. S. Attal, R.Thiruvengadathan, O. Regev, Annal. Chem., 78, 8098 **(2006).**

147. O. Matarredona, H. Rhoads, Z. Li, J. H. Harwell, L. Balzano, D. E. Resasco, J. Phys. Chem. B, 107, 13357, **(2003).**

148. R. J. Chen, Y. Zhang, D. Wang, H. Dai, J. Am. Chem. Soc., 123, 3838 **(2001).**

149. C. N. R. Rao and A. K. Cheetham, J. Mater. Chem., 11, 2887 **(2001).**

150. P. D. Cozzoli, T. Pellegrino, L. Manna, Chem. Soc. Rev., 35, 1195 **(2006).**

151. C. N. R. Rao, G. U. Kulkarni, P. J. Thomas, P. P. Edwards, Chem.–Eur. J., 8, 29 **(2002).**

152 (a). Y. Yin, A. P. Alivisatos, Nature, 437, 664 **(2005).**

(b) D. L. Feldheim, C. D. Keating, Chem. Soc. Rev., 27, 1 **(1998).**

153. (a) B. L. Cushing, V. L. Kolesnichenko, C. J. O'Connor, Chem. Rev., 104, 3893 **(2004).**

(b) A. C. Templeton, W. P. Wuelfing, R. W. Murray, Acc. Chem. Res., 33, 27 **(2000).**

154. (a) M. Hu, J. Y. Chen, Z. Y. Li, L. Au, G. V. Hartland, X. D. Li, M. Marquez and Y. N. Xia, Chem. Soc. Rev., 35, 1084 **(2006).**

(b). P. V. Kamat, J. Phys. Chem. B, 106, 7729, **(2002).**

155 (b) C. J. Kiely, J. Fink, M. Brust, D. Bethell and D. J. Schiffrin, Nature, 396, 444 **(1998).**

156 (a) R. P. Andres, T. Bein, M. Dorogi, S. Feng, J. I. Henderson, C. P. Kubiak, W. Mahoney, R. G. Osifchin and R. Reifenberger, Science, 272, 1323 **(1996).**

(b) R. P. Andres, J. D. Bielefeld, J. I. Henderson, D. B. Janes, V. R. Kolagunta, C. P. Kubiak, W. J. Mahoney, R. G. Osifchin, Science, 273, 1690 **(1996).**

157 (a). E. V. Shevchenko, D. V. Talapin, N. A. Kotov, S. O'Brien, C. B. Murray, Nature, 439, 55 **(2006).**

(b). C. P. Collier, T. Vossmeyer, J. R. Heath, Annu. Rev. Phys. Chem., 49, 371 **(1998).**

158. C. Guarise, L. Pasquato, V. De Filippis and P. Scrimin, Proc. Natl. Acad. Sci. U. S.A., 103, 3978 **(2006).**

159. X.-S. Fang, C. H. Ye, L. D. Zhang, Y. H. Wang , Y. C. Wu, Adv. Funct. Mater., 15, 63 **(2005).**

160. X. S. Fang and L. D. Zhang, J. Mater. Sci. Technol., 22, 721**(2006).**

161 (a). L. S. Li, J. T. Hu, W. D. Yang, A. P. Alivisatos, Nano Lett., 1, 349 **(2001).**

(b) D. J. Milliron, S. M. Hughes, Y. Cui, L. Manna, J. B. Li, L.-W. Wang, A. P. Alivisatos, Nature, 430, 190 **(2004).**

162. S. H. Sun, C. B. Murray, D. Weller, L. Folks and A. Moser, Science, 287, 2000 **(1989).**

163 (a) L. E. Euliss, J. A. DuPont, S. Gratton and J. DeSimone, Chem. Soc. Rev., 35, 1095 **(2006).**

(b) S. H. Sun, Adv. Mater., 18, 393 **(2006).**

164 (a). C. B. Murray, D. J. Norrs, M. G. Bawendi, J. Am. Chem.Soc., 115, 8706 **(1993).**

(b). D. K. Yi, S. T. Selvan, S. S. Lee, G. C. Papaefthymiou, D. Kundaliya, J. Y. Ying, J. Am. Chem. Soc., 127, 4990 **(2005).**

165. G. G. Wildgoose, C. E. Banks and R. G. Compton, Small, 2, 182 **(2006).**

166. B. C. Satishkumar, E. M. Vogl, A. Govindaraj, C. N. R. Rao, J. Phys. D: Appl. Phys., 29, 3173 **(1996).**

167. J. M. Planeix, N. Coustel, J. Coq, V. Brotons, P. S. Kumbhar, R. Dutartre, P. Geneste, P. Bernier, P. M. Ajayan, J. Am. Chem. Soc., 116, 7935 **(1994).**

168. H. S. Kim, H. Lee, K. S. Han, J. H. Kim, M. S. Song, M. S. Park, J. Y. Lee and J. K. Kang, J. Phys. Chem. B, 109, 8983 **(2005).**

169. L. M. Ang, T. S. A. Hor, G. Q. Xu, C. H. Tung, S. P. Zhao, J. L. S. Wang, Chem. Mater., 11, 2115 **(1999).**

170. B. Xue, P. Chen, Q. Hong, J. Lin and K. L. Tan, J. Mater. Chem., 11, 2378 **(2001).**

171. P. Chen, X. Wu, J. Lin and K. L. Tan, J. Phys. Chem. B, 103, 4559 **(1999).**

172. J. Chen, M. A. Hamon, H. Hu, Y. S. Chen, A. M. Rao, P. C. Ecklund, R. C. Haddon, Science, 282, 95 **(1998).**

173. R. Zanella, E. V. Basiuk, P. Santiago, V. A. Basiuk, E. Mireles, I. Puente-Lee and J. M. Saniger, J. Phys. Chem. B, 109, 16290 **(2005).**

174. A. V. Ellis, K. Vijayamohanan, R. Goswami, N. Chakrapani, L. S. Ramanathan, P. M. Ajayan, G. Ramanath, Nano Lett., 3, 279 **(2003).**

175. G. M. Rahman, D. M. Guldi, E. Zambon, L. Pasquato, N. Tagmatarchis and M. Prato, Small, 1, 527 **(2005).**

176 (a). L. Liu, T. Wang, J. Li, Z.-X. Guo, L. Dai, D. Zhang, D. Zhu, Chem. Phys. Lett., 367, 747 **(2003).**

177. D. M. Guldi, G. M. A. Rahman, N. Jux, N. Tagmatarchis, M. Prato, Angew. Chem., Int. Ed., 43, 5526 **(2004).**

178. D. M. Guldi, G. M. A. Rahman, N. Jux, M. Prato, S. H. Qin, W. Ford, Angew. Chem., Int. Ed., 44, 2015 **(2005).**

179. Kinoshita, K. Carbon: Electrochemical and Physiochemical Properties; (Wiley: New York **1988**).

180. McCreery, R. L. in Electroanalytical Chemistry; Bard, A. J., Ed.; Marcel Dekker: New York, Vol. 17, **1991**.

181. Ranganathan, S.; Kuo, T.; McCreery, R. L. Anal. Chem., 71, 3574 **(1999).**

182. Bockris, J. O. M.; Srinivasan, S. Fuel Cells: Their Electrochemistry, McGraw-Hill: New York **1969.**

183. Evans, J. F., Kuwana, T. Anal. Chem., 49, 1632 **(1977)**

184. Chen, P., McCreery, R. L. Anal. Chem. **1996**, 68, 3958. Yang, H.; McCreery, R. L. Anal. Chem, 71, 4081, **(1999).**

185. Conway B E 1999 Electrochemical supercapacitors (New York: Kluwer Academic, Plenum New York, **1999**).

186. Kotz R and Carlen M, Electrochim. Acta 45, 2483 **(2000).**

187. Frackowiak E, Beguin F, Carbon 39, 937 **(2001).**

188. Qu D, Shi H J. Power. Sources 74, 99 **(1998).**

189. Meyer S T, Pekala R W and Kaschmitter J L, J. Electrochem. Soc., 40, 446 **(1993).**

190. Niu C M, Sichel E K, Hoch R, Moy D and Tennent H Appl. Phys. Lett., 70, 1480 **(1997).**

191. Frackowiak E, Metenier K, Bartagna V and Beguin V, Appl. Phys. Lett., 77, 2421 **(2000).**

192. An K H, Kim W S, Park Y S, Choi Y C, Lee S M, Chung D, Bae D J, Lim S C ,Lee Y Adv. Mater., 13 497 **(2001).**

193. Du C, Yeh J and Pan N, Nanotechnology 16, 350 **(2005).**

194. Yoon S, Lee J, Hyeon T and Oh S M, J. Electrochem. Soc., 147, 2507 **(2000).**

195. Chimola J, Yushin G, Gogotsi Y, Portet C, Simon P and Taberna P L, Science, 313, 1760 **(2006**).

196. M. S. Raghuveer, S. Agrawal, N. Bishop, G. Ramanath, Chem. Mater., 18, 1390 **(2006).**

197. R. Muszynski, B. Seger, and P. V. Kamat, J. Phys. Chem. C, 112, 5263 **(2008).**

198. F. Valentini, A. Amine, S. Orlanducci, M. L. Terranova andG. Palleschi, Anal. Chem., 75, 5413 **(2003).**

199. A. Gupta, G. Chen, P. Joshi, S. Tadigadapa, P. C. Eklund, Nano. Lett., 6, 2667 **(2007).**

200. M. A. Pimenta, G. Dresselhaus, M. S. Dresselhaus, L. A. Cancado, A. Jorio, R. Sato, Phys. Chem. Chem. Phys., 9, 1276 **(2007).**

201. A. C. Ferrari, Solid. Stat. Commun., 143, 47 **(2007).**

202. C. E. Banks, T. J. Davies, G. G. Wildgoose and R. G. Compton, Chem. Commun., 7, 829 **(2005).**

203. A. Balducci, R. Dugas, P. L. Taberna, P. Simon, D. Plee, M. Mastragonstino, S.Passerini, J. Power Sources, 165, 922 **(2007).**